DEVELOPMENT OF MASONRY HOUSE WALL STRENGTHENING TECHNIQUES AGAINST EARTHQUAKES USING SCRAP TIRES

A THESIS SUBMITTED TO
THE GRADUATE SCHOOL OF NATURAL AND APPLIED SCIENCES
OF
MIDDLE EAST TECHNICAL UNIVERSITY

BY

MUSTAFA GÖLALMIŞ

IN PARTIAL FULFILLMENT OF THE REQUIREMENTS
FOR
THE DEGREE OF MASTER OF SCIENCE
IN
CIVIL ENGINEERING

JULY 2005

Approval of the Graduate School of Natural and Applied Sciences

_____

Prof. Dr. Canan ÖZGEN
Director

I certify that this thesis satisfies all the requirements as a thesis for the degree of Master of Science.

_____

Prof. Dr. Erdal ÇOKÇA
Head of Department

This is to certify that we have read this thesis and that in our opinion it is fully adequate, in scope and quality, as a thesis for the degree of Master of Science.

_____

Asst. Prof. Dr. Ahmet TÜRER
Supervisor

Prof. Dr. S. Tanvir Wasti (METU, CE) _____

Asst. Prof. Dr. Ahmet Türer (METU, CE) _____

Prof. Dr. Ergin Atımtay (METU, CE) _____

Asst. Prof. Dr. Barış Binici (METU, CE) _____

Asst. Prof. Dr. H. Hüsnü Korkmaz (S.Ü., CE) _____

I hereby declare that all information in this document has been obtained and presented in accordance with academic rules and ethical conduct. I also declare that, as required by these rules and conduct, I have fully cited and referenced all material and results that are not original to this work.

Name, Last Name: Mustafa GÖLALMIŞ

Signature :

ABSTRACT

DEVELOPMENT OF MASONRY HOUSE WALL STRENGTHENING TECHNIQUES AGAINST EARTHQUAKES USING SCRAP TIRES

Gölalmış, Mustafa
M. Sc., Department of Civil Engineering
Supervisor: Asst. Prof. Dr. Ahmet Türer

July 2005, 122 pages

About half of the building stock in Turkey is masonry type and one fourth of the building stock is one-storey brick type masonry buildings. Especially the rural masonry houses are commonly constructed by their own residents without any engineering knowledge. Traditional masonry houses usually have heavy roofs which generate large lateral forces on walls during earthquakes. Readily available retrofitting techniques are mostly complicated and costly making it not feasible for uneducated poor residents to strengthen their own houses. The aim of this thesis is to develop a new alternative strengthening technique using scrap tires that is economic and easy to apply on the walls of one-story masonry houses.

In order to investigate the usage of scrap tires for masonry wall post-tensioning, forty three scrap tire rings (STRs) from nine different brands and nine rim-rings direct tension experiments were conducted. The average tensile load capacities of STRs and rim-rings were found as 132.6 kN and 53 kN, respectively.

Six strip walls (i.e., four brick- and two briquette-walls) strengthened by applying post-tensioning loads with STCs and hybrid system were tested in out-of-plane bending direction. The out-of-plane capacity of the brick and briquette walls

increased up to about 9 times and 5 times with respect to their nominal capacities, respectively.

Finally, two-full scale traditional masonries were tested by the tilting table. The capacity of strengthened house increased 75% with respect to the unstrengthened one.

The results obtained form the conducted tests are highly promising and suggest that the method can be used as a *low-cost* and *simple* strengthening technique for seismically deficient single storey, masonry type houses.

Keywords: Masonry, Out-of-plane, Tensile Strength of Scrap Tire, Tilting Table, Scrap Tire Retrofitting

ÖZ

ATIK OTOMOBİL LASTİKLERİ KULLANARAK YIĞMA BİNA DUVARLARININ DEPREME KARŞI GÜÇLENDİRME ÇALIŞMALARI

Gölalmış, Mustafa
Yüksek Lisans, İnşaat Mühendisliği Bölümü
Tez Yöneticisi: Y. Doç. Dr. Ahmet Türer

Temmuz 2005, 122 sayfa

Türkiye yapı stokunun yaklaşık %50'si yığma binalardan oluşmaktadır. Bu binalar genellikle mühendislik eğitimi almamış, ev sakinleri tarafından inşa edilmektedir. Bu evler genellikle ağır çatı kütleleri ile kapatılmaktadır ve bu çatılar deprem anında, yığma bina duvarlarının, düzlem dışı ve düzlem içi yönünde büyük bir kuvvetle itilmesine ve binanın şiddetli bir şekilde yıkılmasına neden olmaktadır. Hali hazırda bulunan güçlendirme teknikleri çoğunlukla karmaşık ve maliyetinin dar gelirli ev sakinleri tarafından karşılanması güçtür. Bu çalışmanın amacı, kullanılmış araba lastiği ile ard-germe uygulayarak, uygulanabilirliği kolay ve maliyeti düşük, yığma bina duvarları için alternatif bir güçlendirme tekniği geliştirmektir.

Öncelikle, atık araba lastiklerinin güçlü kısımları olan, lastik halkası (yol ile temas eden kısım) ve kenar halkalarının ard-germe malzemesi olarak kullanılmasının, uygun olup, olmadığını araştırmak amacıyla, dokuz farklı lastik markasına ait toplam kırk üç adet lastik halkası ve dokuz adet lastik kenar halkası çekeme deneyi yapıldı. Deneylerden elde edilen sonuçlarına göre, lastik halkası ve lastik kenar halkasıın ortalama çekme dayanımları 132.6 kN ve 53 kN olarak hesaplandı.

Altı adet yığma duvar şeridi (dört tuğla, iki biriket), lastik halka zinciri ve hibrid sistem ile ard-germe kuvveti uygulayarak güçlendirildi ve düzlem dışı yönünde test edildi. Bu deneylerden elde edilen sonuçlara göre, ard-germe uygulanan tuğla duvarın zayıf yöndeki yanal yük dayanım artışı, ard-germe uygulanmayan duvara göre yaklaşık 10 kat artmıştır. Bu oran biriket duvarda ise, 5 kat olarak görülmüştür.

Son olarakta, iki adet birebir ölçekli yığma ev, eğilme masası kullanarak test edildi. Bu iki deneyden elde edilen sonuçlara göre, güçlendirilmiş evde, güçlendirilmemiş eve göre, yaklaşık %75'lik bir dayanım artışı gözlenmiştir.

Bu çalışmada yapılan deneylerden elde edilen sonuçlar, önerilen ard-germe methodu için umut vericidir. Sonuç olarak, bu çalışmada önerilen ard-germe tekniği ile, sismik dayanımı yetersiz olan bir katlı evler için, maliyeti düşük ve uygulanabilirliği kolay basit bir güçlendirme tekniği sunulmaktadır.

Anahtar Kelimeler: Yığma Ev, Düzlem Dışı, Lastik Çekme Dayanımı, Eğilme Masası, Atık Lastikle Güçlendirme

To my family and my darling, Kevser…

ACKNOWLEDGEMENTS

This study was conducted under the control of the Asst. Prof. Ahmet Türer. I wish to express my sincere thanks and appreciations for his support, guidance, encouragement and criticisms during this study. It was a great honor and pleasure to work with him.

I also would like to extend my thanks to my parents and my darling for their encouragement and assistance throughout this long and difficult study.

I should mention the names Asst. Prof. Dr. H. Hüsnü Korkmaz, Atilla Akaydın, Çağdaş Şimşek, Hasan Metin and Gökhan Özdemir to appreciate them for their great friendship and assistance.

I would like to thank Bayezıd Özden for his comments and important suggestions through out my research.

This study formed a part of "Seismic Performance Improvement of Masonry Houses" project, financed by World Bank DM-2003 and TÜBİTAK İÇTAG I599/01. The help of the Project liaison, Mr. İbrahim Sirer, is also kindly acknowledged.

TABLE OF CONTESTS

PAGE

LIST OF TABLES

PAGE

LIST OF FIGURES

PAGE

LIST OF SYMBOLS

STR	: Scrap tire tread ring
STC	: Scrap tire tread ring chain
URM	: Unreinforced masonry
P	: Post-tensioning load (kN)
T	: Torque values (N.m)
δ	: Crack opening (mm)
Δ	: Lateral displacement (mm)

CHAPTER 1

INTRODUCTION

Turkey is located in active seismic regions, and a large part of the country is under an earthquake risk. In the last fifteen years, many large earthquakes have occurred in Turkey (Erzincan-92, Dinar-95, Adana-Ceyhan-98, İzmit-99, Düzce-99, Afyon-Sultandağı-2002, Bingöl-2003, and Erzurum-2004) killing about 20000 people, during these earthquakes. A majority of the people that lost their lives in Erzincan, Afyon, Bingöl, and Erzurum were living in masonry houses.

Masonry construction constitutes a major portion of the building stock in developing countries. For example, masonry buildings in Turkey constitute 51% of the building stock (21% is brick, 11% hollow brick, 9% stone, and 10% others) according to DIE-2000 [1] values. A majority of masonry houses were built without engineering services. Turkish rural masonry houses commonly have heavy soil type roofs creating large lateral forces during earthquakes. The heavy roofs are carried by wooden log beams placed on opposite walls and cause masonry walls to be pushed in out-of-plane and in-plane directions causing sudden collapse of the walls. Although the compressive strength capacities of masonry wall building blocks are high enough to carry these heavy static vertical loads of roofs, they become vulnerable under tensile loads which are created during earthquakes. In order to improve the seismic performance of masonry houses, they would need to be strengthened using post-tensioning which reduces tensile stresses and makes use of the high compressive strength of masonry walls.

Many strengthening methods have been developed and used to increase the strength of masonry houses against seismic forces. One of the common retrofitting methods

is surface treatment, which incorporates different techniques. The first one is the use of ferrocement composites that is made by closely placed multiple layers of fine rods and mesh which are embedded in a high strength cement mortar layer. For the reinforced plaster technique, steel bars are arranged as diagonal bars or as a vertical and horizontal mesh. A thin layer of plaster is then applied over the steel bars. The last one is the shotcrete overlays that are sprayed onto the surface of a masonry wall over a mesh of reinforcing bars.

A repair technique commonly used is grout and epoxy injecting to restore the original integrity of the wall and to fill the voids and cracks of walls.

External reinforcement is another commonly used strengthening technique. Steel systems, such as steel plates or tubes, are attached directly to the existing wall.

In the recent years, a new strengthened technique which is made of fiber reinforced polymers (FRP) has been developed to increase seismic performance of masonry and infill walls. FRP are made of high-modulus fibers bonded with a resin matrix. FRPs possess many advantages which are high corrosion resistance, high tensile strength to weight ratio, electromagnetic neutrality and ease of handling. The most common fibers types used and researched are made of glass (GFRP), aramid (AFRP), and carbon (CFRP) fibers. These fibers are commonly adhered on the surface of the masonry walls using strong epoxy adhesive. The application of FRP usually gives less discomfort to the residents. In order to investigate the seismic performance improvement of masonry walls strengthened using FRP, many experiments have been done on the walls in out-of-plane and in-plane directions. Some studies conducted using these materials are given in the following section and the results obtained from these works will be discussed.

Another well-known technique which was also investigated in this study in order to strengthen masonry wall is post-tensioning of the masonry walls. Until now, the best usage of this technique has been applied on the masonry walls with steel bars. During the construction of the masonry walls, steel bars are passed through the

center hole of the bricks. After finishing the construction of masonry walls, steel bars are tensioned against masonry blocks.

In this study, an alternative post-tensioning technique was tired to develop using STC and hybrid system. Unlike the traditional post tensioning application, the post-tensioning process here was made differently by the STC and hybrid system which are wrapped on the surface of the masonry walls after constructions. Using the nut-bolt arrangement on the connection, the determined post-tensioning forces are applied on the masonry house walls.

This thesis contains the following sections. Chapter 1 provides a general background on the strengthening technique types on masonry walls. In Chapter 2, the construction materials in masonry wall and the strengthening material are detailed. Chapter 3 presents the test set-up preparations and the results of the experiments conducted in this thesis. In Chapter 4, analytic studies are made on the four brick wall tests in the out-of-plane direction. Finally, Chapter 5 introduces a summary and the conclusions of this thesis and some recommendations for future researches.

1.1. LITERATURE SURVEY

In the literature, there are many different studies made on scrap tires to improve the recycling process of them in the world and masonry walls to improve the seismic performance of them.

1.1.1. Recycling Process of Scrap Tire

Some of studies about recycling of scrap tires are explained as follows:

About half of the used automobile tires had been recycled until the 1960's, because natural rubber which was expensive at those times was commonly used in the tire

manufacturing process in the US. After that time, increase in the usage of synthetic rubber in manufacturing reduced the manufacturing costs and caused the usage of the natural rubber to decrease. The development of the steel belted tires in the late 1960s almost ended of tire recycling. By 1995, only 2% of the rubber was being recycled in the US [2].

Highway construction industry is a big alternative market for recycling scrap tires. Many researches have been carried out on crumb rubber modified asphalt [3]. In 1995, it was necessary that all federal states in the U.S fund paving projects with tire modified asphalt [4]. As a result of this encouragement, consumption rate of the wasted tires in modified asphalt projects were increased, and in some states of US it was reached to a maximum recycling rate of 20 % [5].

Furthermore Stubblefield et al. [6] studied to evaluate the feasibility and performance of the waste tire modified concrete. It was observed from the experiment results that the usage of the scrap tire crumbs in concrete provided an additional tensile strength while no positive effects on compressive strength. Also, it was stated that the performance of truck tires are better than the car tires due to the high steel concentration in the truck tires.

Eldin and Senouci [7] investigated the strength of the concrete and toughness with a portion of aggregates replaced by waste tire chips. According to the experiment results, the compressive strength of the concrete was reduced, while its toughness and ability to absorb fracture energy were enhanced significantly. They also provide a qualitative explanation of the fracture mechanisms of rubber-filled concrete based on the theory of strength of materials.

1.1.2. Seismic Performance Improvement of Masonry Walls

There is much research conducted to improve the seismic performance of masonry wall in the literature. The study studies relevant to this section are listed and expounded in the following paragraphs.

Ghobarah and Galal [8] investigated the effect of the strengthening operation on unreinforced masonry block walls with opening exposed to extreme out-of-plane loads. Five full scale masonry walls with different opening configurations, such as a single center window, one window off center, two windows, a wide window and a door were constructed. The walls were tested under the uniformly distributed lateral load in out-of-plane direction up to failure and then they were strengthened using carbon fiber-reinforced polymer (CFRP) laminate strips and retested. The failure of unstrengthened walls were occurred along the mortar joints whereas failure of strengthened walls occurred due to cracking of masonry blocks around CFRP strips on the windows corner and debonding between masonry blocks and CFRP strips. Researches have found that the lateral load carrying capacity of the strengthened walls increased five times compared to unstrengthened walls. The ductility demand and energy dissipation capacities of the strengthened walls were increased as well.

Tan and Patoary [9] suggested the usage of three different fiber-reinforced polymers (FRP) to improve the seismic performance of the masonry walls in the out-of-plane direction. The test results pointed out that the load-carrying capacity of walls increased significantly with increasing number of FRP layers. During the experiments, there was only one mode of failure taking place due to the tensile splitting under bending observed on the unstrengthened walls, whereas four different modes of failures, i.e., punching shear through the bricks, flexural bond failure by debonding of the FRP laminates from the masonry substrate, FRP rupture, and flexural compression failure, were observed for the strengthened walls.

Hamoush et al. [10] conducted eighteen compact masonry wall panel tests to evaluate the out-of-plane shear strength of masonry walls reinforced with externally bonded FRP composites for different forms. They stated that using FRP composites augmented the flexural performance and structural integrity of the walls. Conversely, researchers further stated that the reinforcement fiber area and the amount of fiber extension to the supports did not affect the shear strength of the walls significantly.

Ehsani et al. [11] conducted a series of experiments on three half-scale URM walls retrofitted with E-glass fiber-reinforce polymer (GFRP) strips and tested under cyclic out-of–plane load. They stated that the out-of-plane capacity of the strengthened URM walls with GFRP increased to 32 times of the wall weights whereas the walls behaved in a brittle manner.

Hamid et al. [12] presented an experimental study concerning the behavior and strength of concrete masonry walls strengthened with joint reinforcement embedded into the mortar joints. They have constructed five-full scale masonry walls. These walls were tested to designate the effect of amount and type of horizontal steel and bond pattern on wall behavior. It was obtained from the experiment results that joint reinforcement did not influence the cracking load significantly; whereas the flexural strengths of walls were increased significantly. Although, bond pattern did not affect the ultimate moment carrying capacity of the walls, it affected the cracking moment.

Zeiny and Larralde [13] introduced a technique to repair un-reinforced brick walls during past seismic events or to retrofit existing walls by injecting expansive epoxy in the walls. They conducted a series of out-of-plane brick wall tests. They observed form the experiments that using expansive epoxy increased the bond strength among the bricks hence the out-of-plane strength of the walls increased 20%.

Griffith et al. [14] performed eighteen static and dynamic experiments on unreinforced brick masonry walls subject to out-of-plane load. The test program comprised of static, free vibration and dynamic tests using harmonic support, impulse support, and earthquake support motion. They detected that displacement rather than acceleration determined whether unreinforced wall would collapse under internal (seismic) loading.

Rodriguez et al. [15] conducted four post-tensioned masonry wall specimens which were constructed using hollow concrete blocks. During the construction, a-high-strength reinforcing bar was put in the center of the section of the wall (**Figure 1.1**(a)). After 28 days later from the construction of the wall, the post-tensioning

load was applied on the wall by tightening the nut on the treaded steel bars. The post-tensioned load was monitored with load cell located between the steel plate and nut to control the determined level of post-tensioning load. Then, the walls were subjected to out-of-plane load in order to evaluate the effects of the level of the post-tensioned forces, the size of the post-tensioned bars, the reinforcement ratio ρ, and the fixity of the post-tensioned bars inside the cell on the wall behavior. The specimens were tested horizontally using simply supported conditions and applying two concentrated line loads to obtain maximum constant moment in the middle part of the walls (Figure 1.1(b)). Three noteworthy results were obtained from the experiments. Firstly, large deflections were measured in the middle part of the post-tensioned walls before failing. Secondly, the level of applied post-tensioning load on the walls affected the crack pattern distributions on the walls. Lastly, the post-tensioning technique proved to increase both the cracking and ultimate loads of the walls segments. In addition, they also stated that it was efficient and easy to apply this post-tensioning technique on masonry walls.

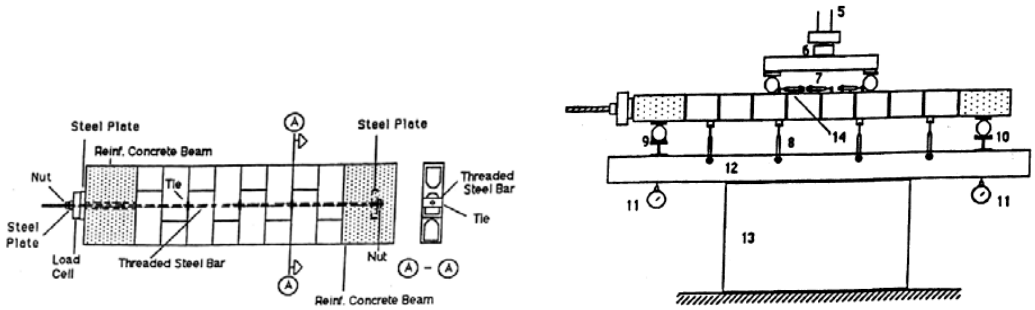

(a) (b)

Figure 1.1 (a) Test Specimen (b) Test Set-up

Laursen and Ingham [16] presented the results of pseudostatic simulated seismic tests on two unbonded post-tensioned concrete masonry (PCM) cantilever walls subjected to in-plane loading. The 67% scale wall models were constructed to represent 4 to 5 story office or apartment building. The results obtained form the experiments indicated that PCM walls withstood after severe cycling simulated earthquake loading was imposed. The ductile response of the walls increased 1.5% but relatively little energy dissipation explored during cycling of the walls.

Abdel-Halim and Bakarat [17] investigated the seismic performance of six 1/3-scale (single story) concrete backed stone masonry walls, subject to cyclic in-plane loading. Three of these samples constructed using an old construction practice and the others were constructed using a new construction practice. In the old construction practice, concrete in the columns and walls are cast simultaneously. On the other hand, in the new method, firstly the columns are cast then walls were built and concrete is cast behind the walls. In this study, the influence of the type of construction, applied vertical loads, and existence of dowels between the infill concrete panel and the base on the lateral resistance, ductility, energy dissipation, stiffness degradation, and failure mechanisms were explored. The experimental results pointed out that the construction type had no influence on the ultimate lateral load resistance of the walls. On the other hand, the lateral strength and stiffness of the walls increased with the increasing amount of applied vertical load on the walls. The existence of the dowels not only caused the diagonal cracks to be shifted upward far from the base of walls, but also gave a better distribution and smaller widths for these diagonal cracks. In the experiments, failures of all concrete-backed stone masonry walls were dominated by diagonal shear cracks.

Rosenboom and Kowalsky [18] presented the results of five large scale clay brick walls post-tensioned with a target force of 1000 kN using steel bars. These walls were subject to in-plane simulated earthquake forces. The main objective of the study was to investigate five basic configurations and determine through the one which had the most appropriate characteristic for seismic performance. In this study, the variables of the interests were bonded versus unbonded post-tensioning steel, confined versus unconfined masonry, grouted versus ungrouted masonry and application of supplemental mild steel. According to the conducted experiment results, the best performing configuration utilized unbonded post-tensioning and confinement of the wall. This wall had little residual deformation after the cycling loading.

Vecchio et al. [19] investigated two large-scale wide-flanged three dimensional walls subjected to reversed cyclic displacements, resulting in the web heavy displacement.

Then, the walls were repaired by removing and replacing the damaged concrete and then re-tested. The test results indicated that there were close to full restoration of strength, stiffness, and energy dissipation characteristics of the walls obtained. However, it was obtained form these tests that, repair scheme, strength of the repair concrete, and residual damage in the unrepaired zones could have a significant influence on subsequent behavior, especially amended the mode of failure.

1.1.3.Usage of Scrap Tires as Confinement Reinforcement

Prof. Dr. Murat Saatçioğlu at Ottawa University, Canada has made studies on the usage of scrap tires as confinement material on circular columns. The scrap tires are piled on the top of each other as vertical reinforcement bars passed through the holes opened at the side of the tires. The concrete which is cast inside the tires are confined by means of rim-rings and tread section of the tires. Successful results were obtained from the experiments but papers have not been published yet.

1.2.OBJECTIVES AND SCOPE

The main objective of this study was the development of a new strengthening technique by using scrap tires for poor masonry dwellers who could easily apply it on the walls of their masonry houses without any help from engineers. To achieve the main objective, additional objectives may be listed as follows:

- Develop simple connectors to form scrap tire chains (STC),
- Develop mechanism to apply post-tensioning force on STC using simple tools,
- Investigate the effect of STC post-tensioning on brick and briquette walls in out-of-plane bending direction using laboratory experiments,
- Investigate the application locations of STC for best performance,
- Investigate the level of post-tensioning for best performance,

- Investigate the ductility, damping, and energy dissipation capability improvements using STC,
- Investigate application of STC post-tensioning on full-scale masonry house (using tilting table tests),
- Obtain material capacities for commonly used hollow bricks and briquettes.

To achieve the objectives listed above; the scope of the study was finalized and is summarized below in bullet list format:

- Conduct direct tension tests on STR and STC using connectors
- Design connectors that are capable of transferring axial tensile forces between STRs and allow application of post-tensioning force by turning bolts.
- Conduct direct compression material tests on bricks, briquette, and mortar to obtain material capacities.
- Conduct six strip wall tests in out-of-plane bending direction to experimentally obtain strength, ductility, energy dissipation, damping changes between original (nominal) and strengthened walls using STC.
- Conduct tilting table tests to investigate strengthening effects on full size masonry laboratory house.

The results obtained from this study are believed to provide experimental and practical information on the use of the scrap tire as a strengthening material for masonry walls.

CHAPTER 2

MATERIALS

This section discusses the properties of the materials used in the post-tensioning process and in the construction of masonry walls.

2.1. TIRE

In this part, a brief explanation about the history of production of the tires and a terminology prepared for the tires are given.

2.1.1. History of Tires

Automotive tires are made of synthetic rubber which is obtained from petroleum. The development of the tires was based on improving the performance of natural rubber which is obtained from the liquid latex secreted by certain plants. In the beginning, natural rubber was used to produce waterproof fabrics and to make balls, containers and shoes by Pre-Colombian people in South and Central America. Until the 18^{th} century, Europeans did not make use of rubber except that they utilized it for manufacturing elastic bands and pencil erasers. Joseph Priestley, who is known to be the founder of the modern science of chemistry, called the material "rubber" due to its usage as an eraser [20].

During the 19th century, Charles Goodyear, a bankrupt hardware merchant from Philadelphia, devoted his life to make rubber more resistant to various chemical

elements. Firstly, he initiated his working by means of blending rubber with various dry powders, and aimed to find a way to boost the stickiness of natural rubbers. In 1839, he applied steam head to rubber under pressure for two days at 270 degrees Fahrenheit and he achieved in obtaining the best product [21].

Following the discovery of vulcanization, manufacturers began producing tires from solid rubber. These tires were strong, absorbed shocks and resisted cuts and abrasions. Even though this was a great progress, the tires were very heavy and did not allow for a smooth ride [22].

In order to decrease vibration and improve traction, Robert W. Thomson, a Scottish engineer, first produced the pneumatic rubber tire which consisted of rubber filled in with air. Unfortunately, the idea was not a commercial success since it was introduced too early for its time. In 1888, John Boyd Dunlop of Belfast, Ireland, who did not know about Thomson's earlier invention, introduced the pneumatic tire to the market once more. The timing was perfect and the pneumatic tire caught the public's attention because bicycles were becoming extremely popular and the lighter tire used at bicycles provided a much better ride [22].

After about half a century, manufacturers started producing vehicle tires comprising two parts, i.e., an inner part and an outer part. The inner part, called the inner tube, contained compressed air and the outer part was a casing protecting the inner tube and providing the tire with a better grip. An important element of the outer part were the layers called plies which were made of rubberized fabric cords embedded in the rubber and they strengthened the casing. They were known as bias-ply tires. The reason why they were named bias-ply tires was that the cords in a single ply spread diagonally from the beads on one inner rim to the beads on the other rim. The orientation of the cords is changed from ply to ply so that the cords crisscross each other [22].

The steel-belted radial tires were first produced in 1948 by Europeans. In those first tires, the ply cords radiate at a 90 degree angle from the wheel rims. Together with

this, a belt of steel fabric that wrapped the circumference of the tire reinforced its casing. Radial tire ply cords consist of nylon, rayon or polyester. The advantages of radial tires include longer tread life, better steering and less rolling resistance. However, radials have a harder riding quality, and are about twice as expensive as the non-radial tires. The production of steel-belted radial tires is illustrated in Figure 2.1 [23].

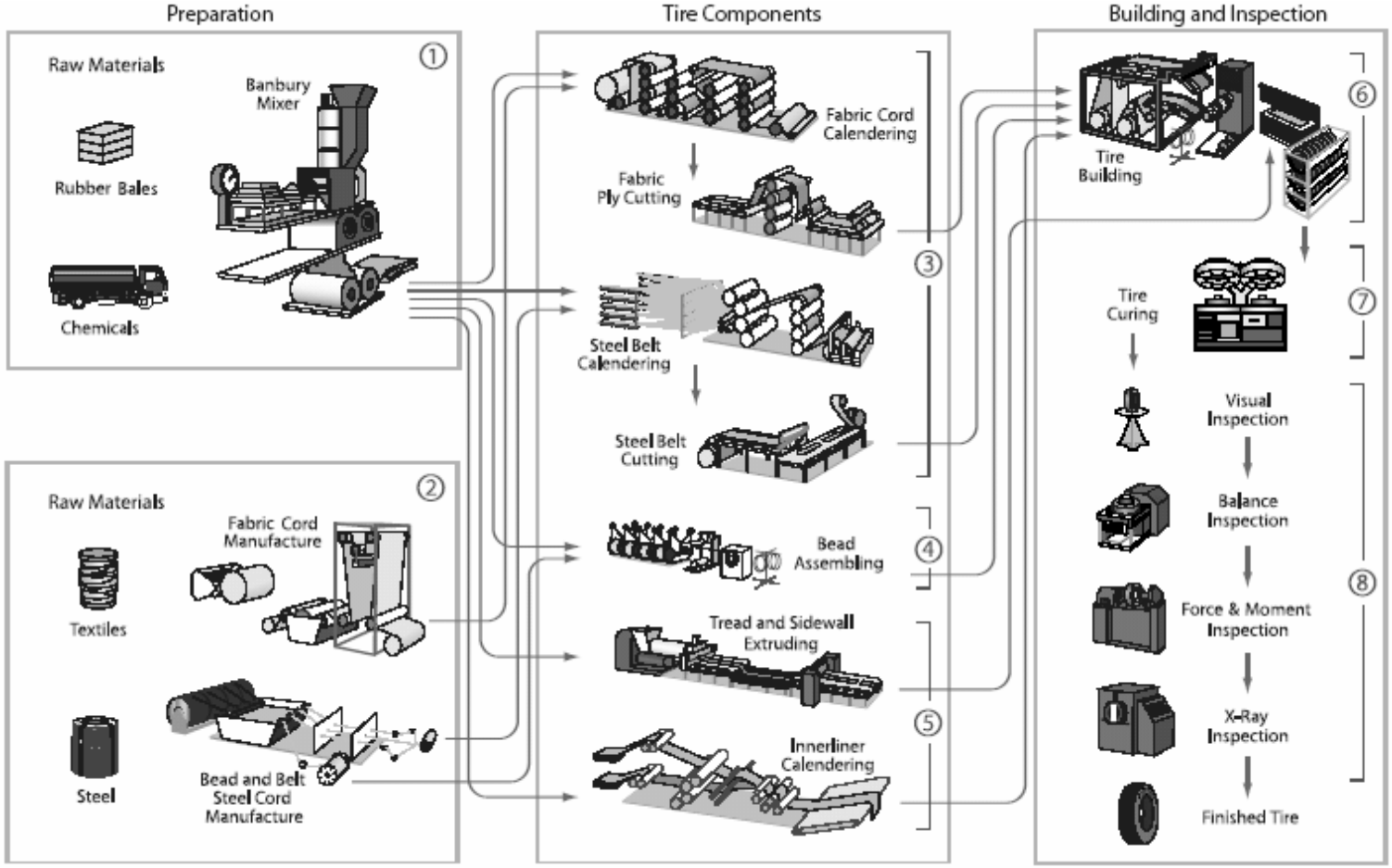

Figure 2.1 Tire production line [23]

2.1.2.Tire Terminology

The automobile tire components are illustrated in Figure 2.2. A tire is formed from four main parts which are the tread, shoulder, sidewall and bead. The steel wires are embedded in the tread and bead parts of tires, making these parts stronger than the other parts. Therefore, in this study, firstly, the tensile strength capacities of these parts were investigated. Secondly, the possibility of using these parts as post-tensioning materials for strengthening masonry walls was explored.

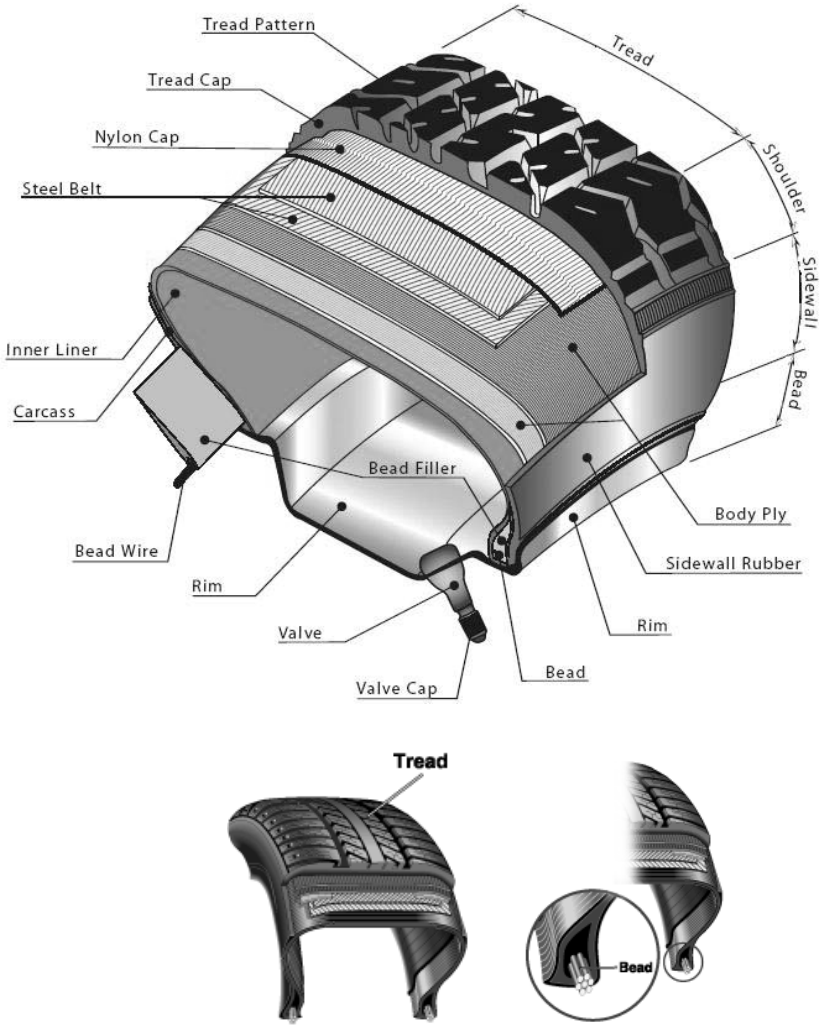

Figure 2.2 Components and sections of automobile tires [23 and [24]

The dimensions and properties of tires are marked on the sidewalls of tires (see Figure 2.3). The numbers, 175 / 70R-13, marked on the sidewalls, denote that tread read section is "175 mm" wide, the percentage of the section height to section width is "70 %" and the diameter of the rim is "13 inches (33 cm)" respectively. In addition, the number 82T gives information about pressure resistance and velocity characteristics of the tire.

Figure 2.3 Tire marking [24]

The terminology used in this study is summarised briefly below. The terms referring to different parts of a scrap tire were developed using the location of each segment (see Figure 2.2). Figure 2.4(a) shows the Scrap Tire Tread-ring (STR) which is the remaining, ring shaped, section of a tire when the sidewalls are cut off. This is the part of a tire that is in contact with the road surface. The sidewall (see Figure 2.4 (b)) is the narrow band, on either side of a tire, connecting rims to the STR. The rim-ring (see Figure 2.4 (c)) is the part of a tire where the wheel edges touch the tire. The rim-ring section has loops of circular continuous steel wires, called bead, which are concentrated at the rim area. The preparation of a scrap tire ring and two rim-rings from a scrap tire is illustrated in Figure 2.5.

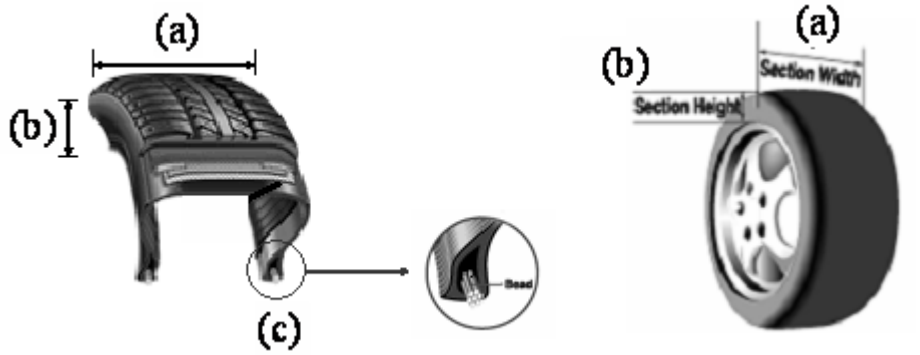

Figure 2.4 Terminology [25]

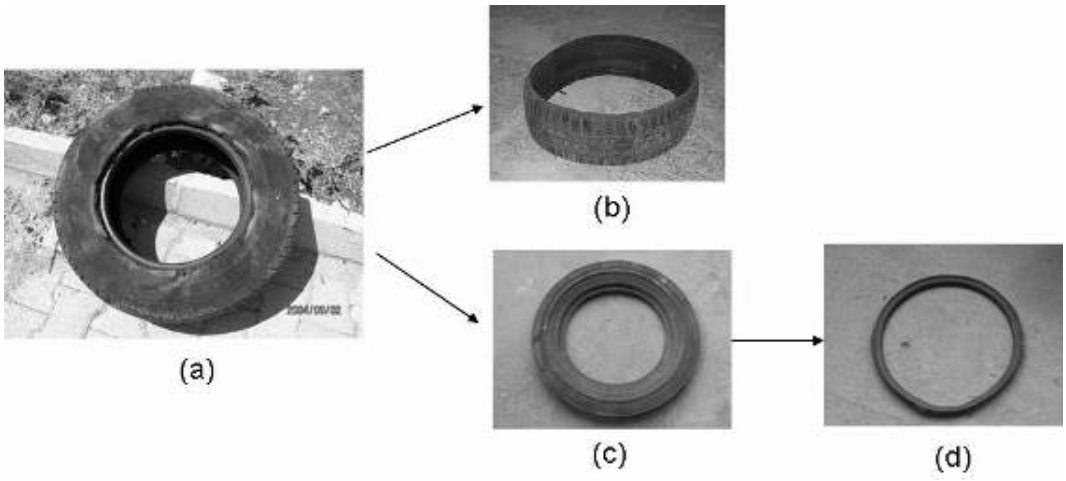

Figure 2.5 Preparation of post-tensioning materials: (a) scrap tire, (b) STR, (c) side wall, (d) rim-ring

2.1.3.Scrap Tire Selection Criteria

Scrap tire that will be used in wall strengthening should be selected based on the following criteria. Scrap tire should be:

- in good apparent quality,
- without major wear and tear,
- no big holes, cracks,
- no significant deterioration.

The long term performance, behavior and strength of tire rings (STRs) are also affected by the net cross-sectional area. Therefore, it is not recommended to use STRs which have with smaller than 185mm.

2.2.BRICK

The width, length, and height of the bricks used in the tested walls were 18.5cm, 29cm and 13.5cm respectively (See Figure 2.6). The void ratio of the bricks was measured as 60% of the total brick area (18.5cm x 29cm). The average axial load

capacity of three-bricks was measured as 431 kN, which was about 8 MPa for the full area including the voids. The average compressive strength of the tested bricks was about half the value given in TC705 [26]. However, the bricks used in this study were the ones commercially available on the Turkish market and are the most commonly used bricks in the construction of masonry houses in the country. The weight of the bricks referred to in TC705 [26] is about twice the weight of the bricks used in the test with exactly the same dimensions. Therefore, the void ratio was half of the ratio for the standard bricks and the material strength was almost equal to the ones referred to in TC705 [26].

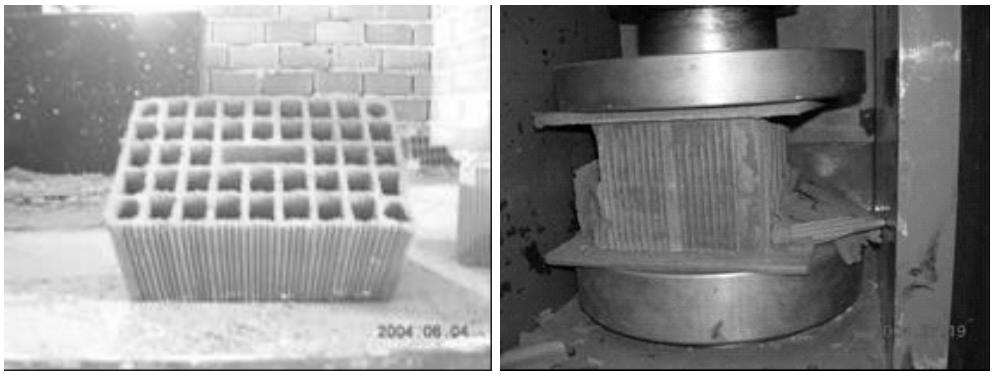

Figure 2.6 Bricks are used in the wall tests and compression test.

2.3.BRIQUETTE

Unlike bricks, briquettes are not commonly used in the construction of masonry houses in Turkey, but they are mostly preferred in secondary construction types such as stables, huts etc. The briquettes used in this study were the type that is commercially available on the market (see Figure 2.7) with width, length, and height dimensions of 40 cm x 20 cm x 40 cm respectively. The void ratio was measured as 60% of the total cross-section area. The compression strength tests, conducted on three briquettes, showed that their average axial compression capacity was 50 kN (or 1.46 MPa) for the full area including voids.

Figure 2.7 Briquette compression test

2.4.MORTAR

The mortar used between the bricks was prepared with 1:1:1½:7 weight ratio mixtures of cement, lime, water and sand respectively, which is the common practice in masonry constructions in Turkey. The average 28 day strength of the mortar samples tested using 7.5cm x 15cm standard cylindrical samples was found to be 3.6 MPa. The obtained strength was also similar to the average mortar strength in common practice.

CHAPTER 3

EXPERIMENTAL PROGRAM

The tests conducted in this thesis consist of two parts which are out-of-plane masonry strip wall tests, and two full scale masonry house tests.

3.1.TENSILE STRENGTH CAPACITY OF SCRAP TIRE PARTS

In this part of the study, the tensile strength capacity of the scrap tire and how the scrap tire would used as a post-tensioning material for masonry walls were investigated and they are briefly explained.

3.1.1. Preliminary Tests

The initial attempt of testing scrap tire parts was conducted by cutting STR in transverse direction and directly pulling it apart using a universal testing machine in the Construction Material Laboratory of the Department of Civil Engineering at Middle East Technical University (METU). The scrap tire band was clamped to the testing machine at each end using two-plated connectors with three bolts (see Figure 3.1 (a)). A premature failure occurred at about 35 kN, which was much lower than the expected tensile strength of scrap tire. This failure occurred due to tearing and slipping of bolts of the scrap tire band (see Figure 3.1 (b)). Additional tension tests, with and without connectors, remained unsuccessful since the bolts continued to tear the tire and slipping occurred between the clamps of the machine. These results showed that tire bands cannot be successfully connected to each other using clamps and bolts. Therefore, it was decided to keep the ring shape of tires unchanged, i.e., in the form of a scrap tire thread-ring (STR) (Figure 2.5(b)).

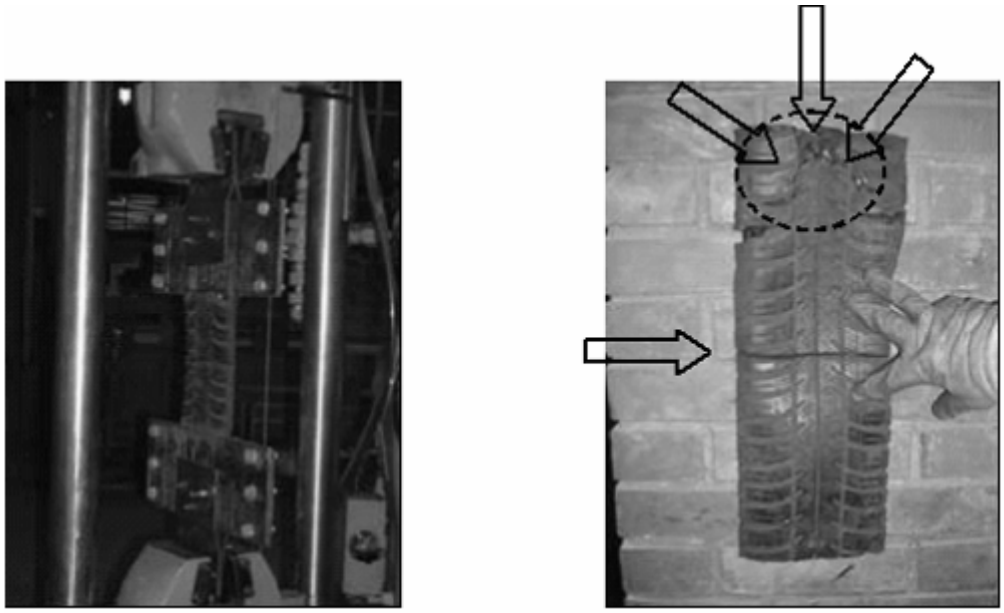

(a) (b)

Figure 3.1 Preliminary test: (a) pull machine, (b) premature connection failure

3.1.2.Test Set-up and Instrumentation

In order to measure the tensile load capacities of STRs and rim-rings, and to design connectors, a test setup with a capacity of 300 kN was designed and constructed in the Structural Laboratory of the Department of Civil Engineering at METU (see Figure 3.2 (a)). The test can be conducted on a single ring or on a chain of connected rings using adaptable test setup (see Figure 3.2 (b)).

One 200mm stroke displacement transducer (LVDT) and a 300 kN load cell were used to measure deformations and axial stretching load applied on the STRs, rim rings and connectors. The load was applied by an adjustable-speed hydraulic pump. A 16-channel data acquisition system was used to synchronously read data from the transducers at 5 samples per second (5 Hz).

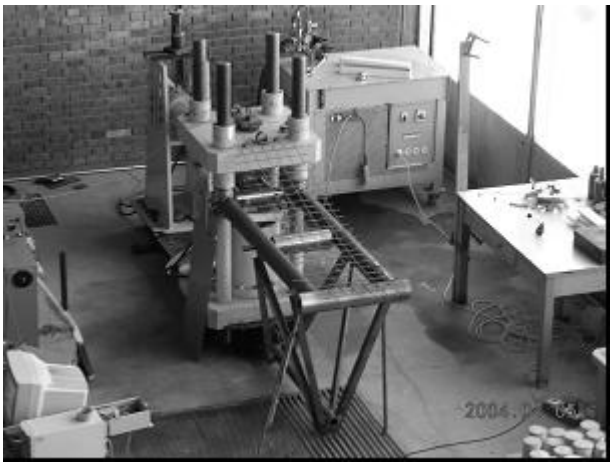

(a)

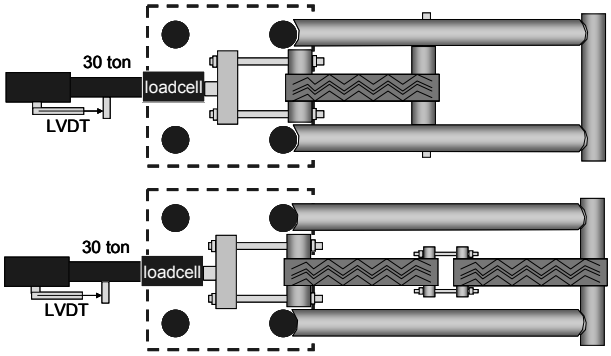

(b)

Figure 3.2. Test setup: (a) testing machine general view,
(b) testing machine schematic view

3.1.3.Experiments and Results

Four different tensile strength tests on the parts of scrap tire (i.e., STR and rim-rings) were conducted and the results obtained from these tests are summarized briefly in the following parts.

3.1.3.1. Scrap Tire Tread Ring (STR) Tests

Forty-three single-STRs which belong to nine different commonly available and mostly used trademarks in Turkey were tested for direct tension (see Figure 3.3). The mean and standard deviation of ultimate tensile load capacities of STRs were found to be 132.6 kN and 27.72 kN, respectively As well as, the minimum and the maximum tensile strengths for the tested specimens were measured to be about 90 kN and 190 kN, respectively (see Figure 3.4).

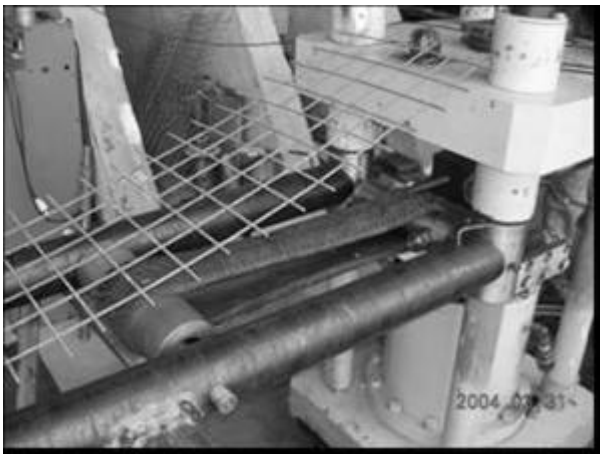

Figure 3.3 Single-STR test

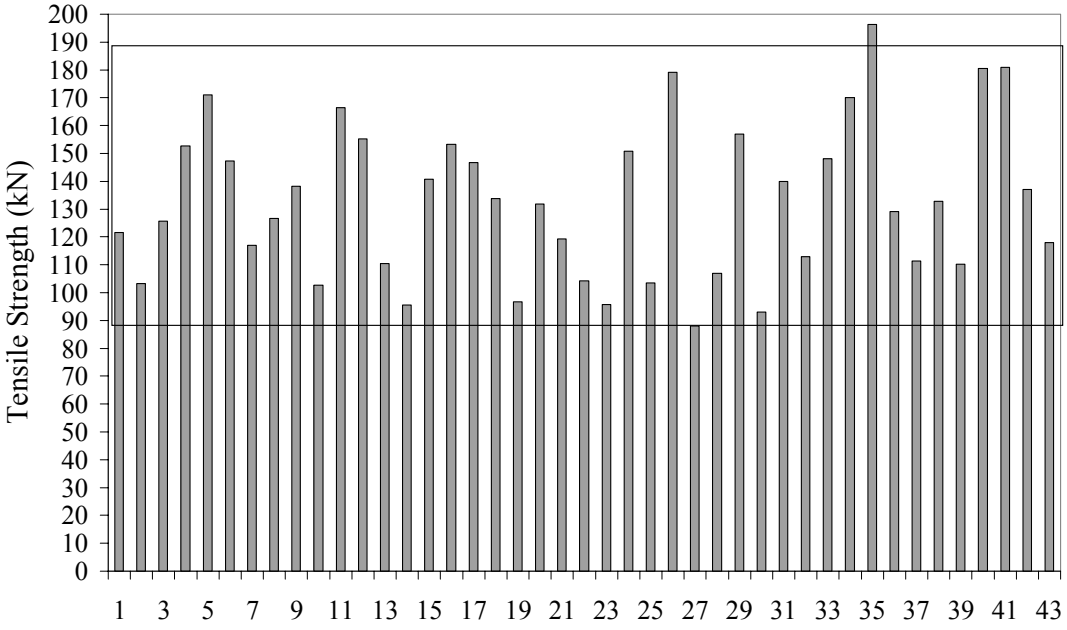

Figure 3.4 Ultimate tensile strength capacity distribution of STRs

STR specimens are tested in direct tension up to failure **(**Figure 3.5). Seventeen STR specimens were tested in April and May 2004 (see Figure 3.6(a)) and twenty-six specimens after being outside about one year were conducted in May and June 2005 (see Figure 3.6(b)). Visual investigation on scrap tires that are exposed to direct sunlight for extended periods of time show that sunlight has unfavourable damaging effects on the rubber of scrap tires

Figure 3.5 Failure of STRs

Although the STRs have steel mesh reinforcement inside them, the overall shape of the curves resembled the behaviour of rubber material. Bi-directional layout of the steel mesh probably affected the load resistance of STRs, and larger resistance is obtained as the reinforcing steel mesh lines up with the direction of load application. This behaviour is somewhat verified since the cross-section of each STR starts to shrink (see Figure 3.3) and fails suddenly as the load is further increased. The sudden failure of STR resembles snapping of rubber band or tensile failure of high strength brittle steel. High strength steel wire mesh is used in tires which also support the failure mechanism observations (Figure 3.5**).**

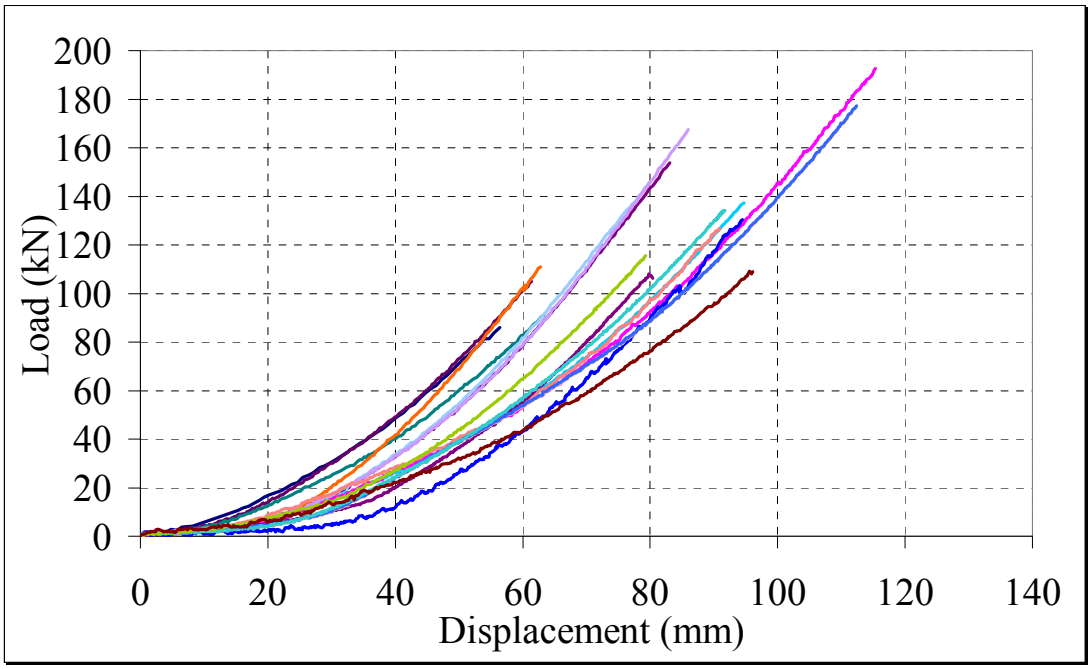

(a)

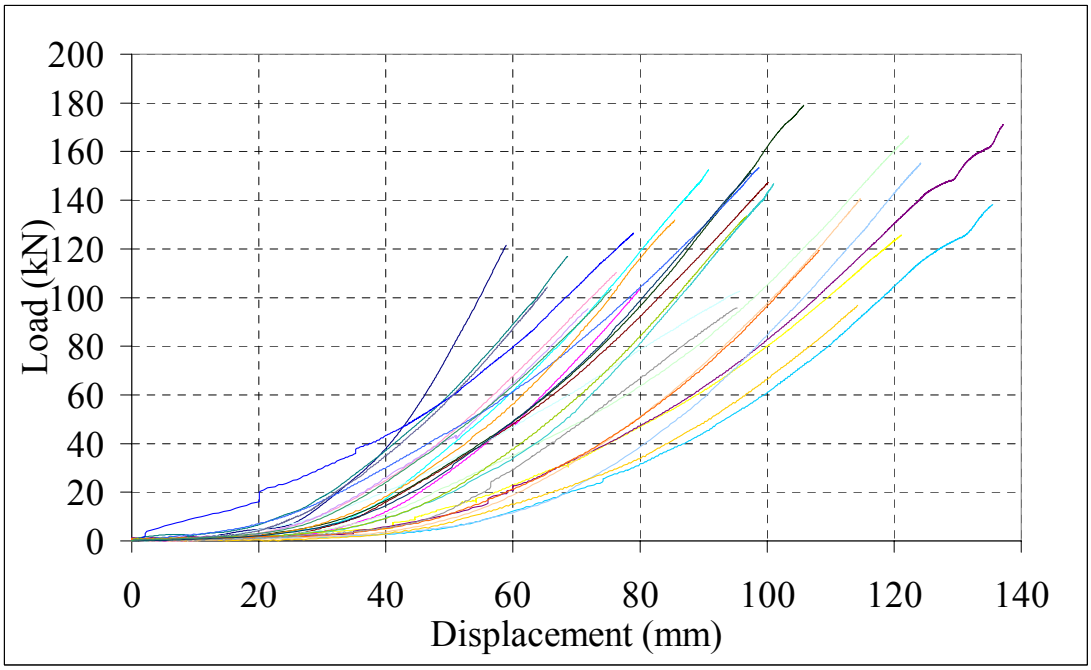

(b)

Figure 3.6 Tensile load vs. displacement of STRs

Performed tests showed that there are five major factors affecting the tensile load capacities of STRs:

- The amount of steel wire mesh used inside STRs changes with respect to the tire brand. STRs exhibit greater tensile load capacity when the amount of steel wire used in the cross-section is high.
- The thickness of the rubber layer in scrap tires also changes between the brands and the amount of usage or the level of wearing. The tensile load capacities observed during the tests were significantly affected by the thickness of the STRs. This observation shows that the tensile load is shared between the rubber and steel mesh layers.
- Some tires have wider section width resulting in a larger cross sectional area. Consequently, the tensile load capacity increases as the width of the tire increases.
- The softness of scrap tires rubber also affects their tensile load capacity. STRs manufactured using hard rubbers have higher tensile load capacity compared to softer rubber tires.
- Time-dependent deterioration (aging) of scrap tires also plays an important role in determining the tensile load capacity. If the deterioration of the tire is extensive (e.g., extensive sun exposure, existence of large holes, cracks, and apparent poor quality), the tensile load capacity is significantly reduced.

3.1.3.2.Connector Tests for STR Chains

A single STR is not sufficient for post-tensioning as it is not long enough to wrap the whole wall. Therefore, a chain of STRs has to be created using connectors between two successive STRs.

First, Φ18 St420 re-bars welded together in a rectangular shape were used to connect two consecutive STRs (see Figure 3.7 (a)). During the test, however, the bars have bent and tore the STRs cutting like a knife. When the tensile load reach about 31 kN

(see Figure 3.8, ct-1), the bending of the re-bars caused stress concentration on their edges and initiated the cutting process. In addition to this, the small diameters of the bars caused additional stress concentration along the width of the STRs. Larger diameter bars or pipes should be used in order to reduce stress concentration on tires as well as prevent bending of the connector.

In the second attempt, ϕ34 St37 water pipes were used in the connector to increase the section moment of inertia as well as to provide a larger bearing surface to reduce stress concentration on STR. The pipes were welded to each other using steel re-bars. The connection failed close to the welding on the re-bar (see Figure 3.7(b)) under about 38.5 kN of tensile load (see Figure 3.8, ct-2). The performance of the welded connection was considered poor and it was decided to use a bolted connection in the following test.

The remaining three connectors were composed of larger diameter pipes with holes on either side for passing and tightening bolts. The connector utilised in the third attempt was constructed using a pair of St37 steel pipes with dimensions of 78mm x 4mm x 380mm for diameter, thickness, and length, respectively. This connector also failed the test but its capacity was measured as 82 kN, which was twice as much as the capacity of the connectors tested in the previous experiments (see Figure 3.8 ct-3). The connector failed where the bolts punched the pipes (see Figure 3.7 (c)). As the diameter of the pipe increases, the section becomes more vulnerable to punching.

The penultimate connector design test was carried out using 72mm diameter pipes with 4mm pipe thicknesses, which has a smaller pipe diameter. Washers were used in addition to better distribute the bolt forces to prevent punching failure. The maximum tensile load was measured to be 82 kN when the STRs broke off suddenly (see Figure 3.8, ct-4). The connector design was somewhat successful since the failure was governed by the STR. On the other hand, although washers were used to reduce the stress concentration around the pipe holes and enlarge the load-bearing area, the pipe have shown indications of bearing failure around the holes of the 72mm diameter pipe (Figure 3.7(d)).

(a) ct-1

(b) ct-2

(c) ct-3

(d) ct-4

(e) ct-5

Figure 3.7 Types of connectors tested for STR

In the last connector test, the pipe diameter was further reduced to 49 mm in order to prevent bearing and punching failure (Figure 3.7(e)). The connector remained elastic and successfully transferred STR tensile forces. The hole diameters were also reduced by using smaller bolts (in an attempt to optimize the cost) and double washers were used at each bolt location. The 49 mm diameter pipe connector did not govern the STC capacity. One of the STRs have failed at about 88 kN axial force, as desired and expected (see Figure 3.8, ct-5).

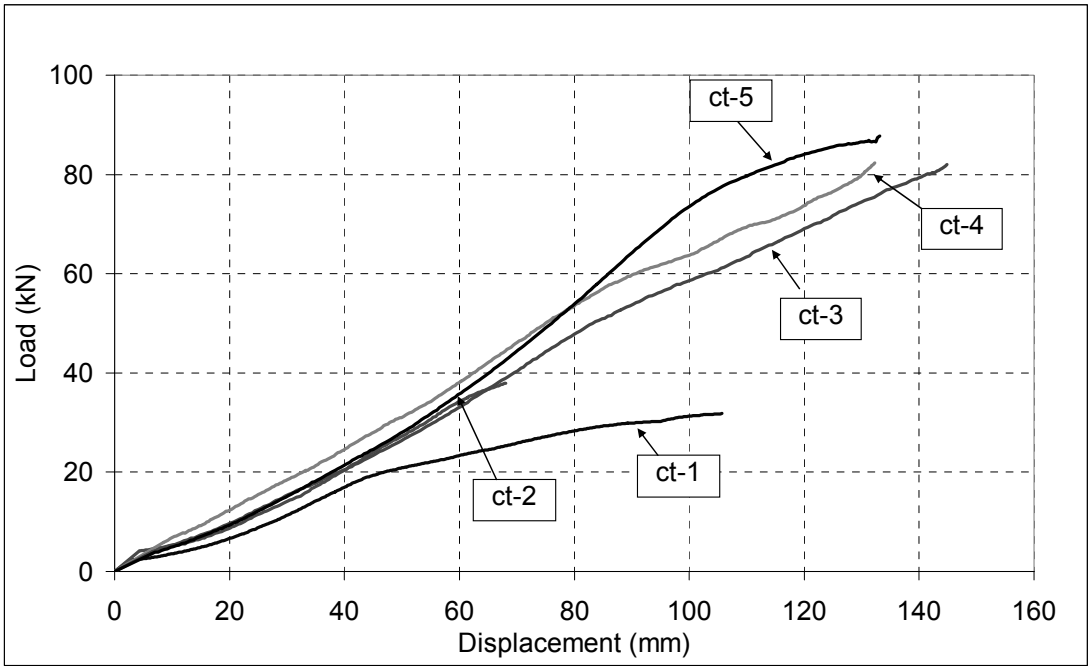

Figure 3.8 Tensile Load vs. Displacement of CA Design Tests

A simple yet effective connector was designed and proof tested. Since the target population of the work is defined as low income group people living in masonry houses, maximum cost reduction was crucial. Therefore, the connection design was one of the most challenging tasks. Simplicity of the connector is another important characteristic. The connector shown in Figure3.9 is simple, more efficient, and cheaper than the initial connector shown in Figure 3.1(a). The details of five different connector types, tested in this study, are summarized in Table 3.1

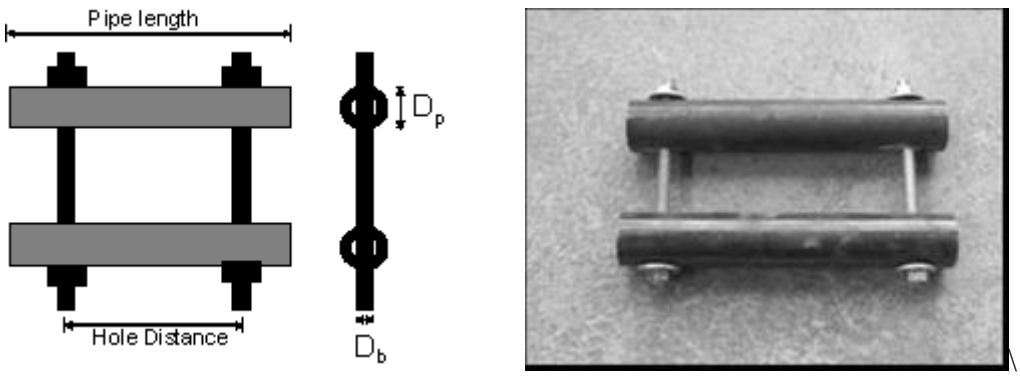

Figure3.9 Connection Apparatus

Table 3.1 Details about the connection apparatuses

Test Number	Pipe or Bar Diameter (mm)	Pipe Thickness (mm)	Pipe Length (mm)	Hole Distance (mm)	Bolt Diameter (mm)	Type of Connection
1	18(St42)	-	205	-	18 (S420)	Welded
2	34(St37)	4	220	-	16(S420)	Welded
3	78(St37)	4	380	250	16 (6.8)	Bolted
4	72(St37)	4	330	250	16 (6.8)	Bolted
5	49(St37)	4	330	250	12 (6.8)	Bolted

3.1.3.3.Rim-ring Tests

Rim-rings (also called as beads) have many layers of continuous wire hoops (Figure 3.10) and are located on either side of the tires at the rim section. In order to investigate the tensile load capacities of rim-rings, nine single rim-ring direct tension tests were conducted. The mean and standard deviation of ultimate tensile load capacities of nine rim-rigs were found to be 53.5 kN and 10.9 kN, respectively. The load-deflection graphs are shown in Figure 3.11. Steel wires found in rim-rings are more densely placed compared to the STRs (Figure 3.10). The load-deflection curves for rim-rings (Figure 3.11) show similarities to tensile load behavior of high-strength steel material.

Figure 3.10 Steel wires distribution in rim-rings compared to STR [25]

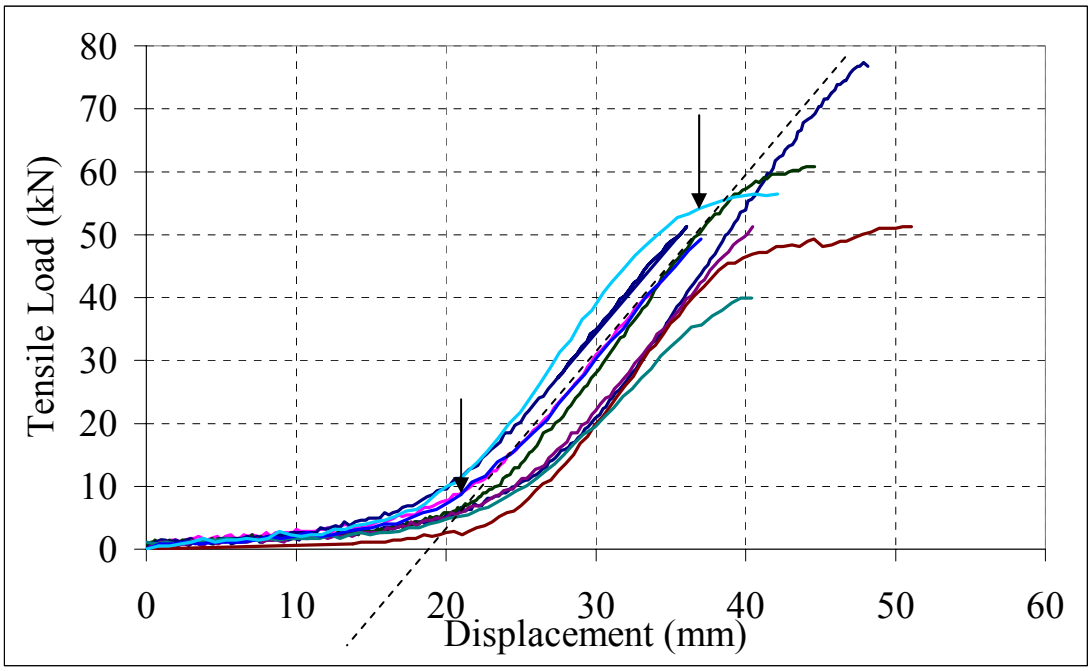

Figure 3.11 Tensile Load vs. Displacement of Rim-rings

The initial low stiffness loading plateau is the part where circular shape of the rim-ring is straightened out and rubber material between the steel cords and tension application apparatus is squeezed tight. The high-stiffness curve observed between 20mm and 40mm deformation in Figure 3.11 is the part where steel rings take the axial tensile load. The approximate total length of a 14 inch rim ring is 112 cm. A total linear deformation of about 1.5 cm (over ring length of 56 cm) refers to about 2.6% strain (26 800με). The tensile load capacity of 53.5 kN (2130 MPa) relates to a ultra-high strength steel level (considering the example shown in Figure 3.10 with a total number of 2 x 16 rim-ring wires of ϕ1 mm diameter located on either side of the ring for a total area of 32 mm^2). The High-Alloy Hardenable Steels and Martensitic Stainless Steels have yielding capacities of 1240 MPa and 1750 MPa, respectively [27]. Ultra-high strength steel types may have ultimate strength as high as 3500 MPa [28, [29]. Although exact steel type used in rim-rings is not known, based on the low-ductility (about 2.6%) and ultra-high strength (about 2130 MPa), the rim-ring wires are expected to be one of the two types mentioned above or their similar equivalents. The tensile capacity of the rim-rings is affected by the brand name; however, the level of deterioration is not expected to have a great influence on the

rim-ring capacity unless the rubber layer is heavily damaged and the steel wires are corroded due to exposure to atmospheric conditions.

3.1.3.4.Connected Rim-ring Tests

Similarly to STRs, A chain of rim-rings can be used to apply post-tensioning. The connection between the rim-rings should be capable of transferring the axial load to the next rim-ring. Furthermore, the connector should be thick enough not to damage the rim-ring and therefore prevent a premature failure. Five connection design tests were conducted in order to achieve adequate strength in rim-ring connections. The first two attempts to bond two rim-rings were made by passing rim-rings inside of each other to form a knot (Figure 3.13 (a), (b)). Excessive bending and stress concentrations at the knot joints caused premature failure of the connections at about 20kN (see Figure 3.12, ct-1) as cracking and snapping sounds were heard. The single rim-ring tension tests revealed much higher capacities, 53 kN on average.

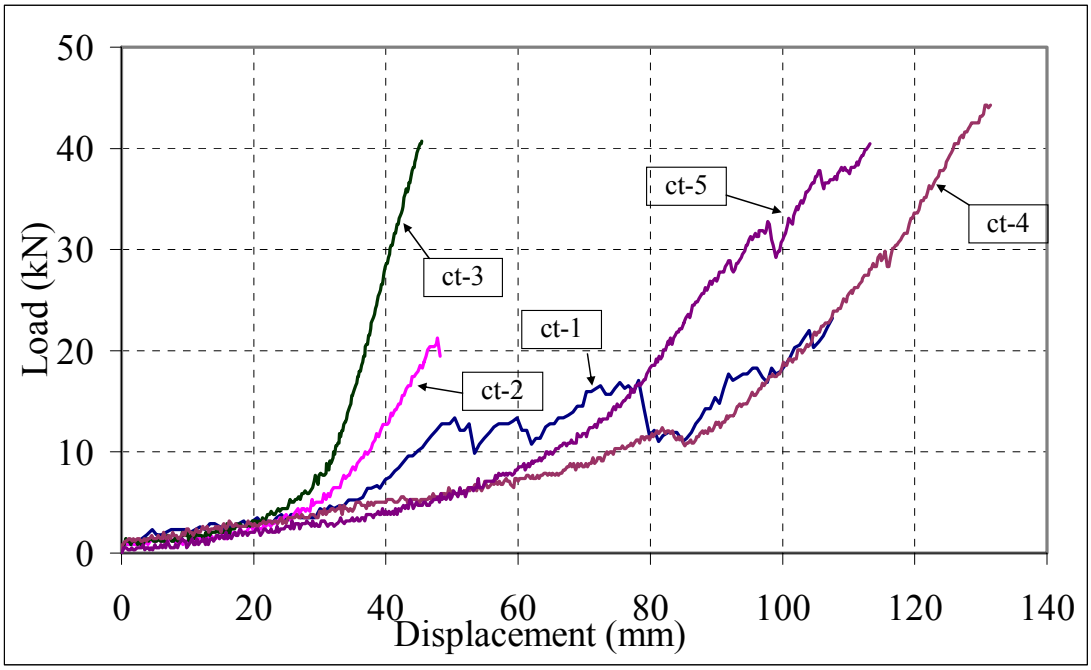

Figure 3.12 Tensile Load vs. Displacement of Connected Rim-ring

In the third and fourth tests, a steel pipe piece and cylindrical wooden log and were passed through the knot region in order to reduce the stress concentration in the knot zone (Figure 3.13 (c), (d), respectively). Consequently, the ultimate strength capacity exceeded 40 kN doubling the capacity of knot connection (Table 3.2). Similarly to the 3rd and 4th trials, an additional 5th trial using a U-shaped steel bolt (Figure 3.13 (e)) was conducted. All of the last three tests (using wooden log, steel pipe, and U-connector) yielded high tensile strengths getting close to about 80% of single rim-ring capacities; however, the use of U-shape steel bolt is more expensive. When the load-deflection curves of the five tests are examined (Figure 3.12, ct-5), the third test with the steel pipe connector (Figure 3.13 (c)) was found to be the best option from the capacity and behaviour points of view. When the knot is directly used without any cushion, the strength is drastically reduced. Usage of a wooden log increases the amount of deformation prior to failure. The pipe piece placed at the eye of the knot has higher stiffness, clean response, and high capacity compared to other connectors. Steel pipe insertion is also a simple and low cost technique compared to U-shape bolt connection.

Table 3.2 Details about connection properties of rim-ring

Test Number	Bond Type	Diameter (cm)	Length (cm)	Ultimate Strength (kN)
1	knot	-	-	23.5
2	knot	-	-	21.3
3	pipe	4	10	40.7
4	Cylindrical wood	8.5	10	44.3
5	Steel U-bolt	-	-	40.5

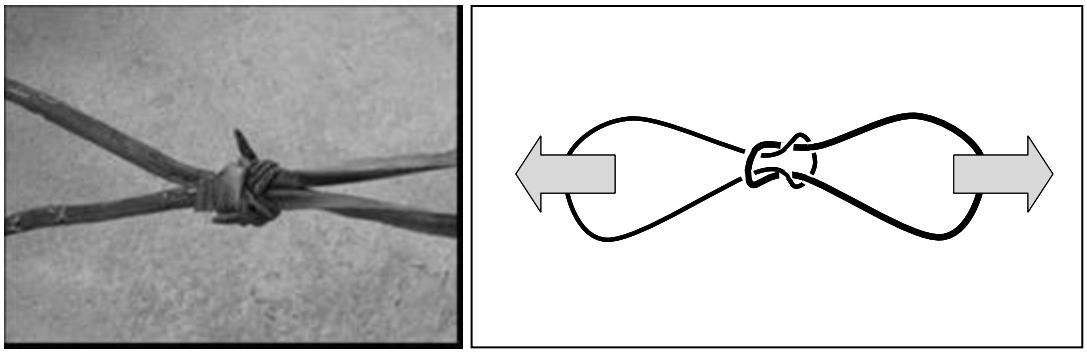

(a) Knot (ct-1) (b) Knot (ct-2)

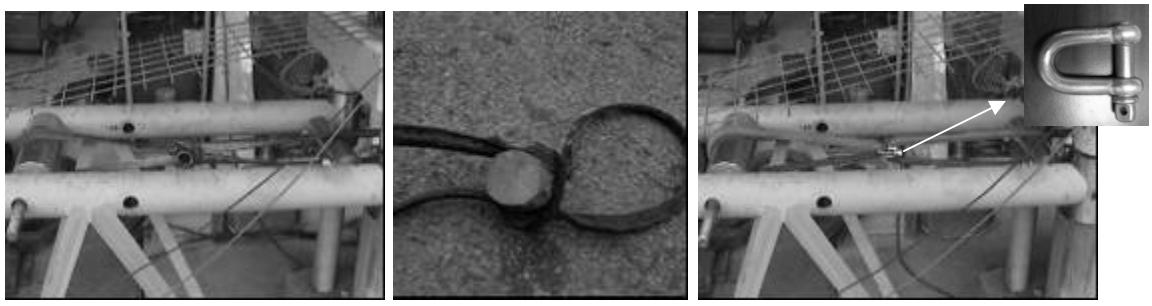

(c) Pipe (ct-3) (d) Wood (ct-4) (e) U-bolt (ct-5)

Figure 3.13 Connection types of Rim-rings

3.2. OUT-OF-PLANE TESTS OF POST-TENSIONED MASONRY WALLS USING SCRAP TIRES

The tensile load-deflection characteristics of scrap tire rings were discussed in detail in the previous part. The axial load capacity of the scrap tire rings (at a range of 90 kN to 190 kN, mean value 132.6 kN, standard deviation 27.72 kN) and elastic behaviour associated with scrap tire rings in tension seems adequate for structural retrofit studies of masonry walls.

There were fifteen out-of-plane tests conducted on six different strip walls (four brick- and two briquette-walls) (Table 3.3). Two of the brick-walls and one of the briquette-walls were strengthened with STR chains, and the other walls were strengthened with the hybrid system (see 3.2.2 on page 37 for definition). All walls were placed vertically (see Figure 3.14(a)) in order to determine the nominal

(without post-tensioning) out-of-plane bending capacity. Similar studies conducted on horizontally placed masonry strip walls (see Figure 3.14(b)) could not measure the nominal strength of the wall due to the loading caused by its own weight [15]. The nominal strength of the wall is insufficient to carry its own weight when placed horizontally. Furthermore, testing of the vertically-placed wall strip may better simulate the actual effects of construction direction and self-weight contribution in vertical direction. Another advantage of placing the wall in vertical direction is the ability to apply cyclic loading while eliminating any uniaxial superposition of the self-weight and the applied load especially in the nonlinear range where they become inseparable.

Table 3.3 Description about out-of-plane tests

		Post-Tensioning Load					
		0 kN	50 kN	100 kN	0 kN	30 kN	50 kN
Test Description	Brick Wall Test #1 (STC)	✓	✓	✓			
	Brick Wall Test #2 (STC)	✓	✓	✓			
	Brick Wall Test #3 (Hybrid)			✓			
	Brick Wall Test #4 (Hybrid)	✓	✓	✓			
	Briquette Wall Test #1 (STC)				✓	✓	
	Briquette Wall Test #2 (Hybrid)				✓	✓	✓

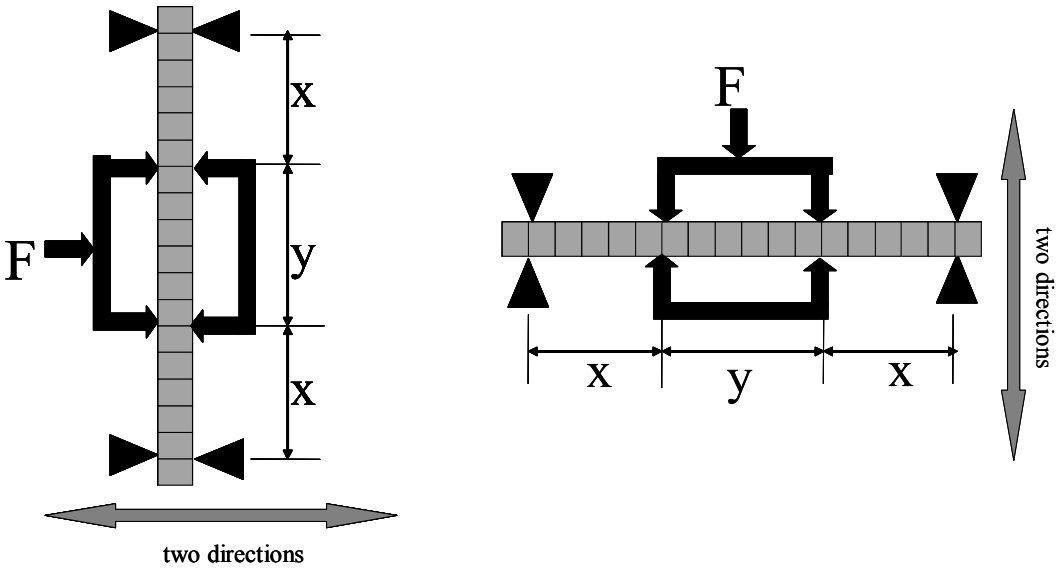

(a) (b)

Figure 3.14 Placing of the wall in (a) vertical and (b) horizontal orientations

3.2.1.Test Specimens

Six masonry wall strips (four brick and two briquette wall strips) were constructed by an experienced mason in the Structural Laboratory of Civil Engineering Department at METU. The width of each brick wall strip was equal to the length of three bricks (885 mm in total including approximately 7.5 mm of mortar thickness between the bricks). The thickness of the walls was 185 mm, and the distance between the supports was 2500 mm. The height of the wall was 2600 mm comprising of 18 brick layers including 10 mm-thick mortar layers (see Figure 3.15). The distance between the middle load application points (Y) was 800 mm leaving about 850 mm of distance (X) to the outer supports (see Figure 3.14 (a)). On the other hand, each briquette wall had length of 2.5 briquettes length (about 1000 mm including mortar), 200 mm thickness, and a distance of 2400 mm between the supports. A total of 12 briquettes layer were used in the vertical direction with about 10 mm mortar thickness in between equaling in total height of 2500 mm. The distance between middle load application points (Y) was 800 mm leaving 800 mm of distance (X) to the outermost supports.

Figure 3.15 Brick wall

3.2.2.Application of Post-Tensioning Load

The post tensioning load is applied through the opened holes at the bottom of strip walls. 1.5 bricks and 1 briquette from the bottom end of the brick and briquette walls respectively were carefully removed using a chisel and hammer. A 400 mm long half-cylindrical (ϕ20 cm) wooden log was placed in the bottom opening of each wall except in the first brick wall where mortar with stone pieces was used instead of a wooden log (this practice has been abandoned for the next five tests since the stone caused crushing of the bricks at the interface). The wooden log was adhered to the strip wall by cement paste so that it can uniformly distribute the applied post-tensioning force from the STR to the wall. At the top edge of the wall, a load cell was placed to measure axial load applied by the STC. For stability purposes a 760 mm long UNP-160 section was used to distribute the post-tensioning load from the load-cell, located between the STR and wall.

The applications of the post-tensioning load on both brick and briquette walls by STR chains (STC) and hybrid system were conducted as follow:
STC: Two STRs were placed on the either side of the wall and connected to each other by six connectors. Then, they were stretched using a wrench until the pre-determined tension value was reached (see Figure 3.16(a)).

Hybrid System: In the hybrid system the STRs on the either side of the wall were replaced by pairs of 1500 mm long Φ12 steel bars welded to 20 mm long ϕ16 bolts. The bolts were then passed through the holes of the steel pipes and stretched by turning the nuts until the pre-determined load was reached (see Figure 3.16(b)).

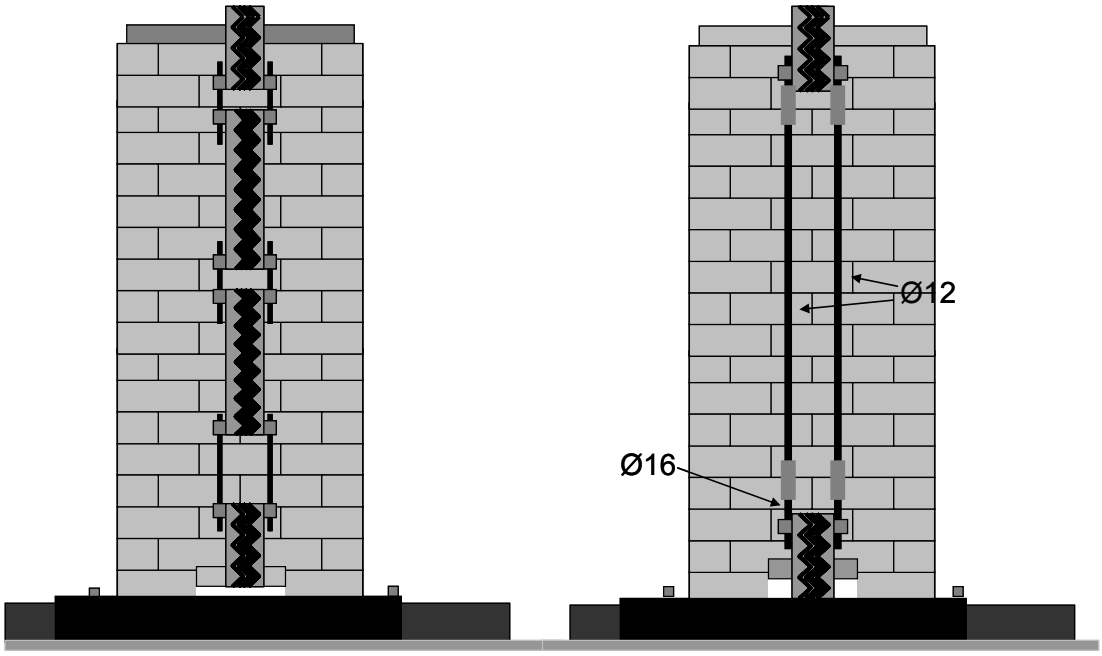

Figure 3.16 Application of post tensioning by (a) STR Chains and (b) Hybrid System

3.2.3.Theory of Post-Tensioning Load Application

The effects of post-tensioning load on masonry are theoretically explained in Figure 3.17. The applied post-tensioned load on the out-of-plane walls in vertical direction increases the bending moment capacity of the wall as shown in Figure 3.17. The initial tensile strength capacity of the wall is demonstrated as $\sigma_{t.}$ and the compression stress on the wall caused by bending is σ_c. When the post-tensioning force is applied on the wall the compression stress increases by σ_w and the tension stress reduces by σ_w. Thus, the tensile stress capacity of wall under the bending moment in the out-of-plane direction increases from σ_t to $\sigma_t + \sigma_w$ akin to in Figure 3.17; however, the compressive stress (σ_w) applied by post tensioning combined with the bending related compressive stress (σ_c) should not exceed total compressive strength of the building material.

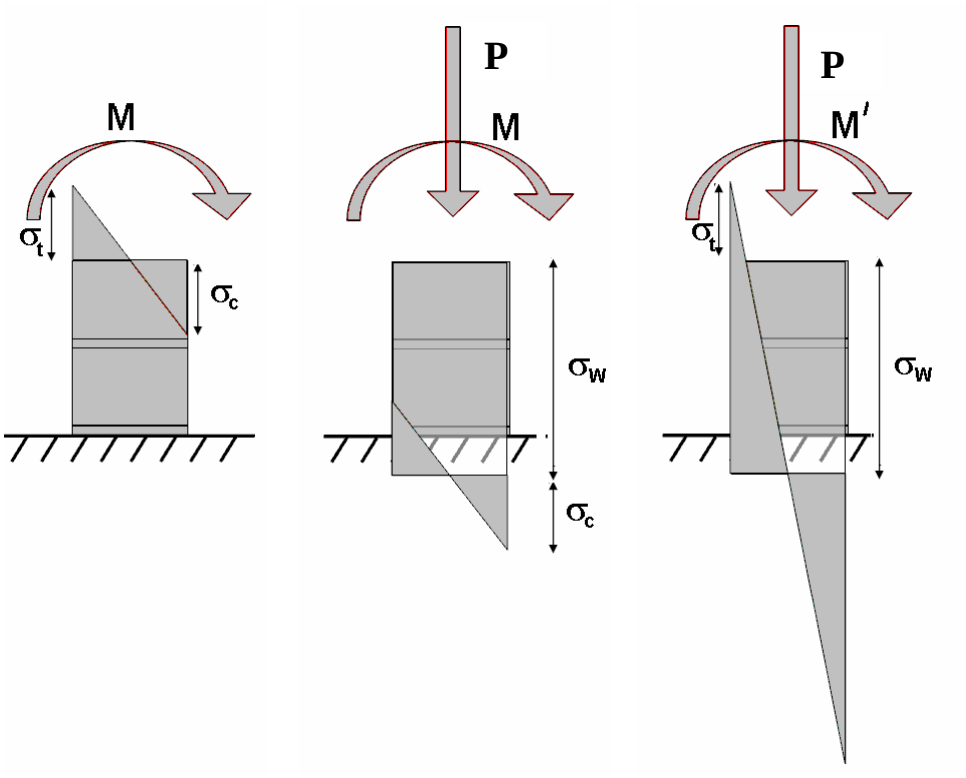

(a) (b) (c)

Figure 3.17 Explanation of increase bending capacity of walls

3.2.4.Setup and Instrumentation

The test setup was prepared so that the wall had constant moment region at the middle 1/3 length with a vertical simply supported layout as shown in Figure 3.18. The test specimen was loaded in horizontal direction by a two-way hydraulic jack, which was connected to an S-shaped load cell (50 kN capacity) to measure the laterally applied load. A simply supported beam was placed at the tip of the S-shaped load cell using a hinge to equally distribute the applied load on the wall by means of medium supports (see Figure 3.18). The placement of mirror beams on either side of the wall allowed the application of cyclic loading. In order to measure the level of actually applied axial load and its variation during testing, a second load cell was placed between the top of the wall and the STR. Four displacement transducers (LVDTs) of 100 mm stroke length were used to measure the displacements in the middle of the test wall in the constant moment region (see

Figure 3.18). Two of the LVDTs were placed close to the edges of the wall at the same height over the maximum deflection point to measure any possible torsional movement (see Figure 3.18-front view).

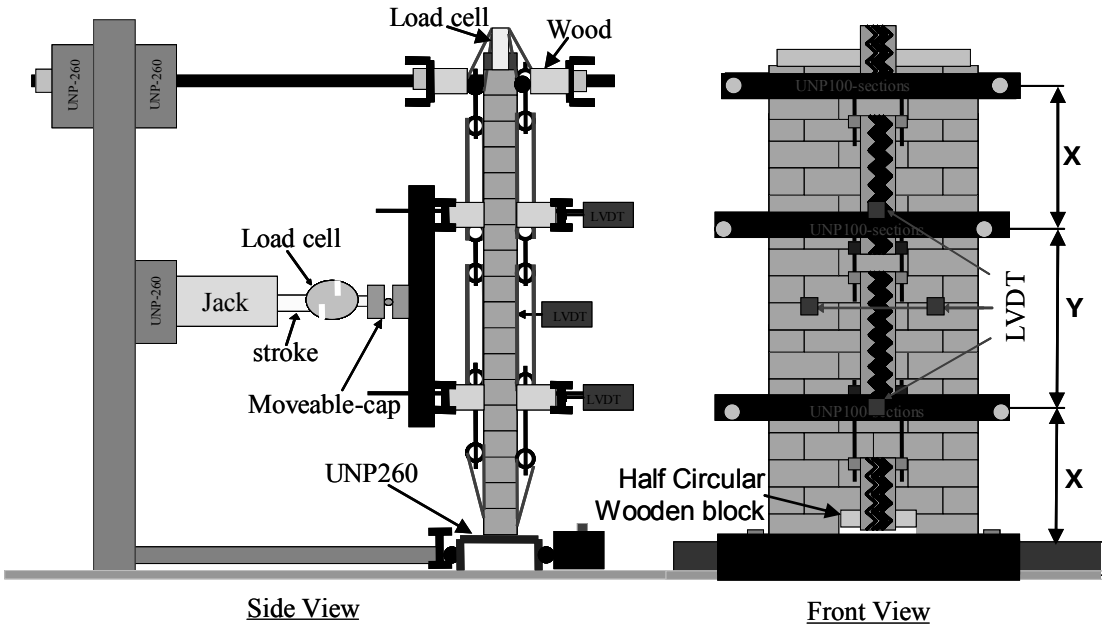

Figure 3.18 Test setup

A 16-channel data acquisition system was used for measurement of the test data. The two load cells and four LVDTs measured simultaneously at a sample rate of five samples per second (5 Hz) throughout the test.

3.2.5. Results of the first brick wall test#1

The out-of-plane tests on the first brick wall strip were conducted in three stages. The first stage involved testing of the wall strip without post-tensioning to obtain the nominal (without strengthening) capacity. The second test was conducted after the scrap tires around the wall were stretched until an axial load of about 50 kN (5 tons) post-tensioning was reached. For the third test, the axial load was increased to about 100 kN (10 tons) and the lateral cyclic loading was repeated. The same specimen was used in all stages without any repair work. The axial load was measured by the

load cell located at the top of the wall below the tires and additional calibration was carried out using a torque wrench for ϕ16 mm bolt or #24 nuts. The applied axial post-tensioning load (P in kN) was calculated by setting torque values (T in N.m) indicated on the torque wrench adjustment tool (Equation 3.1).

$$P = 0.6641\ T + 0.0407 \tag{3.1}$$

The first stage test was conducted on the nominal wall (i.e., without strengthening). The linear capacity of the wall was measured to be 1.206 kN at a lateral displacement of 0.354 mm (k=3.54 kN/mm) when the first crack was observed along the middle of the wall. A small crack was formed on the mortar layer close to the upper side of the loading beam (see Figure 3.19(a)). The maximum lateral load capacity of strip wall was measured as 1.9 kN at a lateral displacement of 3.6 mm. When the lateral displacement reached 27.4 mm, the lateral strength capacity of the wall reduced to 1.2 kN. In order to prevent heavy damage of the wall, the test was stopped (see Figure 3.20).

(a) (b) (c)

Figure 3.19 Crack formation during masonry brick wall tests

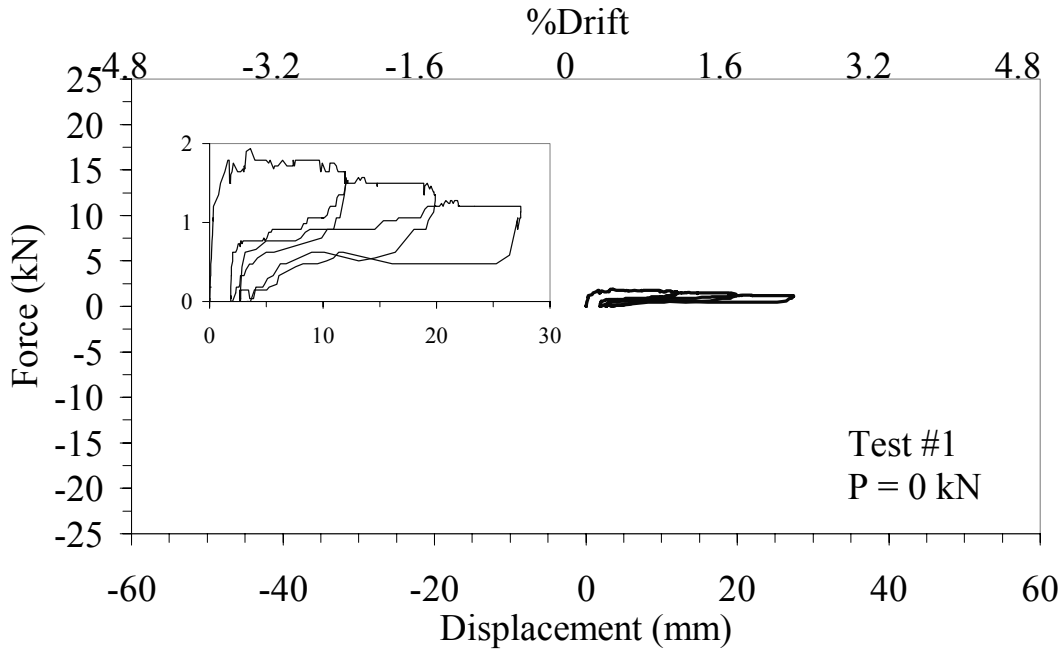

Figure 3.20 Nominal stage test results of the first brick wall

The second stage test was repeated with about 50 kN (5 ton) of axial post-tensioning load, applied on the strip wall using STC. The linear load capacity of the wall was improved to 5.25 kN under a lateral displacement of 1.061 mm (k=4.949 kN/mm). The first crack re-opened in the constant moment region at the same location as in stage 1. The capacity of the wall in the nonlinear range reached to 13.30 kN (at 34.6 mm displacement) which was seven times as much as the capacity of the nominal wall (see Figure 3.21). The initial crack was followed by additional cracks when the specimen was loaded into the nonlinear range (see Figure 3.19(b)). The axial load was reduced to 41 kN from 48.5 kN due to crushing of the mortar layer (see Figure 3.22). The flat plateau seen in Figure 3.22 refers to the linear range of lateral loading. As the linear range was exceeded, an increase in the post-tensioning load was observed parallel to the crack opening. In contrast to lateral force versus post-tensioning load graph, the flat plateau is not apparent in the axial load versus lateral displacement graph, since the displacement required to exceed the linear range is relatively small (see Figure 3.23). On the other hand, the linear relationship shown in Figure 3.23 indicates that the axial post-tensioning force increases linearly as a function of the lateral displacement. The crack opening displacement (δ) is linearly

related to lateral displacement (Δ) using triangles ($\hat{abc}$) and ($\hat{dea}$) as shown in Figure 3.24 (b). Crack opening displacement (2δ) causes stretching of the post-tensioning STC, which increases the post-tensioning load (see Figure 3.23).

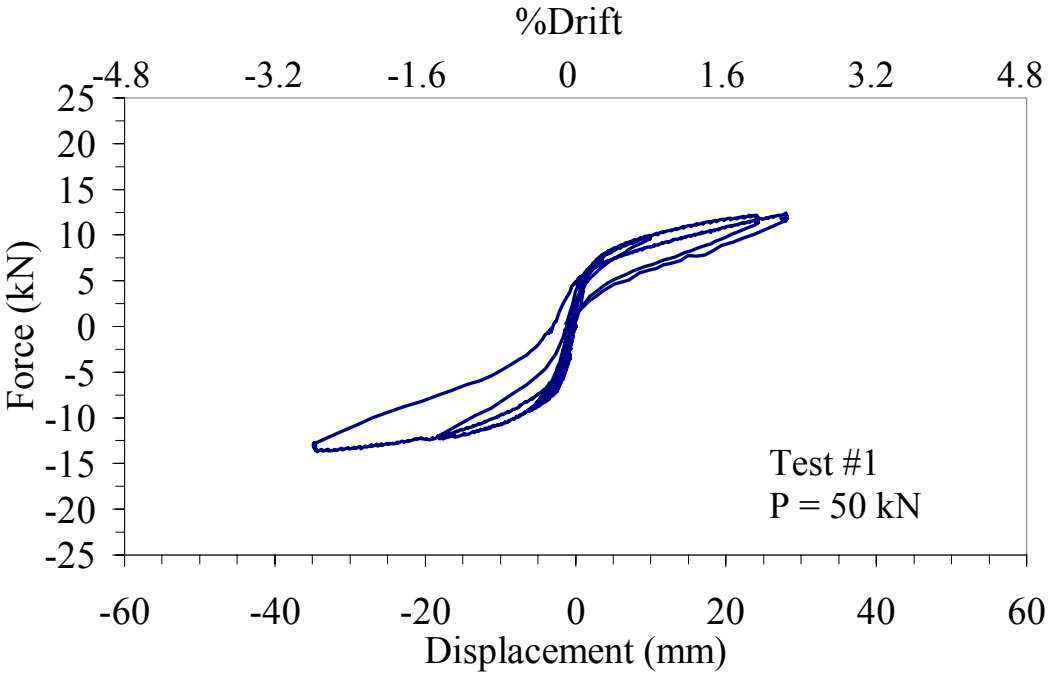

Figure 3.21 Second stage test results of the first brick wall

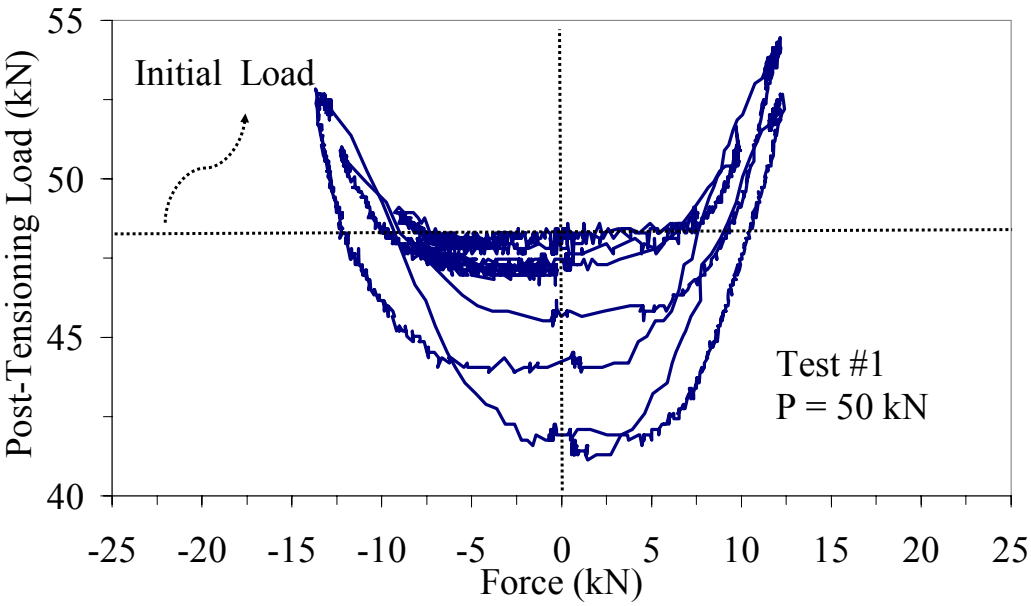

Figure 3.22 Axial post-tensioning force versus horizontal load for stage#2

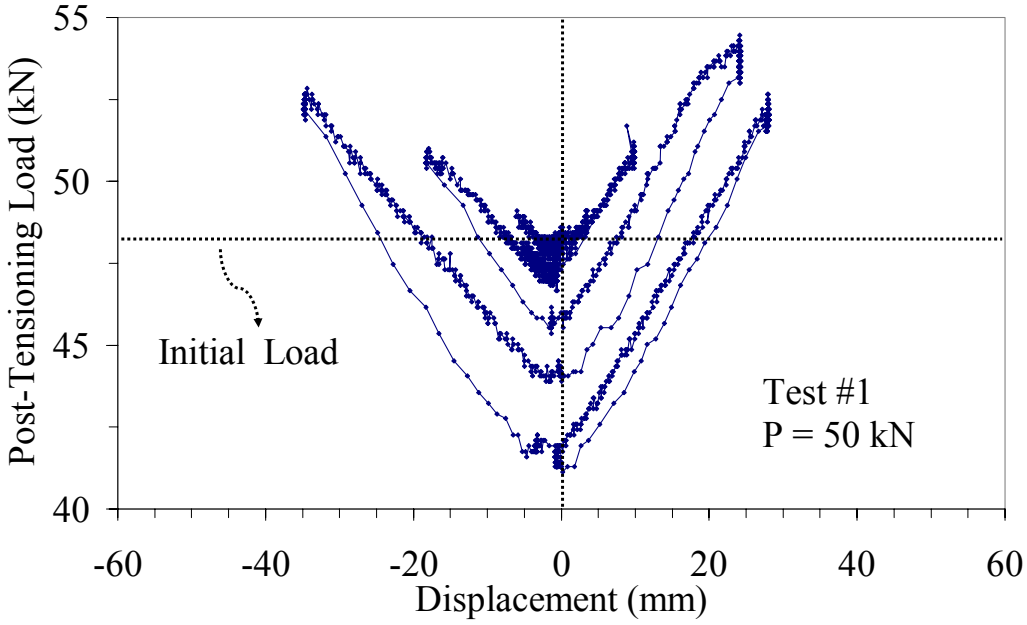

Figure 3.23 Axial post-tensioning force versus horizontal displacement of stage#2

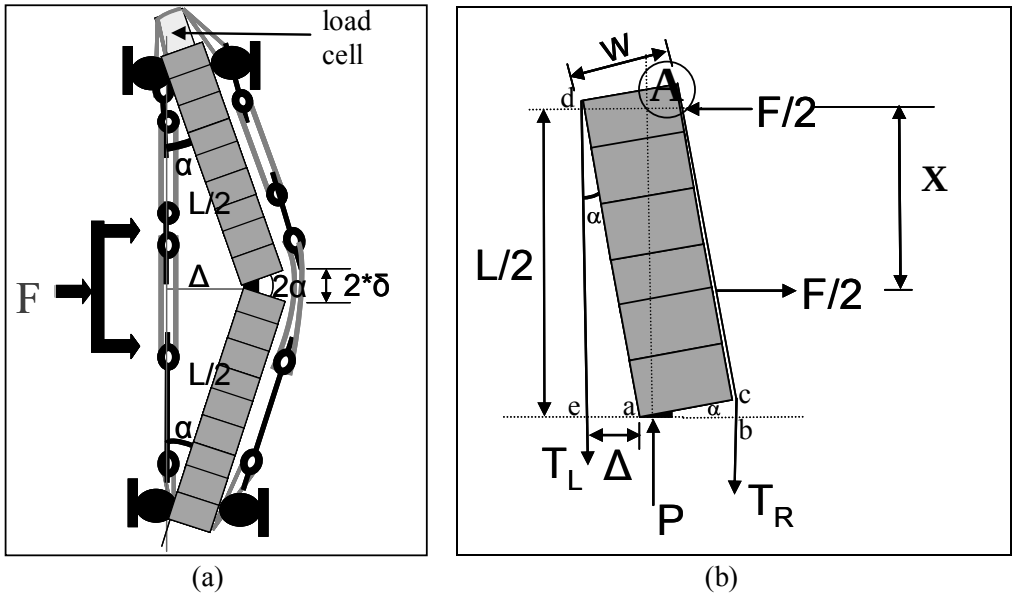

Figure 3.24 Masonry strip wall non-linear range deflection and forces illustration

In the third stage, the axial load applied on the wall was increased to 100 kN (10 ton) and reversal cyclic loading was repeated. The wall showed linear behavior up to the lateral load of 6.34 kN at 0.15mm lateral displacement (k=4.22 kN/mm) and the first

crack was opened. The ultimate capacity was measured as 15.8 kN when the lateral displacement reached 21.3mm (see Figure 3.25). Premature failure was initiated by diagonal shear cracks at the base of the wall when -38.3 mm displacement was applied in the reverse loading direction (see Figure 3.19 (c)). The post-tensioning load level dropped down to 47 kN from the 97 kN initial load (see Figure 3.26 and Figure 3.27) as the scrap tire crushed the bricks at the bottom of the wall (at the location of stone). A half-cylindrical wooden log was used in the second test to evenly distribute stresses from the STR to the wall thus preventing premature failure.

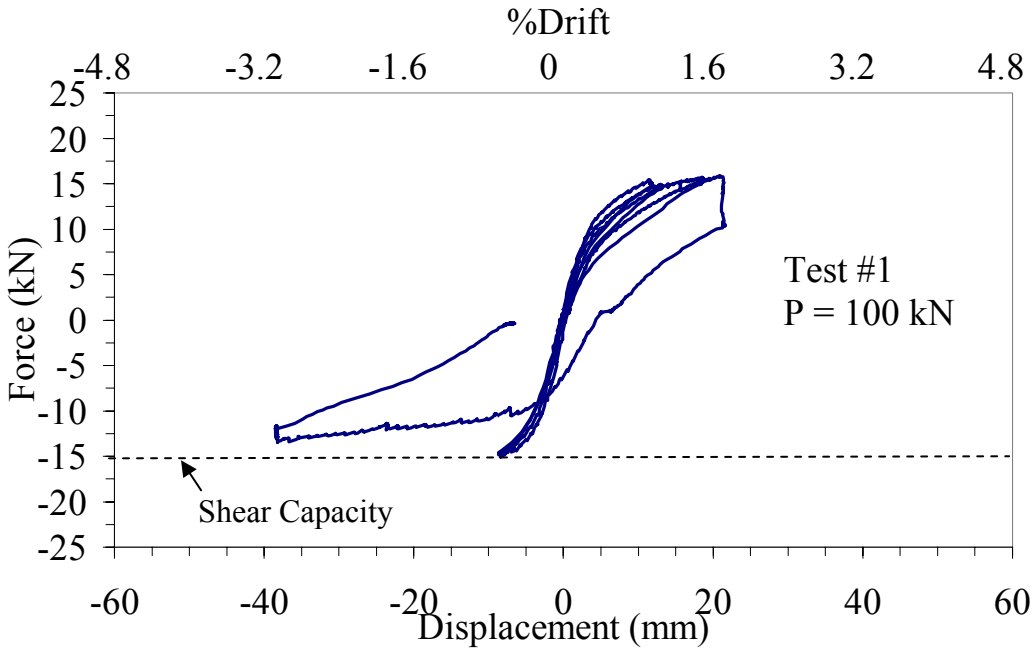

Figure 3.25 Third stage test results of the first brick wall

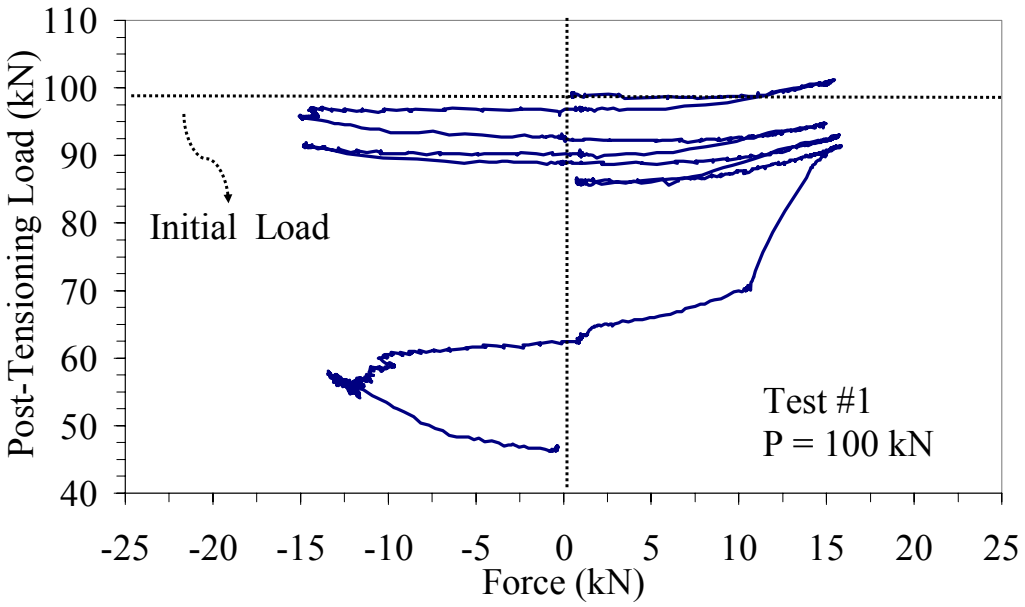

Figure 3.26 Axial post-tensioning force versus horizontal load for stage#3

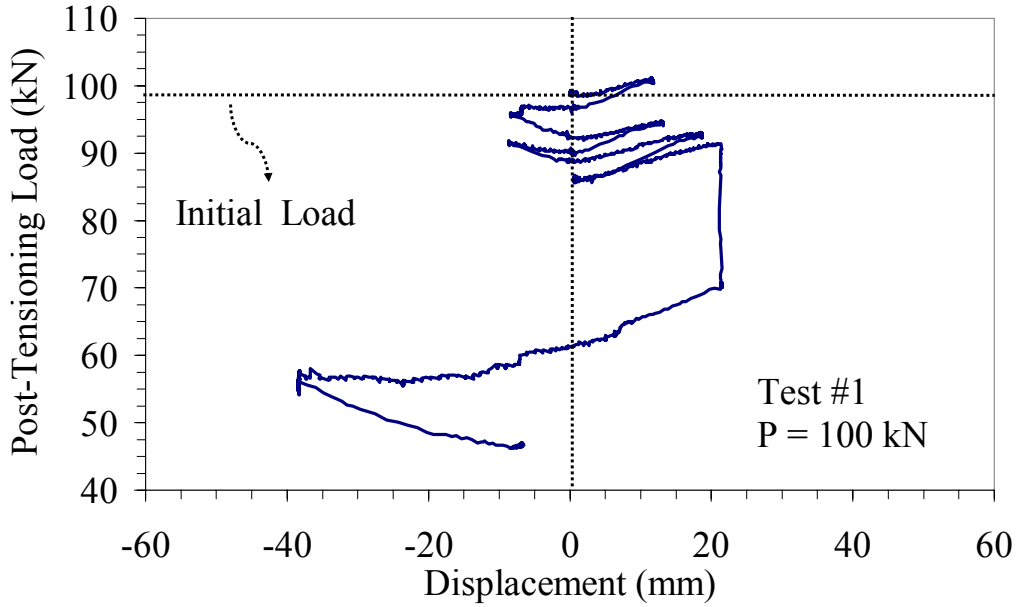

Figure 3.27 Axial post-tensioning force versus horizontal displacement of stage#3

3.2.6. Results of the second brick wall test #2

The second set of brick wall tests were also conducted in three stages with 0, 50, and 100 kN post-tensioning forces applied using STC.

The first stage nominal lateral load capacity of the wall was measured to be equal to 1.1 kN at a displacement of 0.4 mm (k=2.75 kN/mm) (see Figure 3.28). The ultimate load capacity of the wall was measured as 2.16 kN.

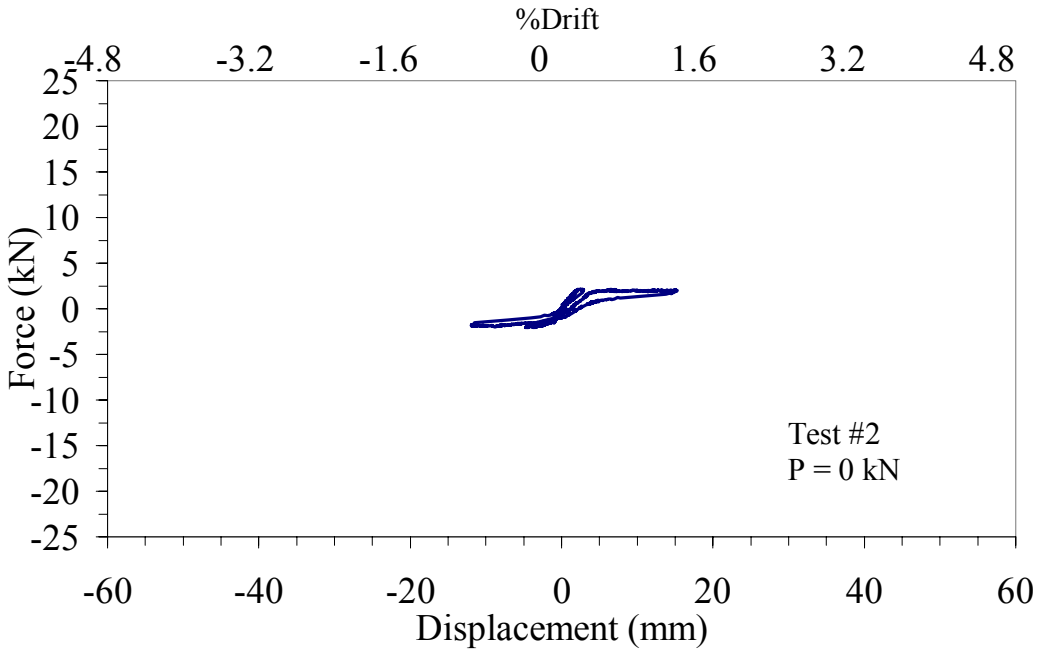

Figure 3.28 Second brick wall test results of stage#1

In stage two, the linear horizontal load capacity of the 50 kN post-tensioned wall specimen was increased up to 5.18 kN with an improvement of about 1.88 times of its nominal value at a displacement of 1.25 mm (see Figure 3.29). The maximum lateral load measured in the second stage test was 12 kN and had the potential to get even larger; however, the cycles were stopped at that level, to prevent extensive damage of the specimen as in stage #1 (see Figure 3.29). Although loading was stopped at an early stage, the capacity was improved about 6 times as compared to

the initial stage. The stiffness increased to 4.15 kN/mm from 2.75 kN/mm.

The flat plateaus shown in Figure 3.30 and Figure 3.34 are similar to that of brick wall test #1 (see Figure 3.26). This indicate that the linear range is better observed at lateral load versus post-tensioning load graph whereas the lateral displacement versus post-tensioning force graph (see Figure 3.34) fails to capture the linear range since the system becomes nonlinear at very low lateral deflections (at about 1mm to 2 mm).

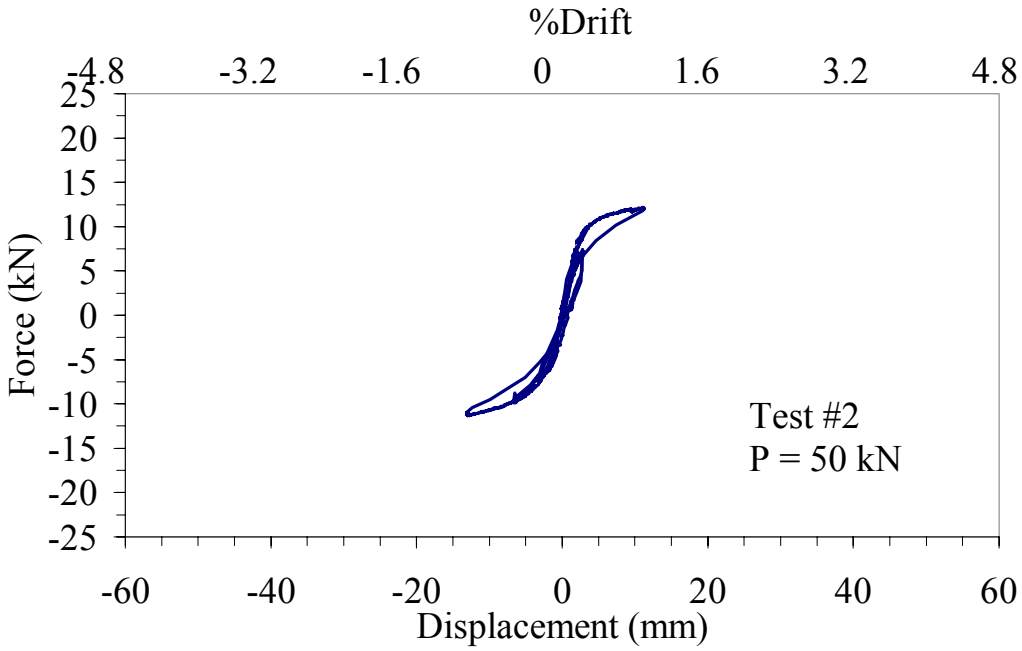

Figure 3.29 Second brick wall test results of stage#2

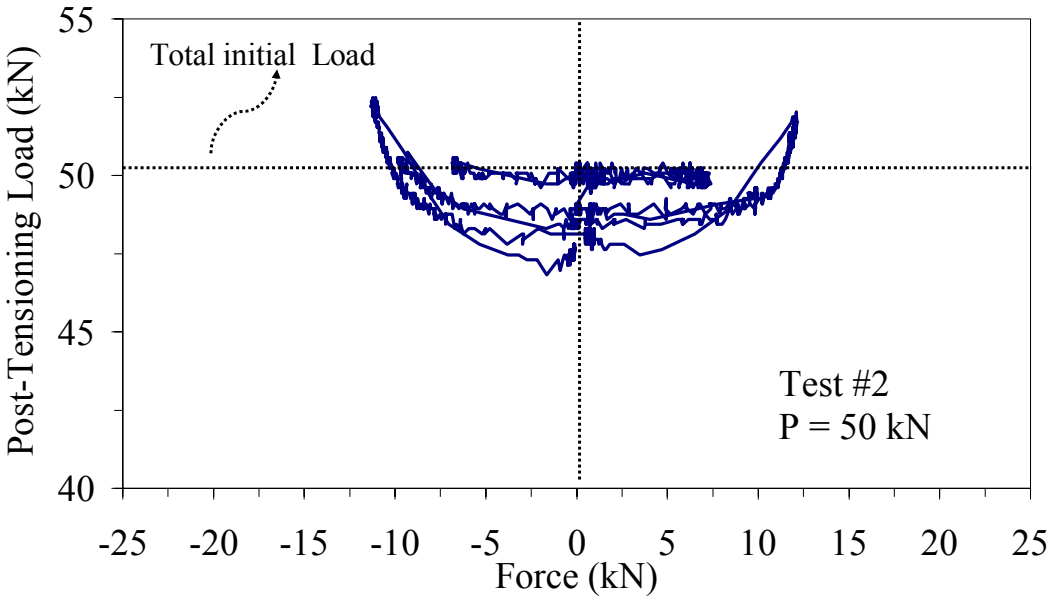

Figure 3.30 Axial post-tensioning force versus horizontal load of stage#2

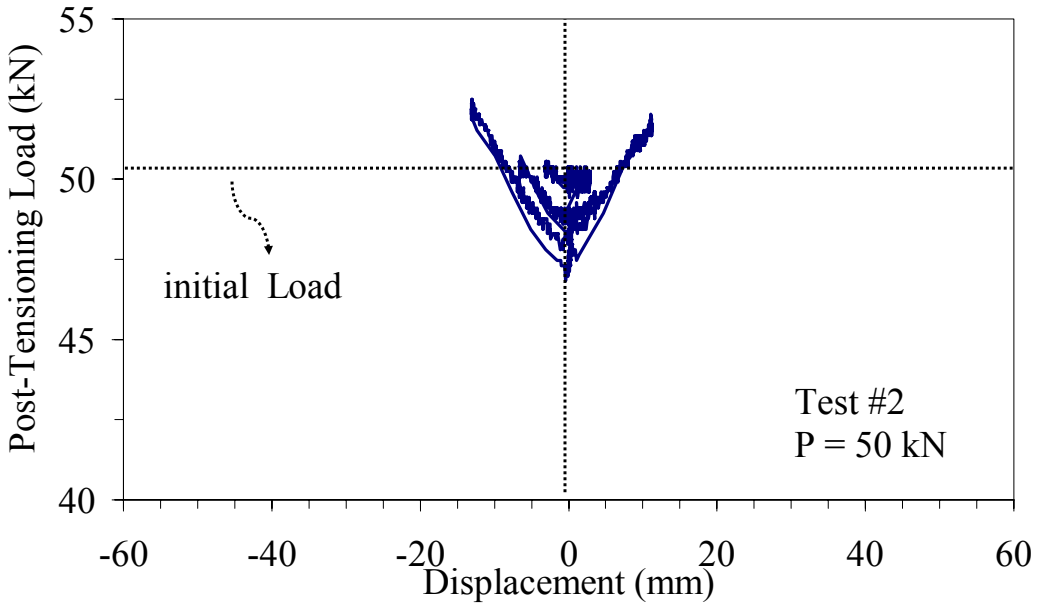

Figure 3.31 Axial post-tensioning force versus horizontal displacement of stage#2

The third test was conducted on the same specimen with post-tensioning axial force of about 100 kN. The linear range was surpassed at about 9.82 kN of lateral force at

a lateral displacement of 2.017 mm. The measured lateral stiffness in the third test increased to 4.87 kN/mm with an increase of about 17.3 % compared to the second stage test The ultimate lateral strength achieved in the third test was about 20 kN (see Figure 3.32) which is about 9.3 times of the nominal strength (see Figure 3.28).

All three stages of wall test #2 were conducted on the same specimen. In other words, the second and third stages were conducted on the already cracked specimen without any repair work. The first crack re-openings during the post-tensioned tests were observed at mid height of the wall at mortar level as the load-deflection curve passed the linear range. Additional cracks in the third stage developed at other horizontal mortar layers, above and below the middle crack, also in the constant moment region, as the lateral displacement was further increased. As the displacement was increased further, one of the cracks grew larger forming a hinge mechanism (Figure 3.24); however, the response was not measured beyond the 50 mm lateral displacement since the deflections exceeded the maximum LVDT measurement range of ±50mm for a maximum lateral drift ratio of 4% (see Figure 3.33 (b)).

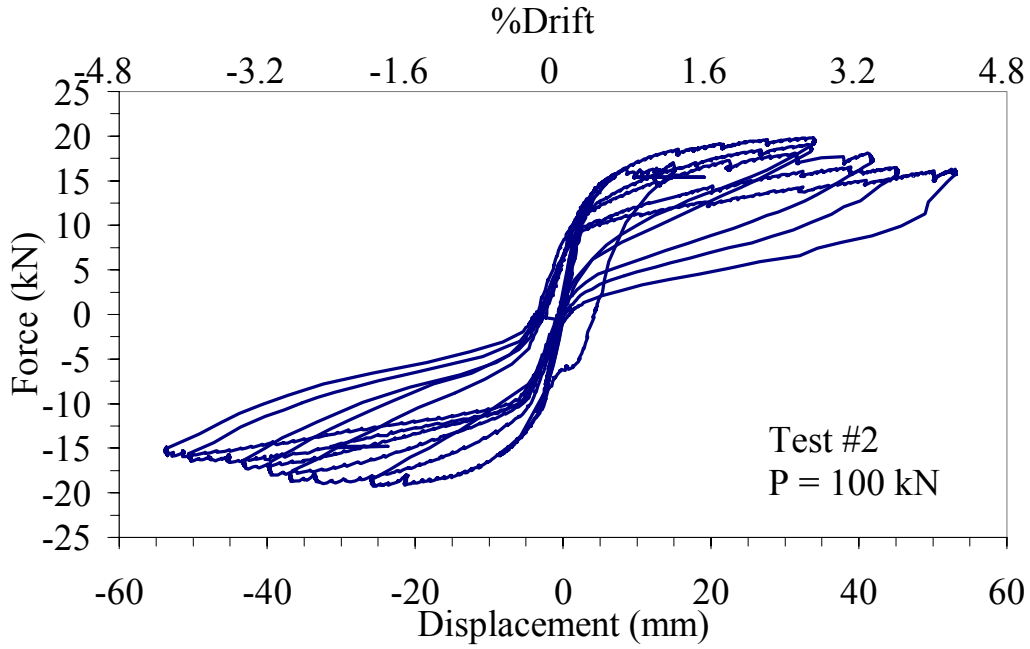

Figure 3.32 Second brick wall test results of stage#3

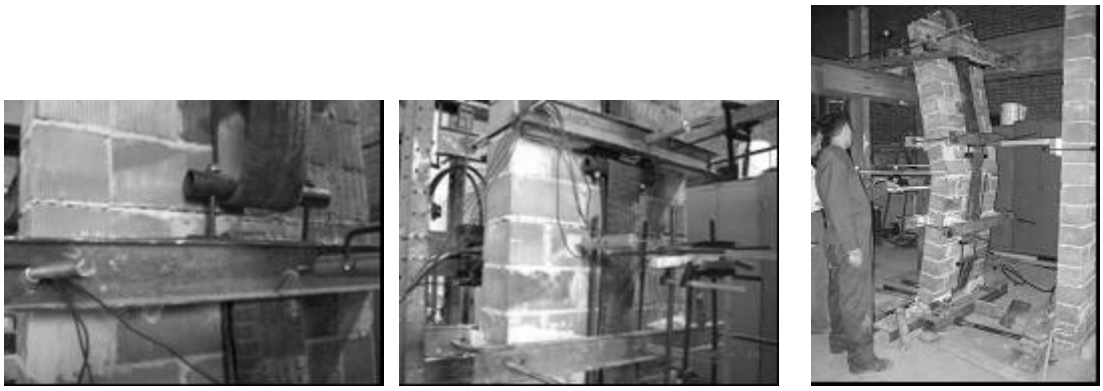

(a) (b) (c)

Figure 3.33 Crack formation during the second brick wall tests

The axial post-tensioning force remained fairly constant in the linear elastic range; however, the measurements from the load cell placed at the top of the wall indicated about 5% to 10% increase in the post-tensioning force when the lateral displacement exceeded the linear range (see Figure 3.34 and Figure 3.35). When the number of cycles in the nonlinear range was increased, the axial post-tensioning force decreased gradually down to 85% of its initial post tensioning force after 10 cycles. This loss of post-tensioning force was attributed to the crushing of the mortar layers and some of the brick edges which shortened the height of the wall.

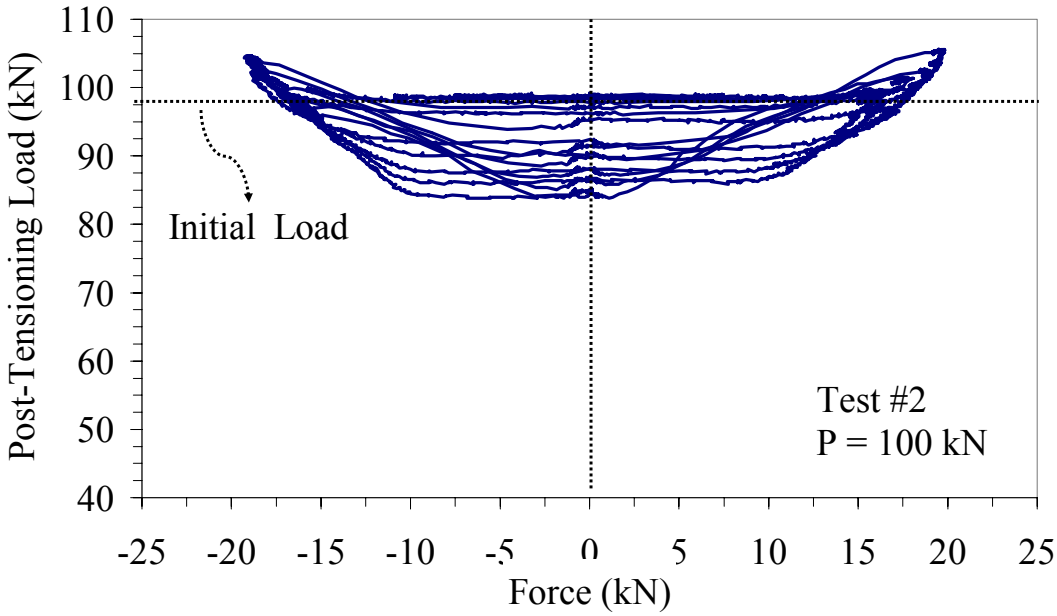

Figure 3.34 Axial post-tensioning force versus horizontal load

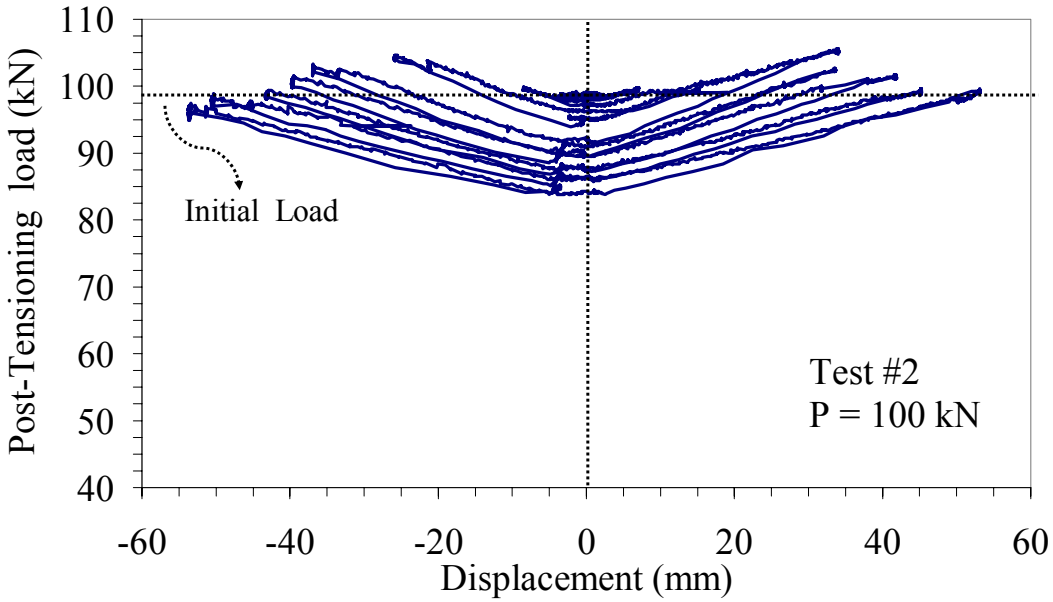

Figure 3.35 Axial post-tensioning force versus horizontal displacement of stage#3

The curves of axial post-tensioning load versus lateral displacement obtained from each cycle (see Figure 3.35) are parallel to each other and show linear behavior with an average slope of 0.3 kN/mm. The increase in post-tensioning force was caused by the crack opening, shown in Figure 3.24 (b), and had positive effect on the overall capacity of the wall especially at large deflections. The effective stiffness of the 2.6m long scrap tire chain on a single side of the wall was calculated to be about 0.64 kN/mm. Based on the similar triangle ratio in Figure 3.24 (b), the total crack opening due to a maximum deflection of 50 mm (4% drift) would be 14.8mm which would increase the post-tensioning force by 9.5 kN which is equivalent to about 20% and 10% of 50 kN and 100 kN post-tensioning forces, respectively. Additional post-tensioning force of about 13 kN at 50 mm displacement was measured during test #2 (Figure 3.35) which also supports the analytical calculation.

3.2.7.Results of the third brick wall test #3

The third brick wall test was conducted in only one stage. It was strengthened by hybrid system, composed of two STRs and four steel bars (Φ12 st420). 100 kN of

post-tensioning load was applied on the wall in the vertical direction similar to the previous tests.

The linear range was exceeded at about 13.4 kN of lateral force and lateral displacement of 1.186 mm (see Figure 3.36). The measured stiffness of the wall was calculated as 11.29 kN/mm, which was twice as much as the third stage of second wall tests. The relatively high stiffness of the wall is attributed to uncrushed original material of the mortar layers and bricks. The ultimate lateral strength obtained in this test was about 22.8 kN, which was about 10.67 times greater than nominal strength of the second wall (see Figure 3.32(a)).

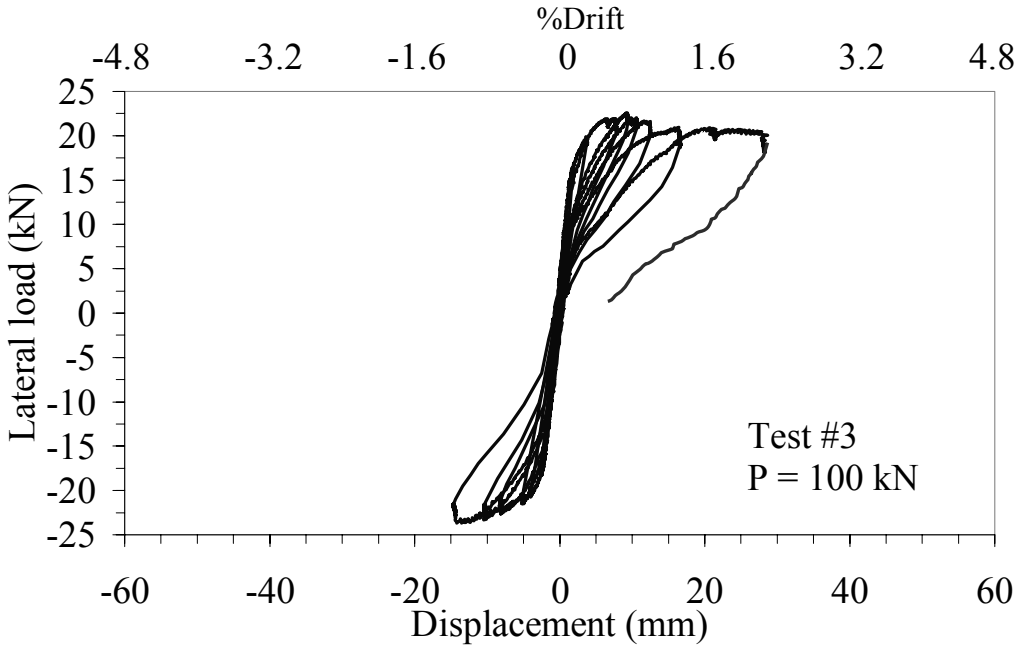

Figure 3.36 Masonry strip wall tests #3, 100 kN post-tensioning load (hybrid)

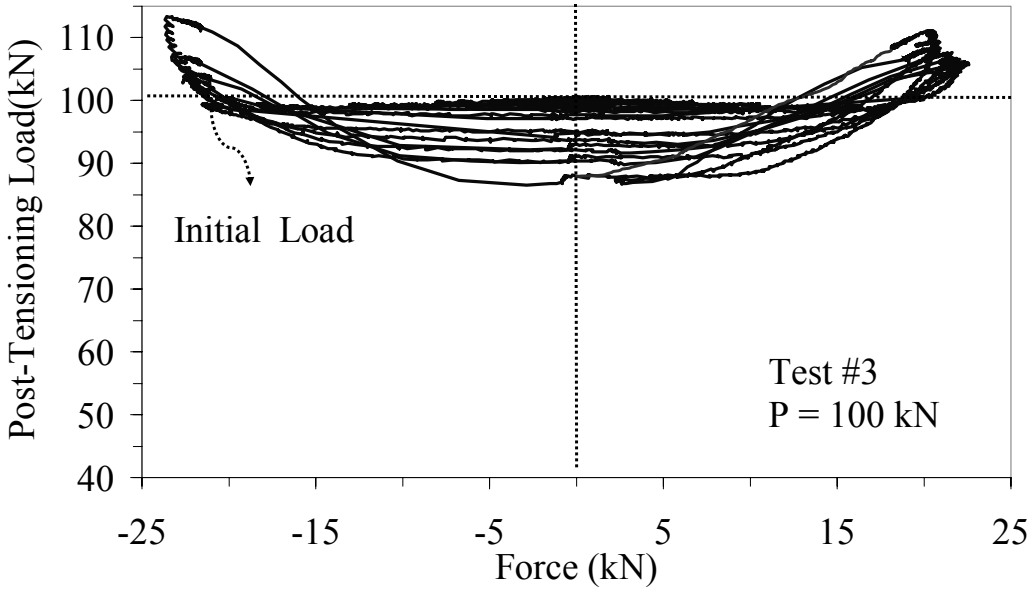

Figure 3.37 Axial post-tensioning force versus horizontal load

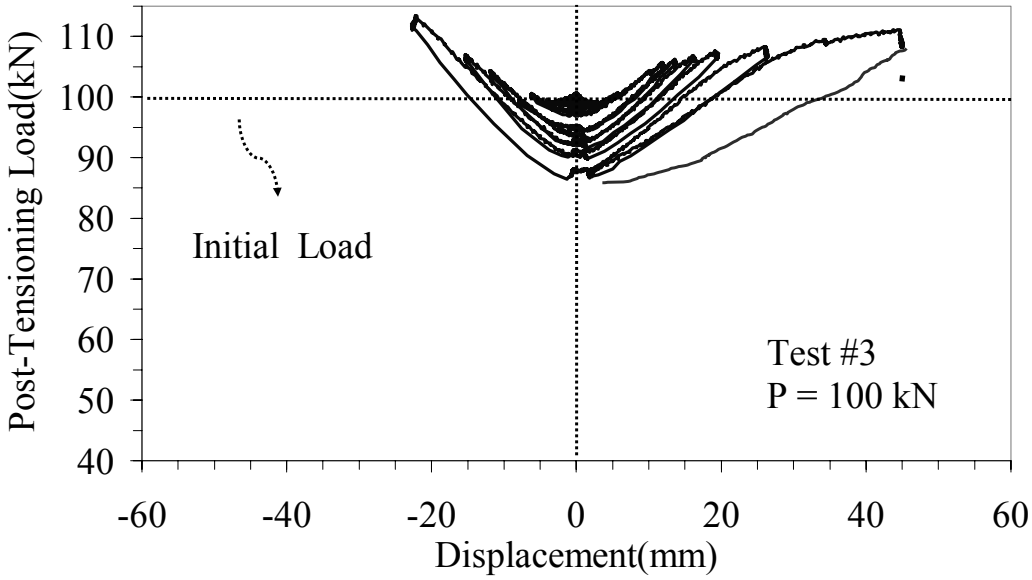

Figure 3.38 Axial post-tensioning force versus horizontal displacement

Similarly to the results of previous wall tests, the axial post-tensioned force remained relatively constant in the linear range until about 1 mm to 2 mm lateral displacement (see Figure 3.37). When the wall passed into the non-linear range, the axial post-

tensioning force started to increase and continued to increase proportionally to the lateral displacement. After 11 cycles, the value of the applied axial post-tensioning force on the wall decreased to 87% of its initial value due to the crushing of the mortar layer and some of the bricks (see Figure 3.37 and Figure 3.38).

First crack formation on the wall was observed on the mortar layer, just beneath the upper load application frames. When the opening grew larger, a hinge mechanism was formed at that level, followed by new small crack formations at the middle section mortar layers of the walls (see Figure 3.39).

Figure 3.39 Crack formation during the third brick wall tests

3.2.8.Results of the fourth brick wall test #4

The fourth brick wall set of tests were also conducted in three stages with 0, 50, and 100 kN post-tensioning forces applied using hybrid system.

The nominal strength of the wall was measured as 2.01 kN at a displacement of 0.405 mm (see Figure 3.40) and by using these values; the lateral stiffness of the wall was calculated as 4.96 kN/mm. The lateral load capacity of the unstrengthened wall was measured to be 2.76 kN which was the greatest value of the nominal brick wall test results.

After applying 50 kN post-tensioning load, the linear capacity of the wall was increased to 5.32 when the lateral displacement reached 1.036 mm (Figure 3.41). From these values, the lateral stiffness of the wall was calculated as 5.133 kN/mm. In the experiment, the maximum strength of the wall was measured as 9.23 kN. The change of post-tensioning load with respect to lateral force and lateral displacement are shown in Figure 3.42 and Figure 3.43 respectively. The initial applied post-tensioning force decreased from 50.2 kN to 48.25 kN.

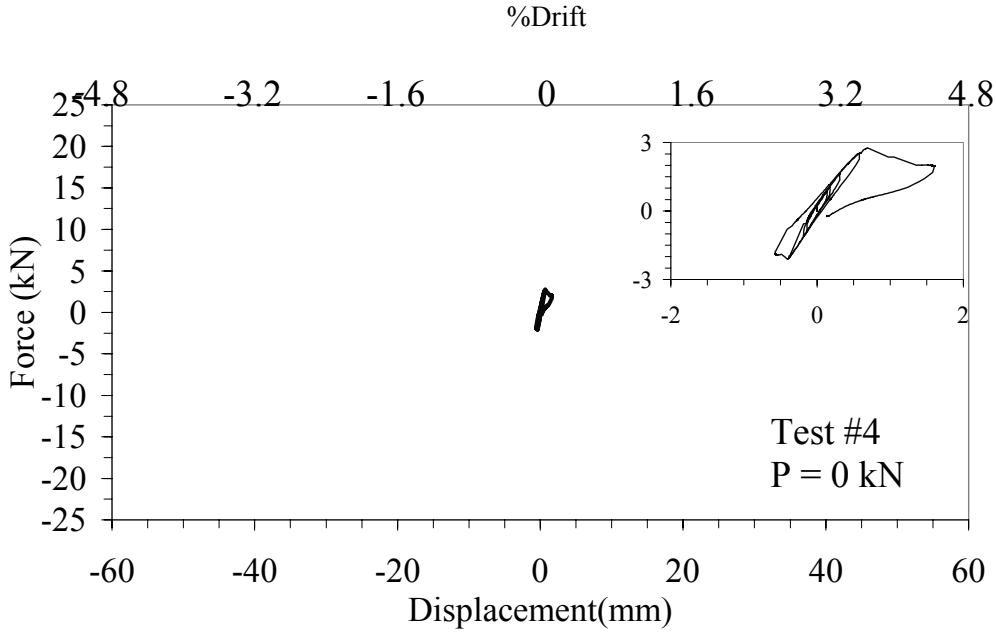

Figure 3.40 Fourth-brick wall test results in nominal case

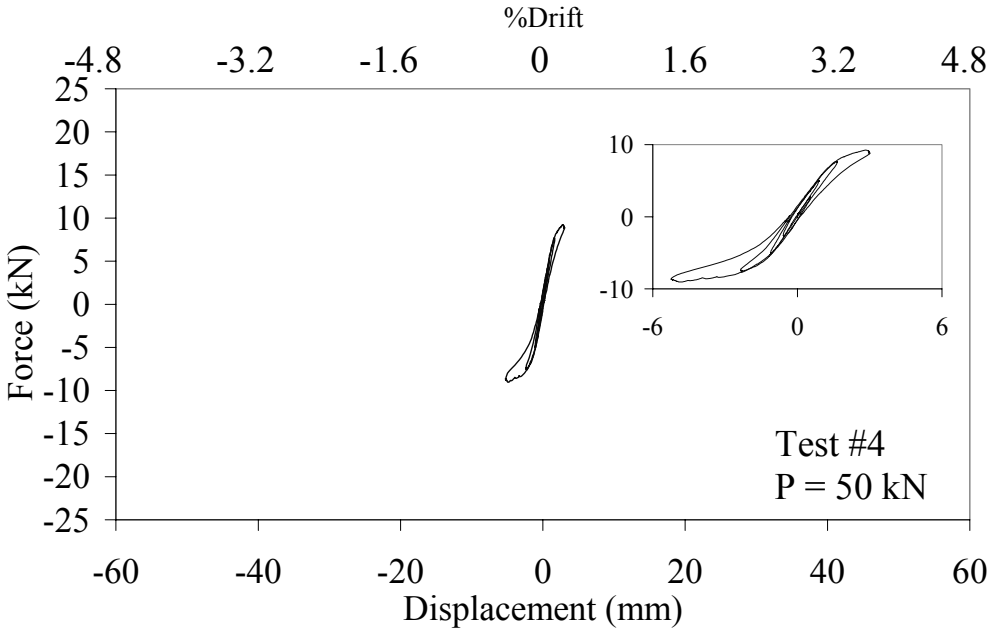

Figure 3.41 Fourth-brick wall test results in 50kN stage

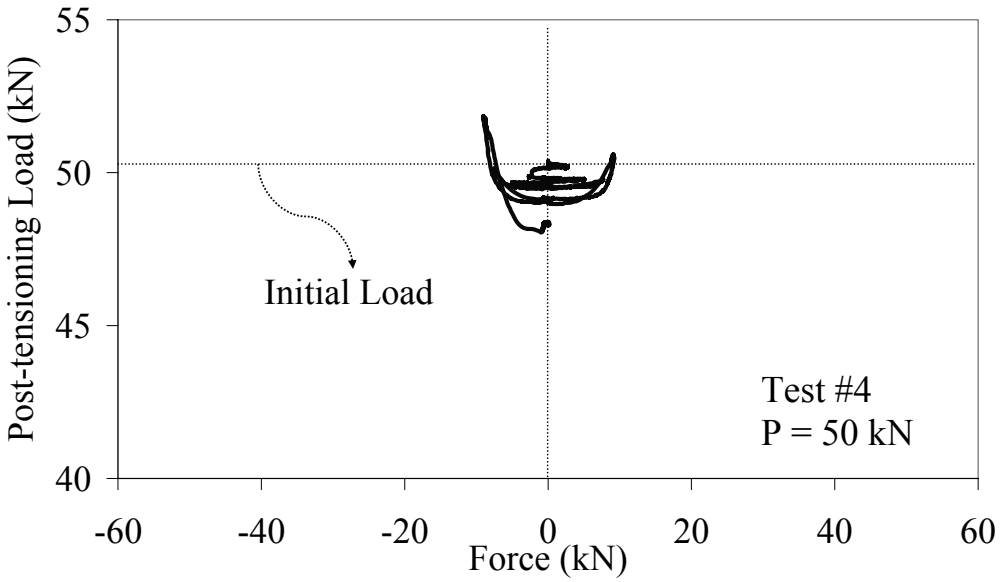

Figure 3.42 Axial Post-Tensioning Force versus Horizontal Load

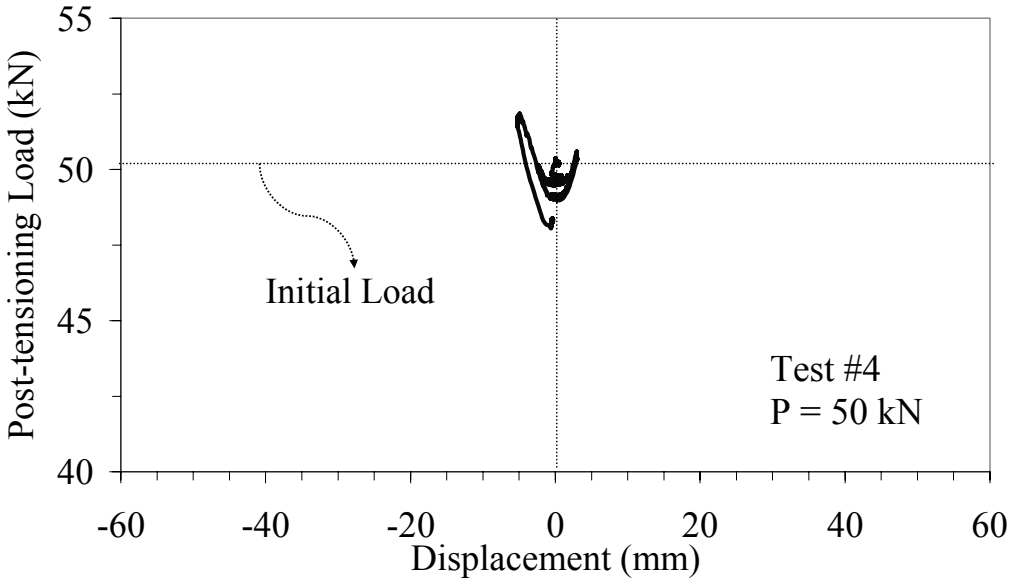

Figure 3.43 Axial Post-Tensioning Force versus Horizontal Displacement

In the third stage, the post-tensioning load on the wall was increased to about 100 kN. The linear range stiffness of the wall was measured as 9.14 kN at 1.56 mm lateral displacement and the lateral stiffness was computed as 5.8 kN/mm. The ultimate lateral strength of the wall was gauged as 20.5 kN. During this test, the post-tensioning loads were decreased from about 99 kN to 78 kN (see Figure 3.45 and Figure 3.46); in other words, 21% of the initial post-tensioning load was lost due to crushing of mortar layers and brick edges.

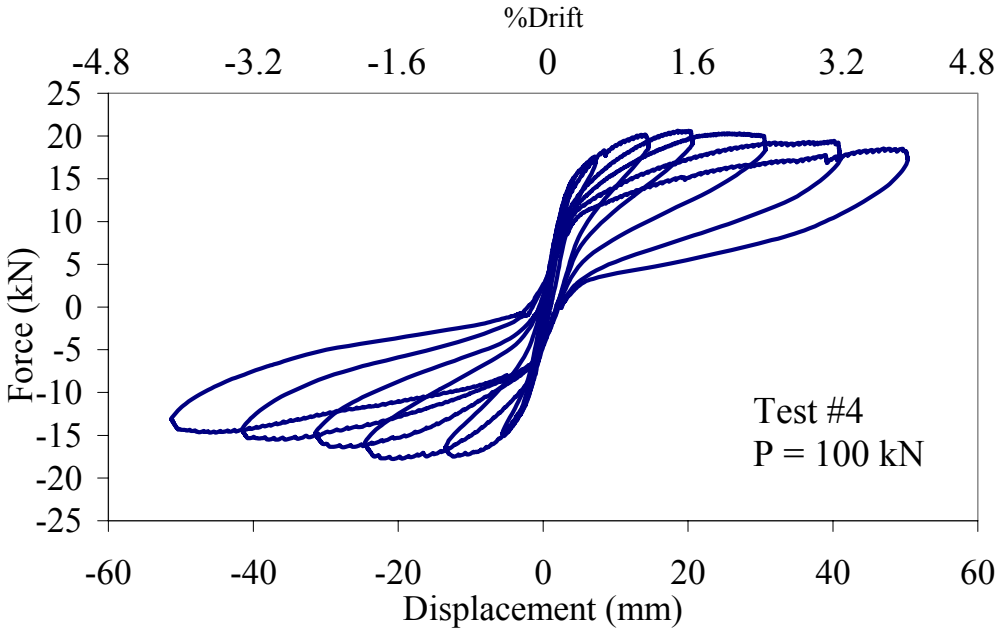

Figure 3.44 Fourth-brick wall test results in 100kN case

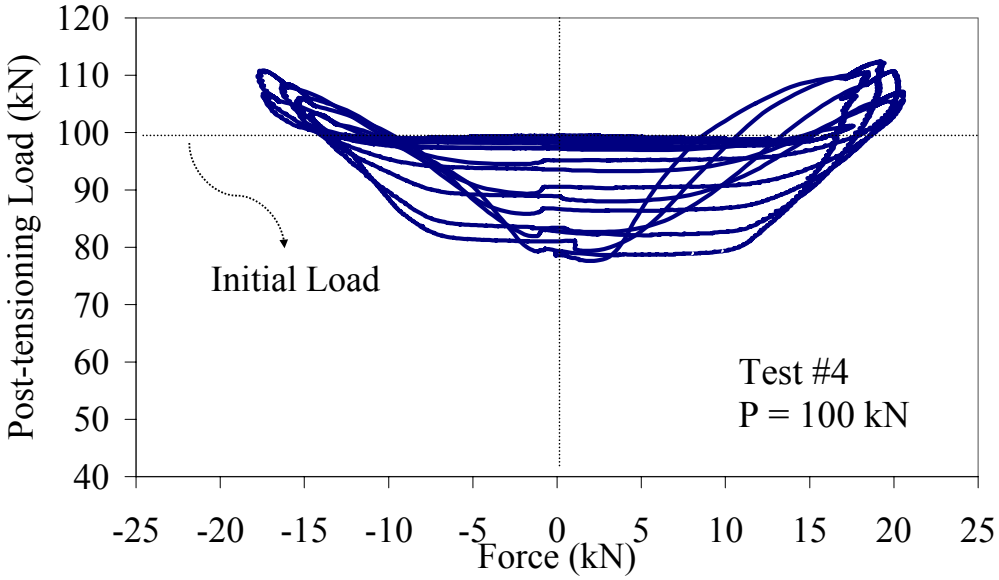

Figure 3.45 Axial Post-Tensioning Force versus Horizontal Load

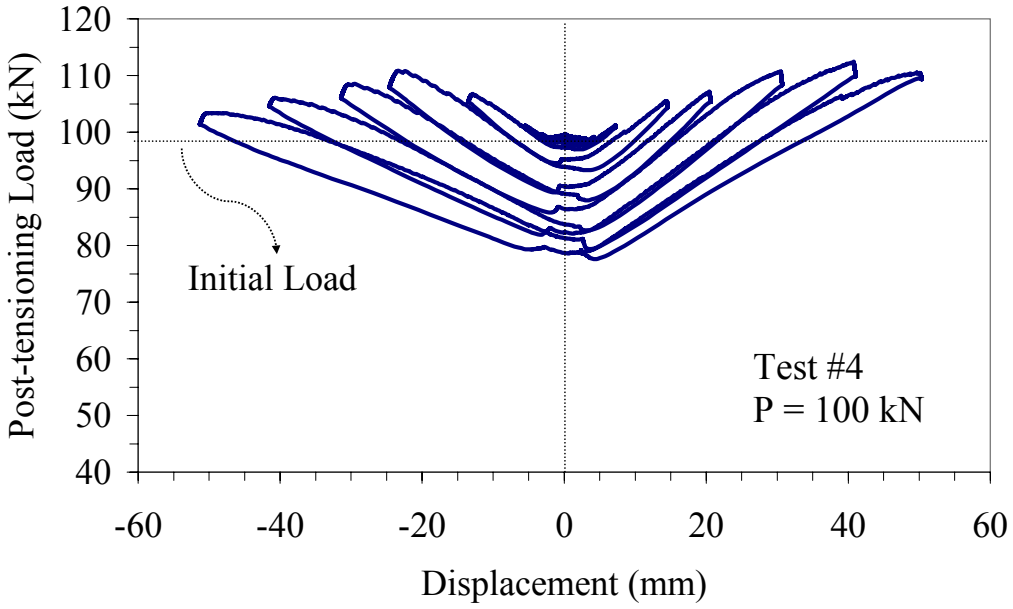

Figure 3.46 Axial Post-Tensioning Force versus Horizontal Displacement

The first crack was formed in the stage #1 (0 kN axial load) on the mortar layer located closest to the upper leg of load application frame (Figure 3.47 (a)). In the second stage (50 kN axial load), this crack was re-opened and followed by additional small cracks at the middle range of the walls (Figure 3.47 (b)). Since the maximum lateral displacement of the wall in stage #2 (50 kN axial load) was kept smaller than 5 mm, excessive damage to the wall was prevented. In the third stage, the lateral displacement of wall was increased up to 50 mm (4% drift ratio). The crack formed in the second stage at the middle layer was opened again as seen in Figure 3.47(c)&(d).

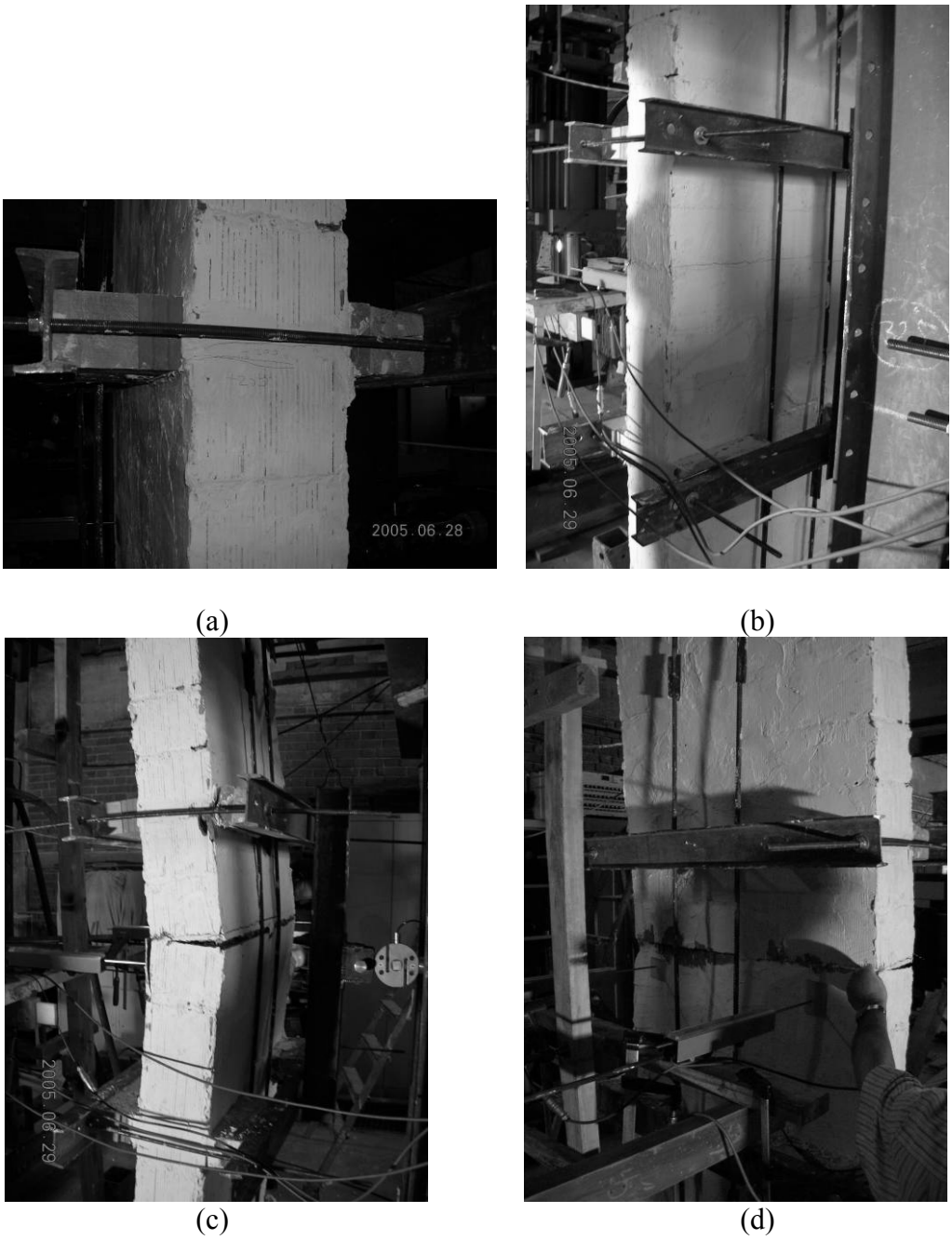

(a) (b)

(c) (d)

Figure 3.47 Crack formation during the fourth brick wall tests

3.2.9. Results of the first briquette wall test #1

The out-of-plane tests on the first briquette wall strip were conducted in two stages. In order to obtain the nominal capacity of the wall, the first stage involved testing of the briquette wall specimen without post-tensioning force. The second stage test was performed after applying 30 kN post-tensioning axial load by stretching the STC. The reason for this small applied post-tensioning force on the briquette wall compared to that of brick walls was the small compression strength capacity of briquettes. The test results obtained from these two stages are given in Figure 3.48 to Figure 3.52.

In the first stage, the briquette wall acted linearly until 1.0 kN of lateral force at a lateral displacement of 0.27 mm (Figure 3.48). The measured lateral stiffness of the wall was calculated as 3.704 kN/mm. The maximum lateral resistance of the wall during the experiments was measured to be 5.4 kN at a lateral displacement of 4.5 mm in the negative direction. A thin crack formation appeared in the maximum moment region. The wall was pushed up to the 5.4 mm lateral displacement in the positive direction. In order to prevent unexpected large damage of the wall, the test was stopped.

In the second stage, 30 kN post-tensioning force was applied on the briquette wall by stretching STC in the vertical direction similar to the previous brick wall tests. The linear resistance capacity of the wall was measured as 10.64 kN at a lateral displacement of 2.38 mm. The stiffness of the specimen was calculated to be 4.47 kN/mm. After surpassing the linear range, small cracks were observed in the middle part of the wall as shown in Figure 3.51(a). When the displacement in the positive direction reached 41 mm, the lateral resistance of the wall increased to 21.5 kN premature diagonal shear cracks, similar to the cracks in the third stage of the first brick wall tests, appeared at the lower part of the wall (see Figure 3.51 (b)).

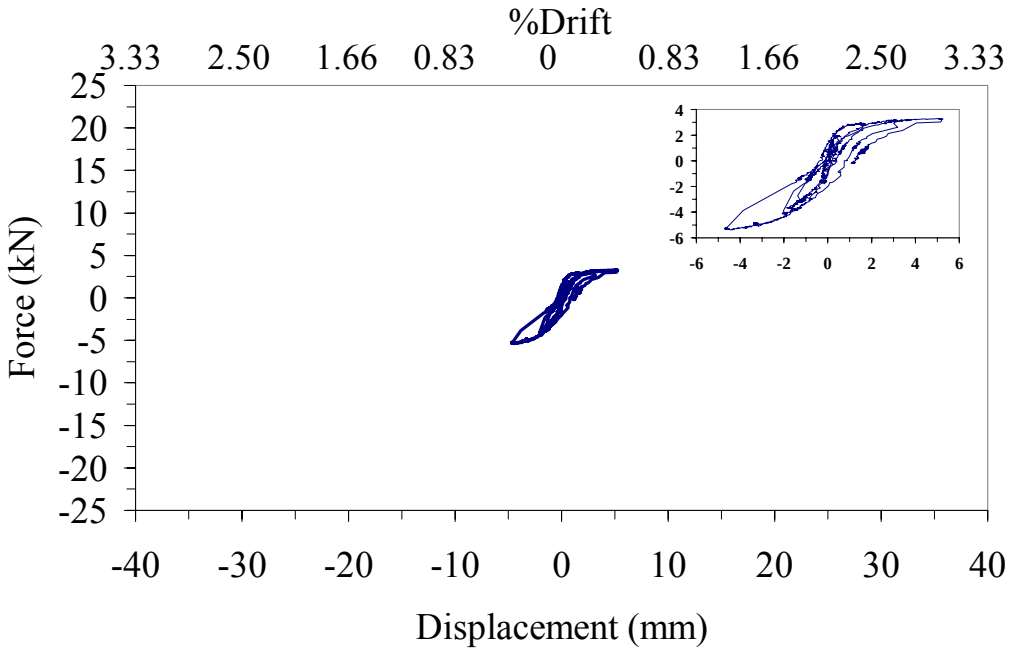

Figure 3.48 Briquette wall test results

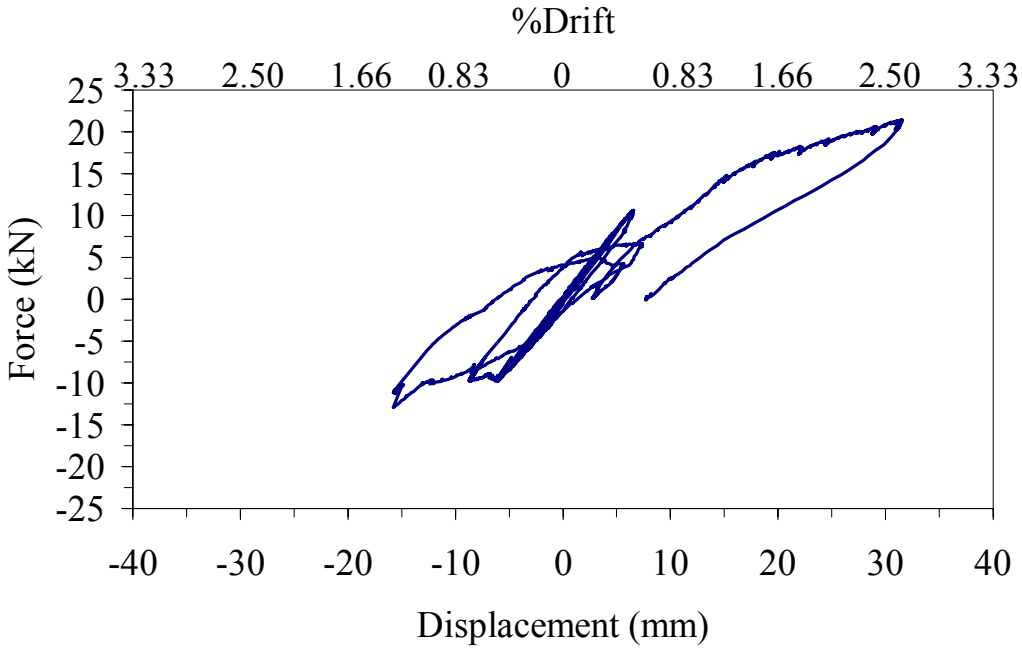

Figure 3.49 Briquette wall test results

During the second stage experiment, the axial post tensioning force remained reasonably constant in the linear range when lateral displacement was less than about 12.5 mm (see Figure 3.50 and Figure 3.52). After passing into the non-linear range,

the axial post-tensioning force measured by the load cell at the top of the wall began increasing proportionally to the lateral displacement increase. At the end of the cycle, the post-tensioning force decreased from 30 kN to 27 kN in the nonlinear range.

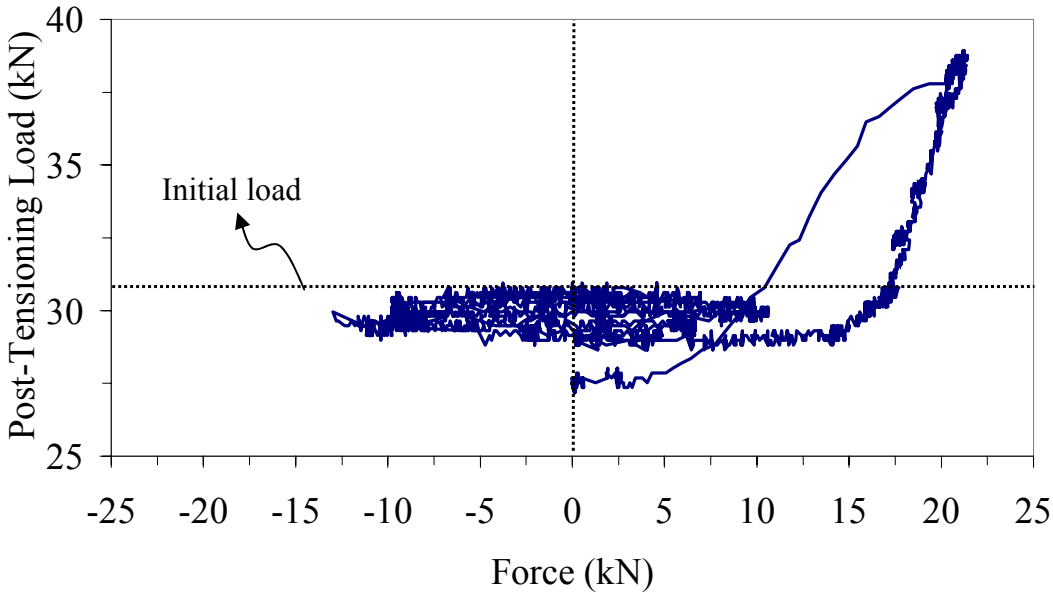

Figure 3.50 Axial Post-Tensioning Force versus Horizontal Load

(a) (b)

Figure 3.51 Crack formation during first briquette wall tests

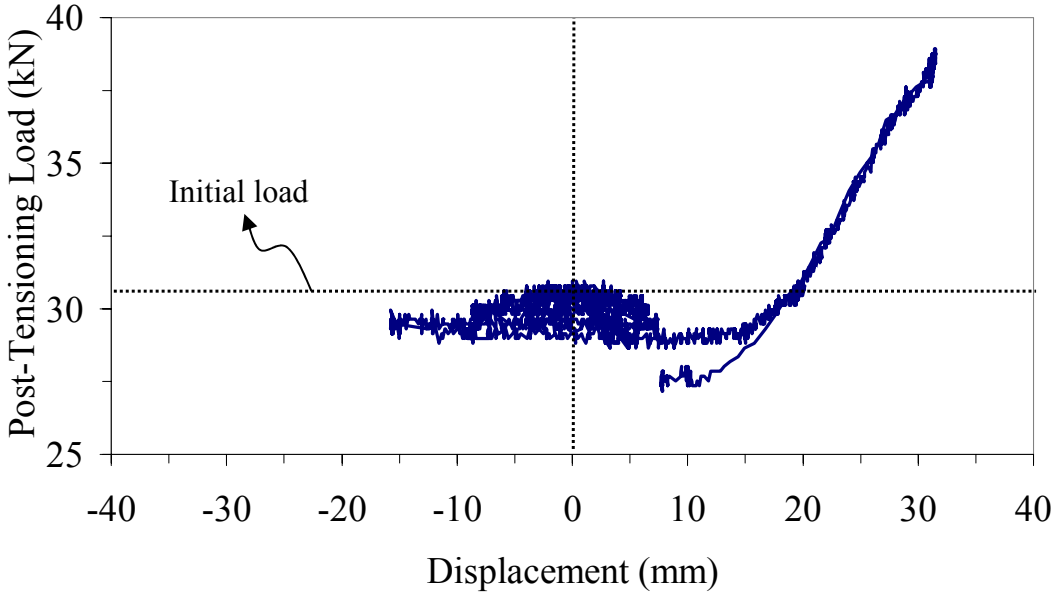

Figure 3.52 Axial Post-Tensioning Force versus Horizontal Displacement

3.2.10.Results of the second briquette wall test #2

The out-of-plane tests on the second briquette wall strip were conducted in three stages with 0, 30 and 50 kN post-tensioning load respectively. The post-tensioning load was applied on the wall in vertical direction by *hybrid system*.

The briquette wall showed linear behavior up to 1.5 kN lateral force at a lateral displacement of 0.34 mm, and using these values, the linear lateral stiffness of the wall was calculated as 4.41 kN/mm (see Figure 3.53). The ultimate nominal strength of the wall was measured equal to 3 kN under the lateral displacement of 1.615 mm. After the formation of small cracks at the middle mortar joint of the briquette wall, the test was stopped to prevent extensive damage of the wall.

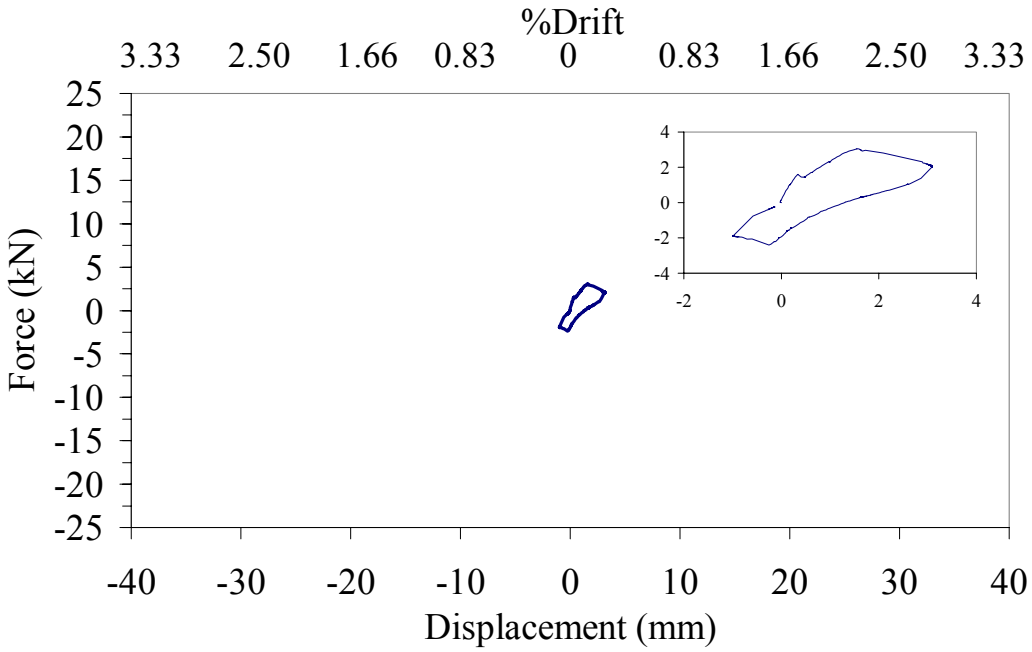

Figure 3.53 Briquette wall tests of stage#1

After that, the hybrid system wrapped on the wall was stretched until the post-tensioning force reached about 30 kN. The linear resistance capacity of the wall was measured as 10 kN at a lateral displacement of 2 mm. Using these values, the stiffness of the wall was calculated as 5 kN/mm. The cracks formed in the previous stage started to re-open when the wall went beyond the linear range. The maximum out-of-plane load resistance of the wall for this stage was measured as approximately 18 kN at a lateral displacement of about 20 mm. During the experiment, the post-tensioning force remained fairly constant up to the lateral displacement of 5 mm (see Figure 3.56) or lateral force of 10 kN (Figure 3.55). In addition, the applied post-tensioning force decreased from 33 kN to 27 kN.

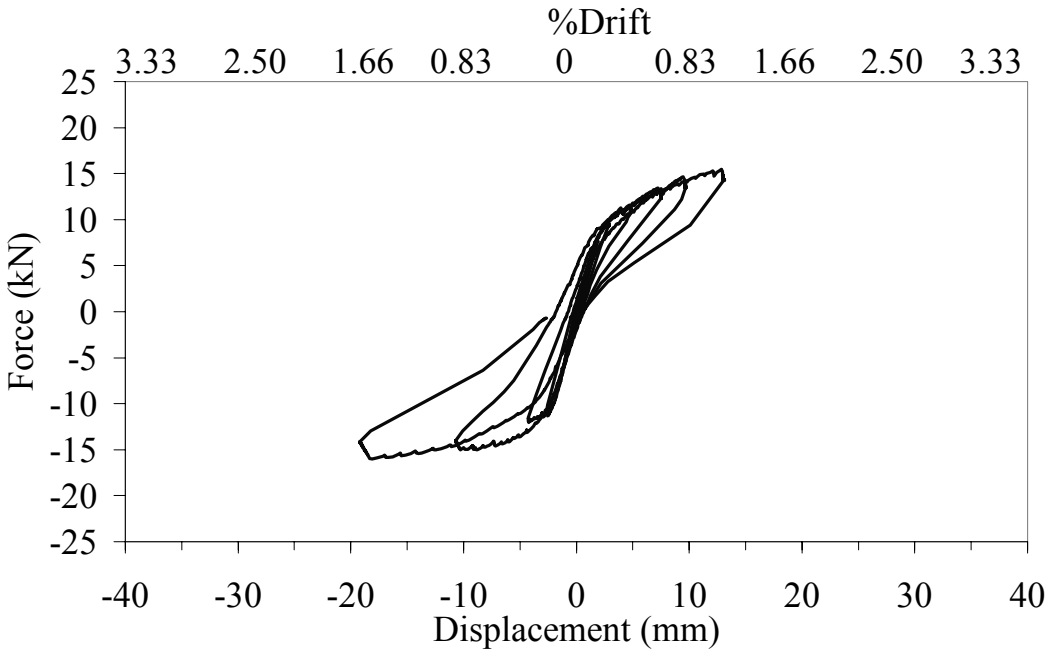

Figure 3.54 Briquette wall tests of stage#2

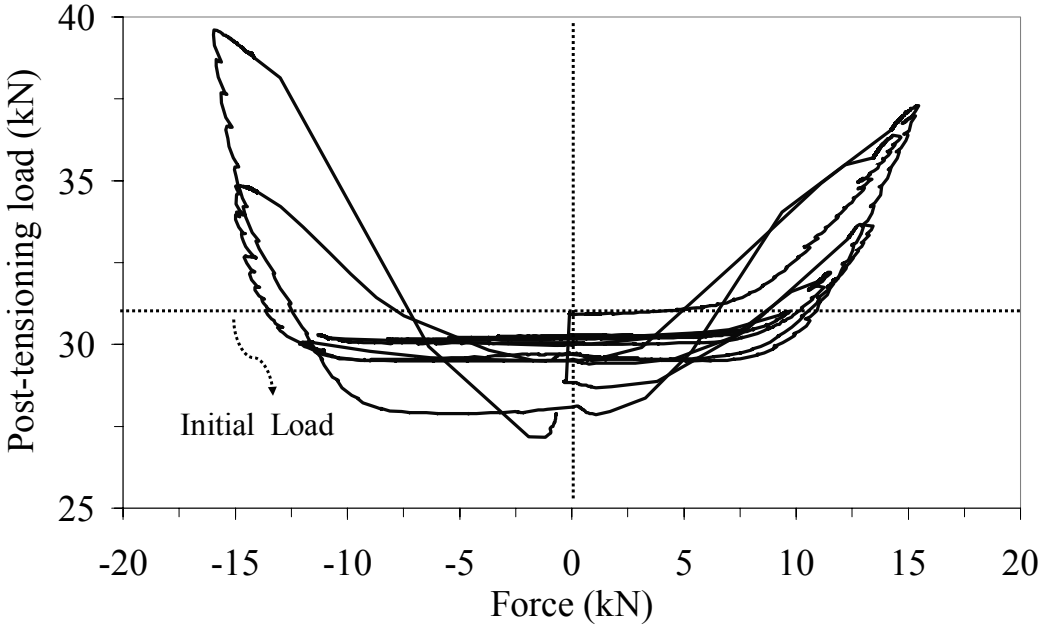

Figure 3.55. Axial post-tensioning force versus horizontal load of stage#2

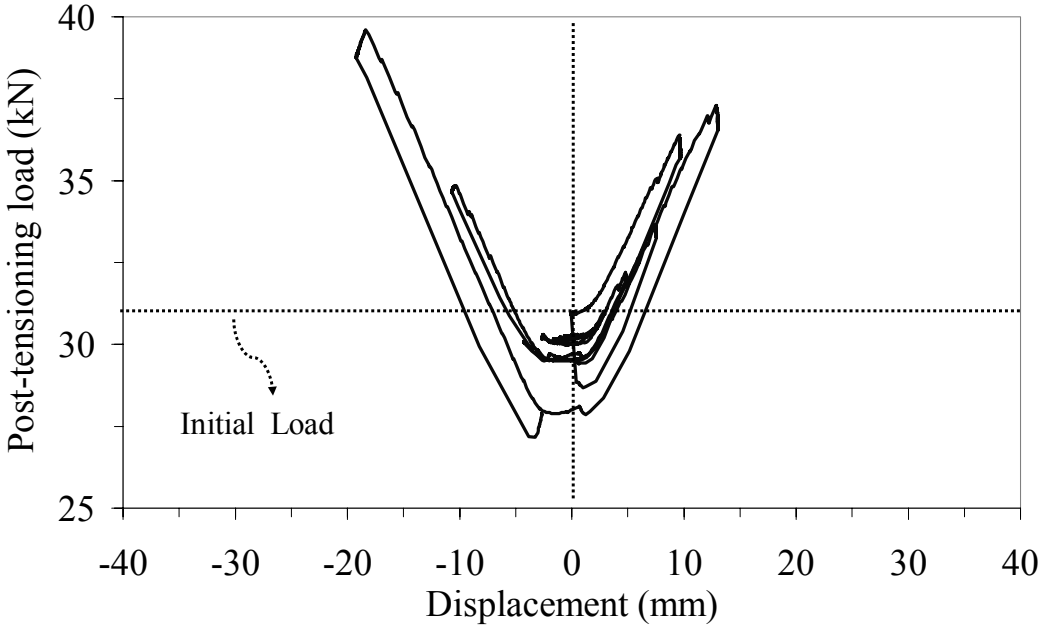

Figure 3.56 Axial Post-tensioning force versus horizontal displacement of stage#2

In the third stage, in order to investigate the behavior of the briquette walls under high post-tensioning force with respect to its compression strength capacity, the post-tensioning force on the wall was increased to about 50 kN. The wall failed prematurely, after the application of only two cycles. Large diagonal cracks were formed close to the bottom support indicating shear failure. The ultimate lateral load resistance capacity of the wall was measured as 20 kN in the positive direction. Diagonal shear cracks were formed at the lower part of the walls when the applied post-tensioning force decreased from 50 kN to 32.5 kN (see Figure 3.58 and Figure 3.59). Therefore, during the experiment, stable hysteretic loops similar to the ones from the previous test were not obtained.

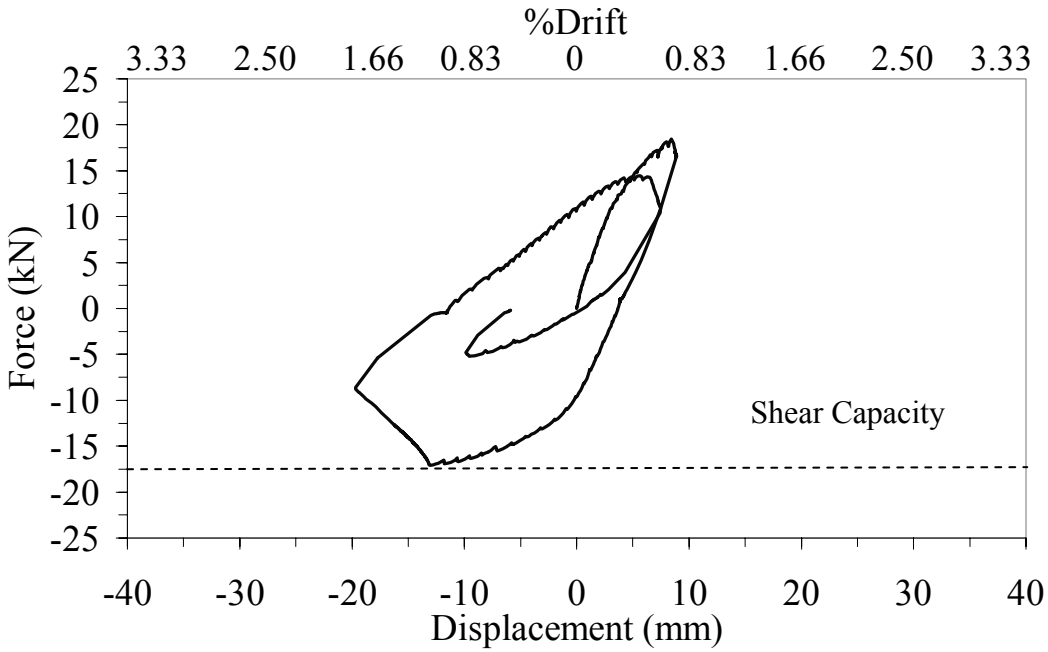

Figure 3.57 Briquette wall tests of stage#3

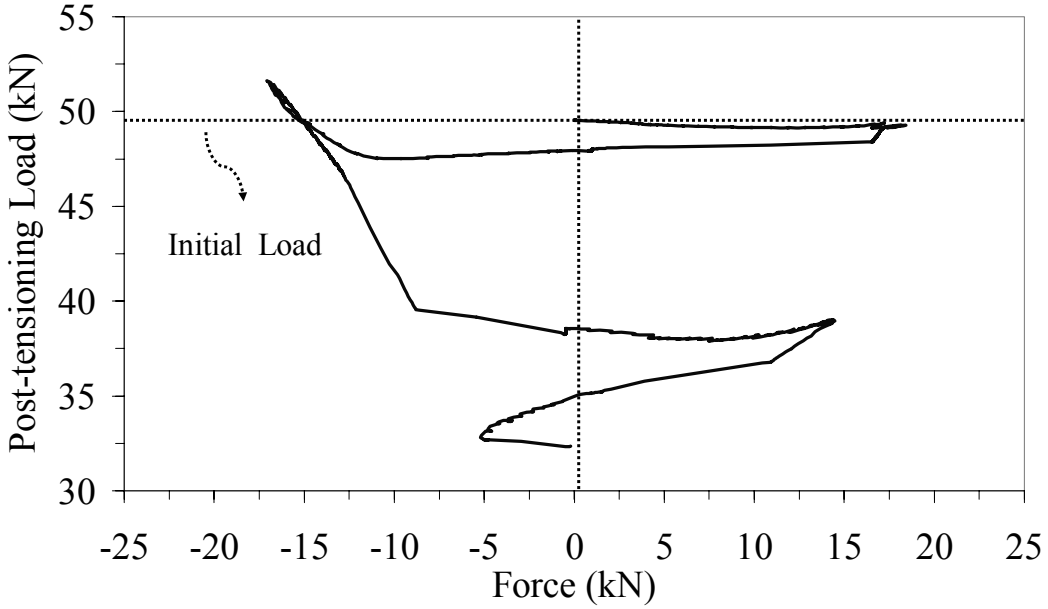

Figure 3.58. Axial post-tensioning force versus horizontal load of stage#3

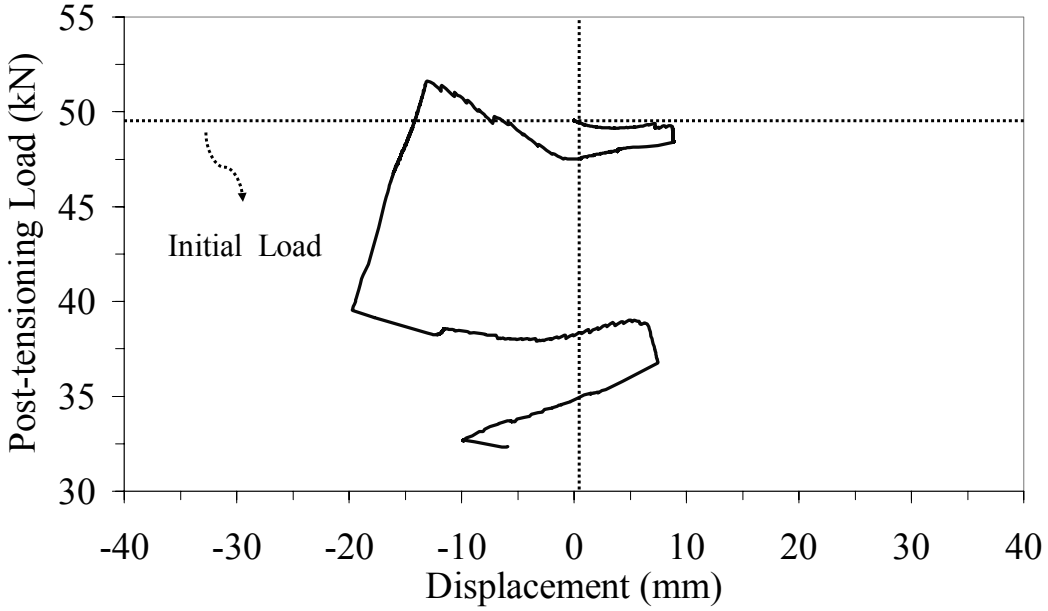

(b)

Figure 3.59 Axial Post-tensioning force versus horizontal displacement of stage#3

3.2.11. Discussion of the out-of-plane test results

The obtained data from the out-of-plane tests were discussed in the four parts as follow.

3.2.11.1.Maximum Lateral Force Capacities

The measured maximum out-of-plane force capacities of the brick and briquette walls in the out-of-plane direction are shown in Table 3.4 and Table 3.5. According to the obtained results, the nominal lateral load capacities of the brick walls can be increased to about 5.3 and 8.35 times by applying 50 kN and 100 kN axial post-tensioning force Table 3.4.

On the other hand, the nominal lateral load capacity of the briquette walls in the out-of-plane direction can be increased up to about 4 times by applying 30 kN axial post-tensioning force using STC and about 6 times using hybrid system (Table 3.5). However, the ultimate nominal strength of the first briquette wall (5.4 kN) was measured to be greater than that of the second briquette wall (3 kN). The ultimate capacities of strengthened briquette walls were within proximity.

Table 3.4. Maximum .out-of-plane force capacities of brick walls measured during tests

Brick Wall	Stage	Post-tension force (kN)	Maximum Resisting Force (kN)	Maximum Resisting Force value ratios (w.r.t. nominal)	Failure Modes
#1 (STC)	1	0	1.90	1.00	Bending
#1 (STC)	2	50	13.30	7.00	Bending
#1 (STC)	3	100	15.90	8.37	Shear
#2 (STC)	1	0	2.16	1.00	Bending
#2 (STC)	2	50	12.00	5.56	Bending
#2 (STC)	3	100	20.00	9.26	Bending
#3 (Hybrid)	3	100	22.80	-	Bending
#4 (Hybrid)	1	0	2.76	1.00	Bending
#4 (Hybrid)	2	50	9.23	3.34	Bending
#4 (Hybrid)	3	100	20.50	7.43	Bending

Table 3.5. Maximum .out-of-plane force capacities of briquette walls measured during tests

Briquette Wall	Stage	Post-tension force (kN)	Maximum Resisting Force (kN)	Maximum Resisting Force value ratios (w.r.t. nominal)	Failure Modes
#1(STC)	1	0	5.40	1.00	Bending
#1(STC)	2	30	21.50	3.98	Shear
#2(Hybrid)	1	0	3	1.00	Bending
#2(Hybrid)	2	30	18	6.00	Bending
#2(Hybrid)	3	50	20	6.67	Shear

It can be concluded form the result given in Table 3.4 and Table 3.5 that the maximum out-of-plane load capacity of the wall was increased by using either STC

or hybrid system similarly.

3.2.11.2. Flexural Rigidity Changes

Theoretically, the amount of applied post-tensioning force in the linear range is not expected to have any effect on the flexural rigidity (i.e., EI) of the section, since the same bending action takes place at a larger level of compression field. EI is commonly recommended to be used constant in codes (e.g., TSE 500). If the compressive stress is beyond linear range of material, concrete and mortar like materials are expected to have reduction in their modulus of elasticity (E) which would cause reduction in the EI value. On the other hand, experimental studies have shown that reinforced concrete columns would have increased EI values as the axial load gets closer to the axial load capacity [30]. This behavior is attributed to the confinement effect of ties in R/C columns.

The effective flexural rigidity values (EI) are calculated using the out-of-plane bending test results of six strip walls were calculated for all loading stages and given in Table 3.6 and Table 3.7. Although, all of the walls were constructed by the same mason, the EI values of the brick and briquette walls in testing stage #1 (zero axial load) were not constant among themselves. The main reason for the differences in the first stages can be attributed to the deficiency of rate of loading. The hydraulic jack was difficult to operate and application of small forces at the beginning of the test was not identical. In addition, the material quality of the walls, amount of used mortar (thickness and width) would influence the EI values each nominal strip wall.

Although the mortar layers located at the middle section of the strip walls were cracked in the first stage of wall tests (except test #3) and no repair work has been done (e.g., injecting grout, plastering, etc.) the EI values of the sections were not reduced to zero due to the application of the post-tensioning force. The even compressive stress field generated by the post-tensioning causes bending stresses to remain in compression preventing development of tensile stress. At the lack of tensile stresses, the crack would not open and continue to transfer compressive and shear stresses.

Table 3.6. Linear Range Load-deflection values obtained in bricks wall tests

Brick Wall	Stage	Post-tension force (kN)	Initial crack displacement (mm)	Initial Crack Force (kN)	Experimental EI values (108*kN.mm2)	Experimental EI value ratios (w.r.t. nominal)
#1	1	0	0.35	1.21	9.57	1.00
#1	2	50	1.06	5.25	13.90	1.45
#1	3	100	1.50	6.34	11.87	1.24
#2	1	0	0.40	1.10	7.72	1.00
#2	2	50	1.25	5.18	11.64	1.51
#2	3	100	2.07	9.82	13.32	1.73
#3	3	100	1.19	13.40	31.73	-
#4	1	0	0.41	2.01	13.94	1.00
#4	2	50	1.06	5.32	14.08	1.01
#4	3	100	1.56	9.14	16.46	1.18

Table 3.7. Linear Range Load-deflection values obtained in briquette wall tests

Briquette Wall	Stage	Post-tension force (kN)	Initial crack displacement (mm)	Initial Crack Force (kN)	Experimental EI values (10^8*kN.mm^2)	Experimental EI value ratios (w.r.t. nominal)
#1	1	0	0.27	1.00	9.09	1.00
#1	2	30	2.38	10.68	11.01	1.21
#2	1	0	0.34	1.50	10.82	1.00
#2	2	30	2	10.00	12.27	1.13

3.2.11.3. Stiffness Changes

The stiffness values of four bricks wall tests in stage #2 and #3 were computed by taking the initial linear slope of force vs. displacement graphs of each cycle. Then, the drift ratios, which is the mid point lateral displacement divided by the mid point to support distance, are calculated for each cycle by taking the average value of maximum displacements in negative and positive directions for each cycle. The stiffness versus the drift ratio graphs are obtained and shown in Figure 3.60 and Figure 3.61 for 50 kN and 100 kN, respectively.

In each cycle, additional cracks and crushing were formed in the mortar layer, hence the effective moment of inertia of the wall decreased. This result caused the stiffness of the wall in the next cycle to decrease as in Figure 3.60 and Figure 3.61.

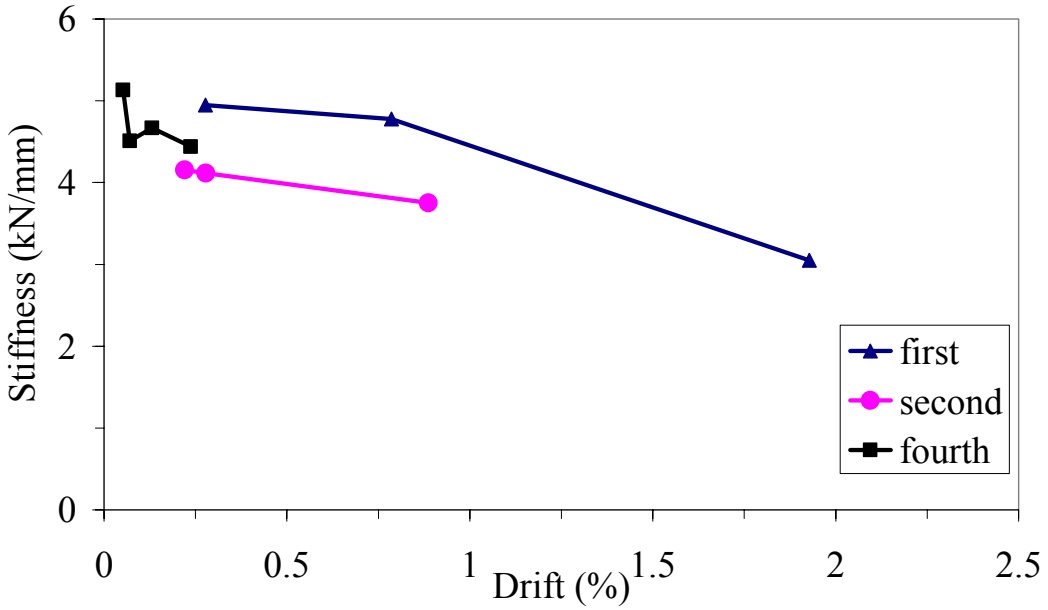

Figure 3.60 Stiffness vs. Drift (%) graphs of bricks walls under 50kN axial load

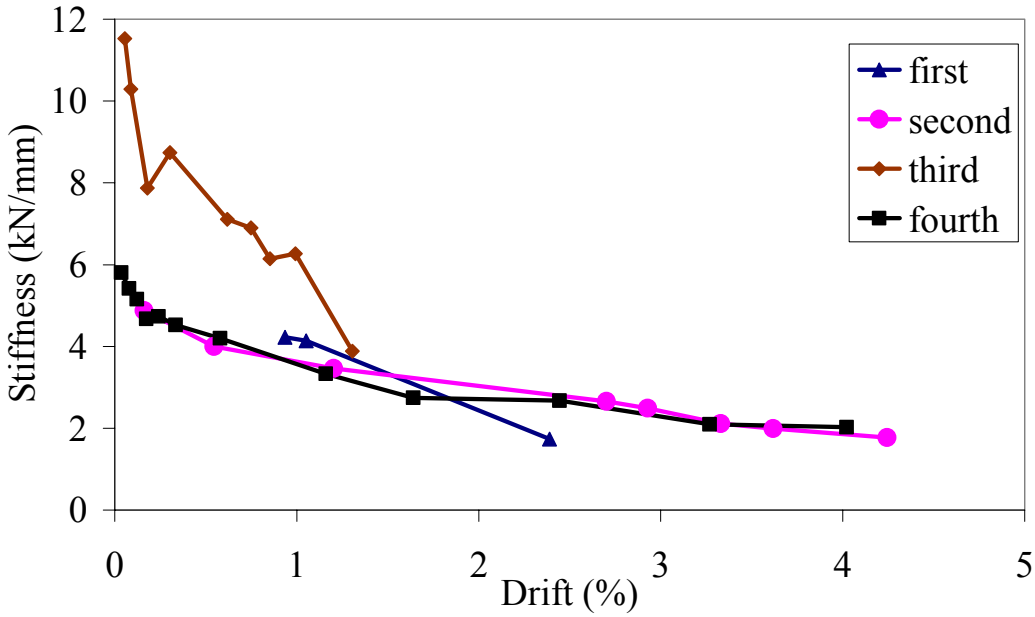

Figure 3.61 Stiffness vs. Drift (%) graph of bricks walls under 100kN axial load

Different from other wall tests, the third brick wall test was conducted as one stage only, under 100 kN of post tensioning load. As no crack and crushing were induced on the mortar layer of the wall prior to testing, the stiffness values of the wall for each cycle were found to be higher than others under drift ratios less than 1% (see Figure 3.61). When the drift ratio with the cycle number increases, the stiffness of the third wall becomes similar to others (Figure 3.61)

3.2.11.4.Energy Dissipation and Damping

The energy dissipation of each cycle of brick wall test results were calculated by considering the enclosed area (E_D) of each hysteretic loop as shown in Figure 3.62. The strain energy, which is dissipated in each cycle of motion (Figure 3.62), is calculated using Equation 3.2 [31].

$$E_{so} = \frac{k * u_o^{\,2}}{2} \tag{3.2}$$

The dissipated energies (E_D) of each cycle obtained from the experiments results are calculated for 50 kN and 100 kN post-tensioning load stages and plotted against the drift ratio corresponding to each cycle in Figure 3.63 and Figure 3.64, respectively. From these figures, it can be concluded that, the energy dissipation of the walls increase as the number cycles and drift ratios increase.

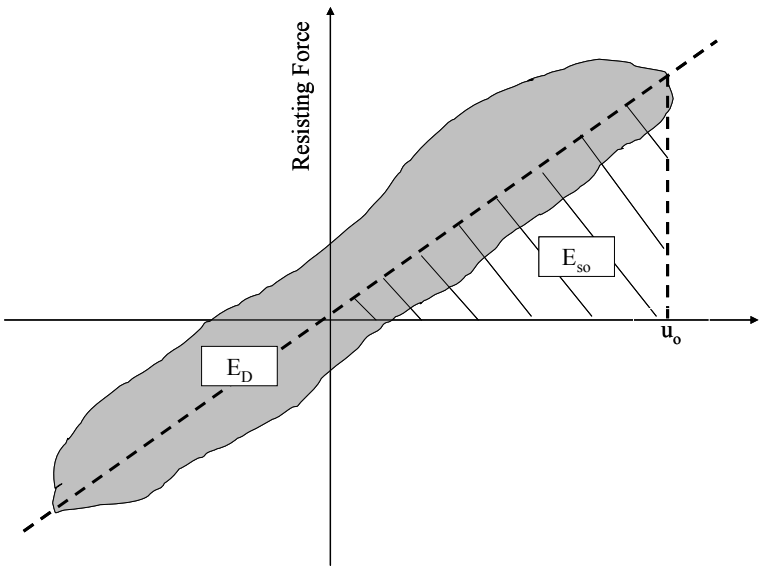

Figure 3.62 E_D in a cycle of hysteric loop and maximum strain energy

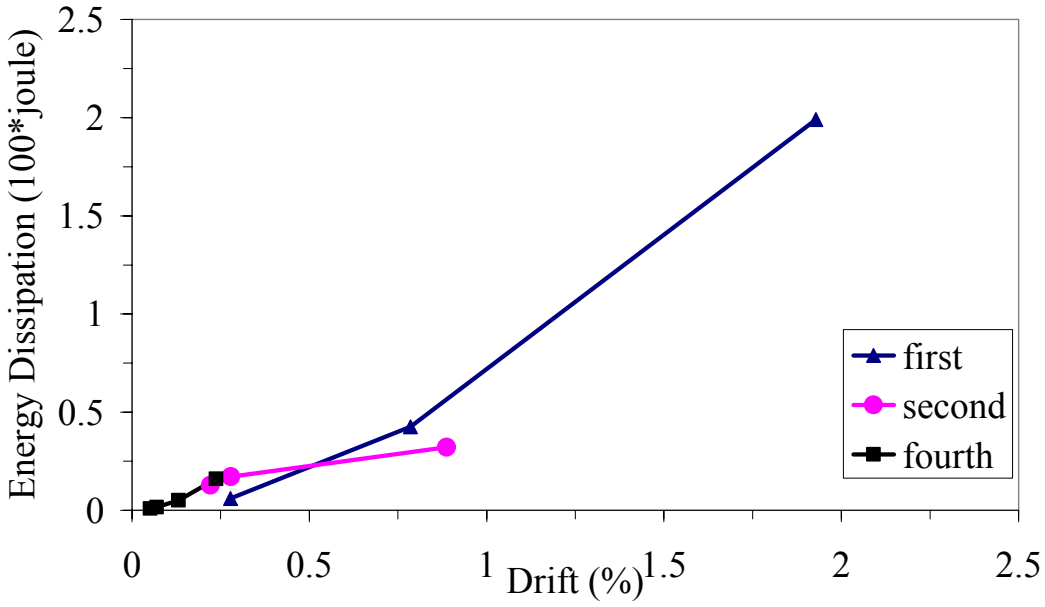

Figure 3.63 E_D vs. Drift ratio (%) graphs of bricks walls under 50kN axial load

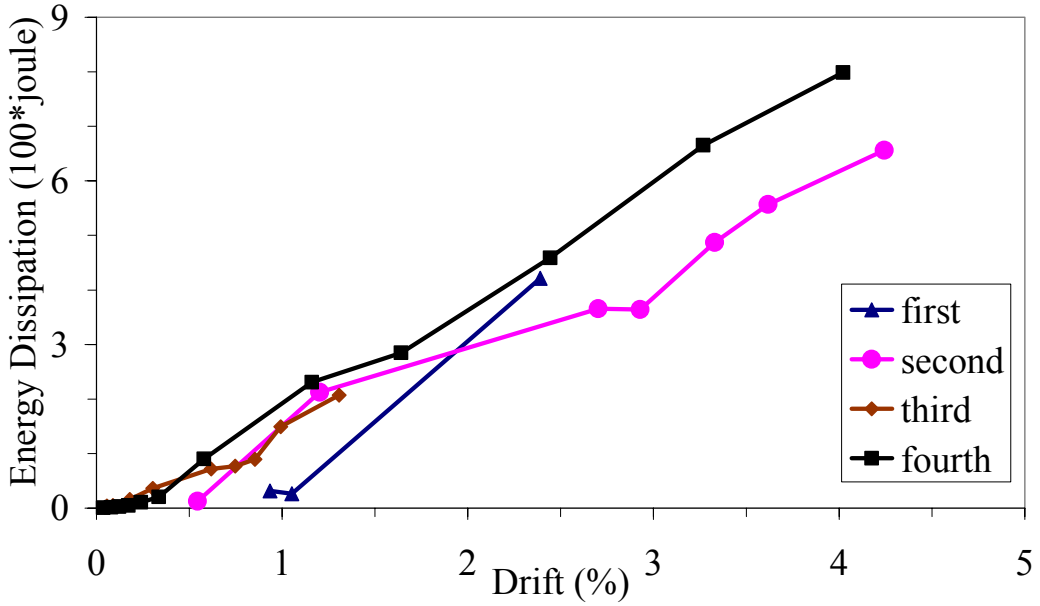

Figure 3.64 E_D vs. Drift (%) graph of bricks walls under 100kN axial load

Specific damping ratio, ξ, is calculated using Equation 3 [31] for each hysteric loop of the brick wall test results and plotted for 50kN and 100 kN tests in Figure 3.65 and Figure 3.66, respectively.

$$\xi = \frac{1}{2\pi}\frac{E_D}{E_{SO}} \tag{3.3}$$

The damping ratios of the walls are inconsistent for the 50 kN tests, but 100 kN axial post tensioning test results reveal that the specific damping factors tend to increase as the cycle numbers and drift ratios in each cycle increases.

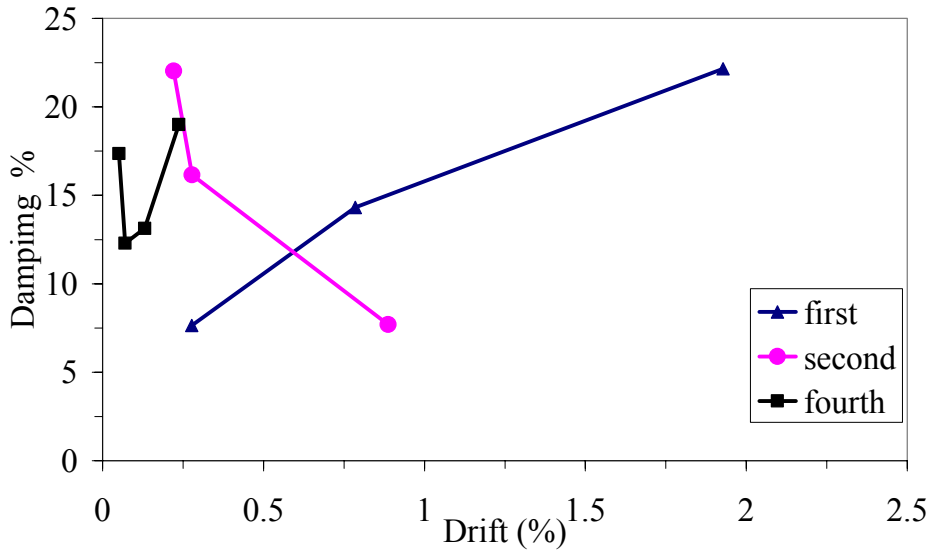

Figure 3.65 Damping vs. Drift (%) graph of bricks walls under 50kN axial load

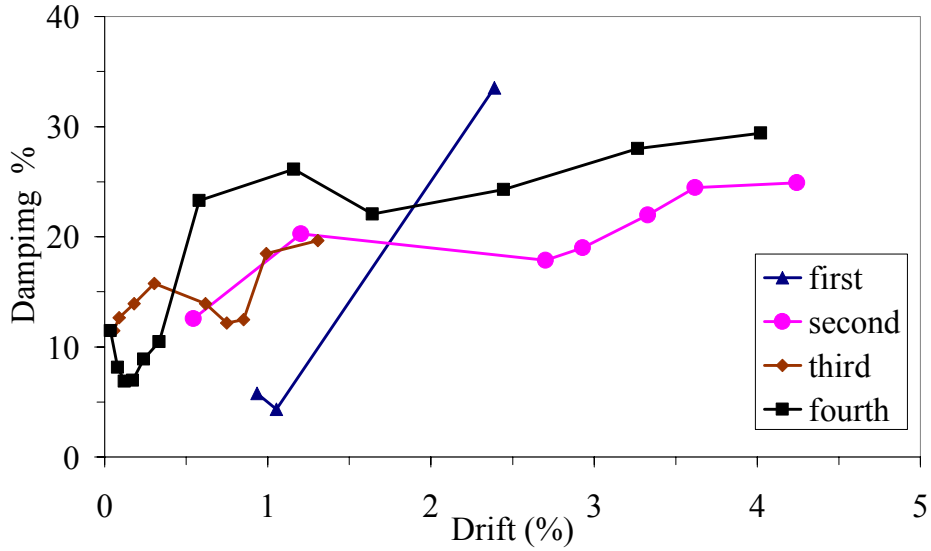

Figure 3.66 Damping vs. Drift (%) graph of bricks walls under 100kN axial load

3.3.TILTING TABLE FULL-SCALE MASONRY TESTS

3.3.1. Test Specimens

Two full scale one-storey masonry houses with identical dimensions of 3m x 4m x 2.40 m width, length, and height, respectively were constructed by an experienced mason on the tilting table. Following the construction, the walls of the masonries were covered with 5mm-thick gypsum to easy identification of crack formation and locations. Both constructed masonry houses were similar to each other and had a single room with two windows and one door (see Figure 3.67).

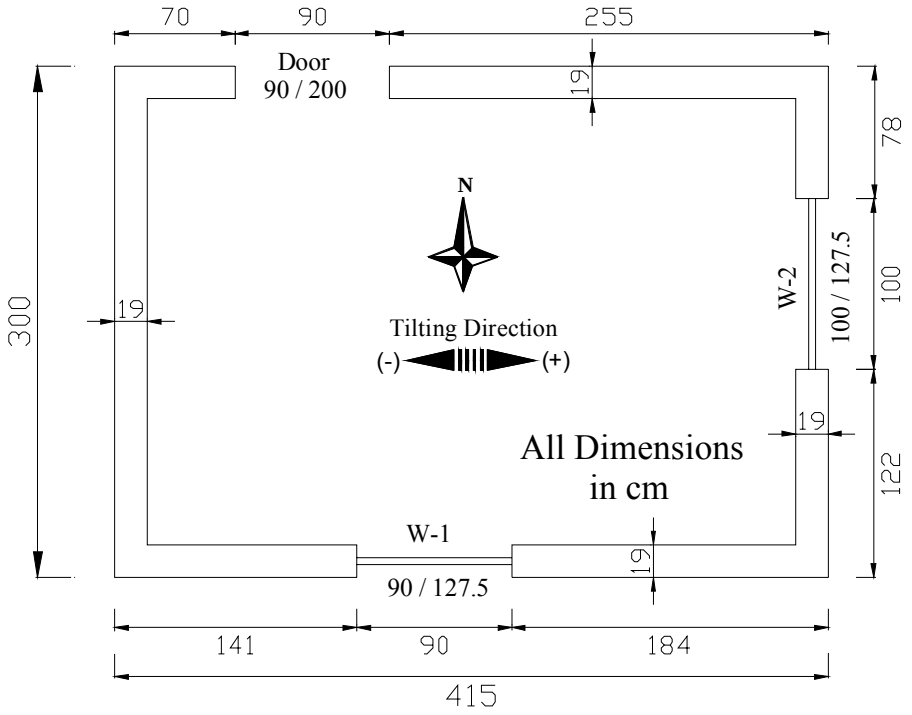

Figure 3.67 Plan view of masonry house

Figure 3.68 Masonry house roof construction

In order to simulate the weight of the roofs found in practice, both models were subjected to 55 kN roof weight carried by five INP-260 sections on reciprocal walls in the tilting direction (Figure 3.68). In the unstrengthened model, sand bags were used as a substitute of the soil-type roof mass in practice; whereas, in the strengthened model, two concrete blocks were used to substitute the same mass for simplicity of placement-removal process and also to provide additional security during the test. The second specimen was post-tensioned by applying Sacs in vertical and horizontal directions (9 Sacs in vertical and 1 STC in horizontal direction). The application of bi-directional post-tensioning was determined after examination of the damage pattern of the first original model test (see Figure 3.75 and Figure 3.76). The strengthening operation in both directions was applied as follows.

- 1.5 bricks were extracted from the bottom end of the wall.
- In order to reduce stress concentration on the tire, half-circular wooden logs were placed in the created gap at the bottom and the top end of the wall.

Both wooden logs were adhered to the wall with cement paste.

- The Sacs were then passed through the gap bellow the bottom wooden log and above the top wooden log, thus wrapping the wall. The post-tensioning load of 50 kN, imposed on the walls was determined using Equation 3.1 (Section 3.2.5), and was applied by turning the bolts of the STR connectors.
- 8-half-circular logs were placed on the upper sides of the wall each corners and horizontal STC are post-tensioned over those logs to eliminate stress concentrations at the corners of the house (see Figure 3.69).
- The STC is then stretched up to 25 kN in the horizontal direction along the periphery of the house close to the roof level (see Figure 3.69).

Figure 3.69 Strengthening operation of the test specimen

3.3.2.Test Setup and Instrumentation

In order to scrutinize the effect of earthquakes forces on a masonry house, a powerful steel tilting table setup was constructed in the Structural Laboratory of METU. The tilting table can be inclined in two directions via a central piston with capacity of 700 kN (see Figure3.70). The direction of the tilting is controlled by the pins of the table located at either side of the table as shown in Figure3.70. During the experiment, the total collapse of the house is prevented by the safety shields constructed to protect the laboratory equipment and personnel from an abrupt collapse. On the other hand, the shields do not touch to the house and do not prevent the specimens from a collapse. Tilting table is designed to tilt 45^{o} on either side and apply lateral acceleration of 0.71g.

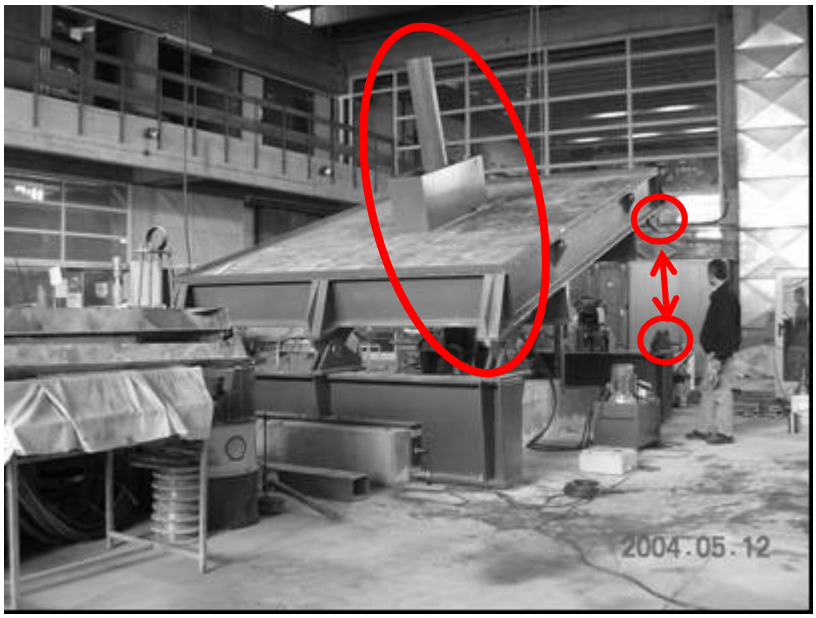

Figure3.70. Tilting Table

In order to measure the deflections of the walls in the out-of-plane and in-plane directions ten displacements transducers (Lads), six of which have 200mm stroke length and four of which have 500m, were used.

Two Lads of 200 mm stroke were placed on the foot corners to measure the slope values during the tests. A 16-channel data acquisition system was used for the measurement of the generated test data. The twelve Lads measured simultaneously at a sample rate of five samples per second (5 Hz) throughout the whole test.

3.3.3.First Model: Unstrengthened Masonry Test

The test of the first model was conducted with the aim of investigating the behavior of unstrengthened full-scale masonry building exposed to cyclic static loading test simulating earthquake acceleration given in Figure 3.71. The measured displacement values of walls in the in-plane and out-of-plane directions are given in Figure 3.72 (a)&(b), and Figure 3.73(a)&(b) respectively.

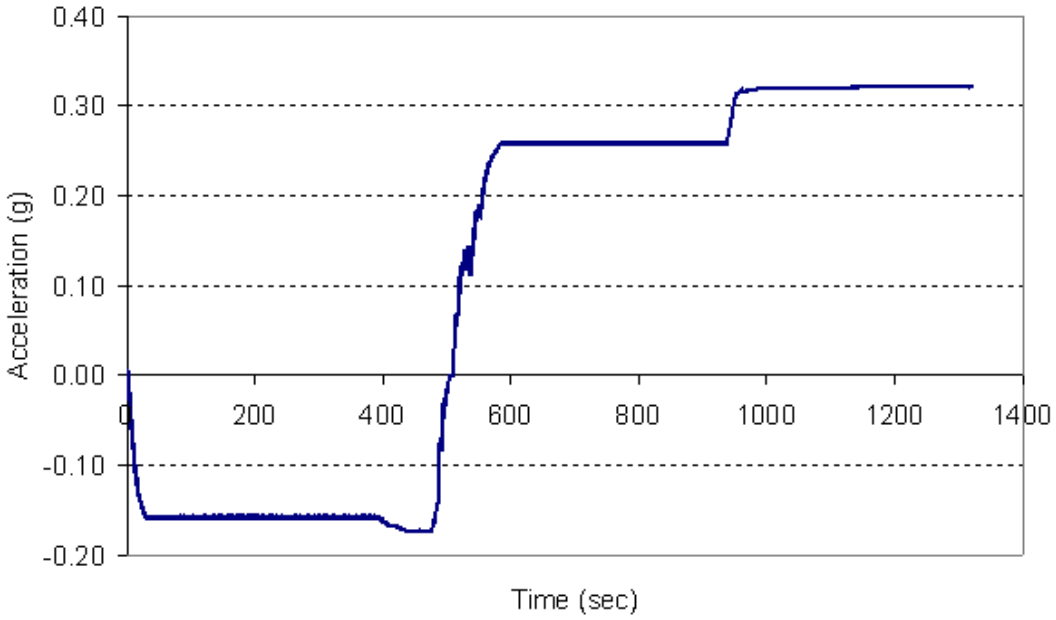

Figure 3.71 Applied acceleration value Model #1

The weight of the roof is carried by five INP-260 sections placed on two reciprocal walls in tilting direction. During the experiment on the tilting table, the lateral load from the roof is transferred onto the walls in out-of-plane direction as a function of

sinus of the tilt angle. The walls that are exposed to lateral load in their out-of-plane direction experience bending in their weak directions. The load is transferred from out-of-plane walls to the support and dominantly to the adjacent orthogonal walls. The orthogonal walls carry the load in their in-plane direction and shear stress (tensile stresses in principal direction) concentrations develop especially around the corners of the doors and windows (see Figure 3.74).

The walls of the unstrengthened masonry house showed linear behavior until the model collapsed suddenly at 18.8 degree of tilting referring to a lateral acceleration of 0.31g in the positive tilting direction.

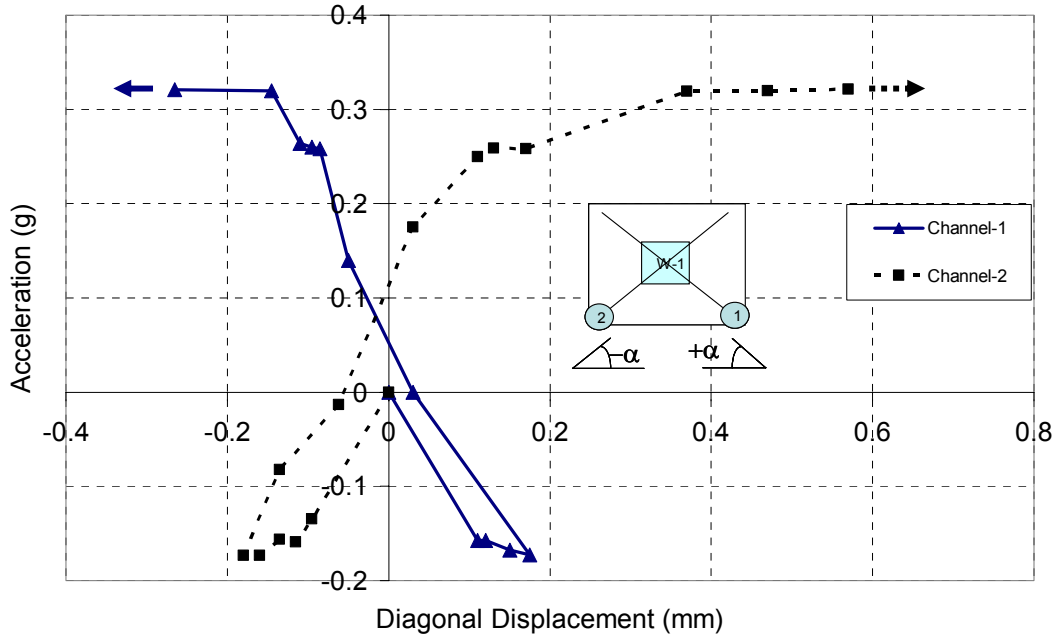

(a)

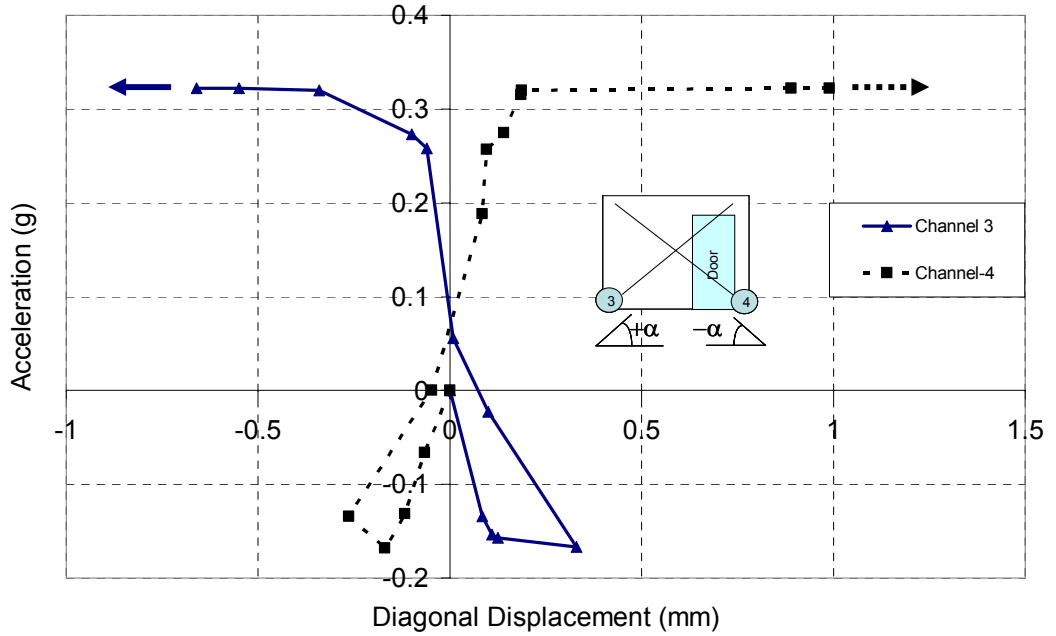

(b)

Figure 3.72 Bi-diagonal acceleration vs. in-plane diagonal displacements (Model #1)

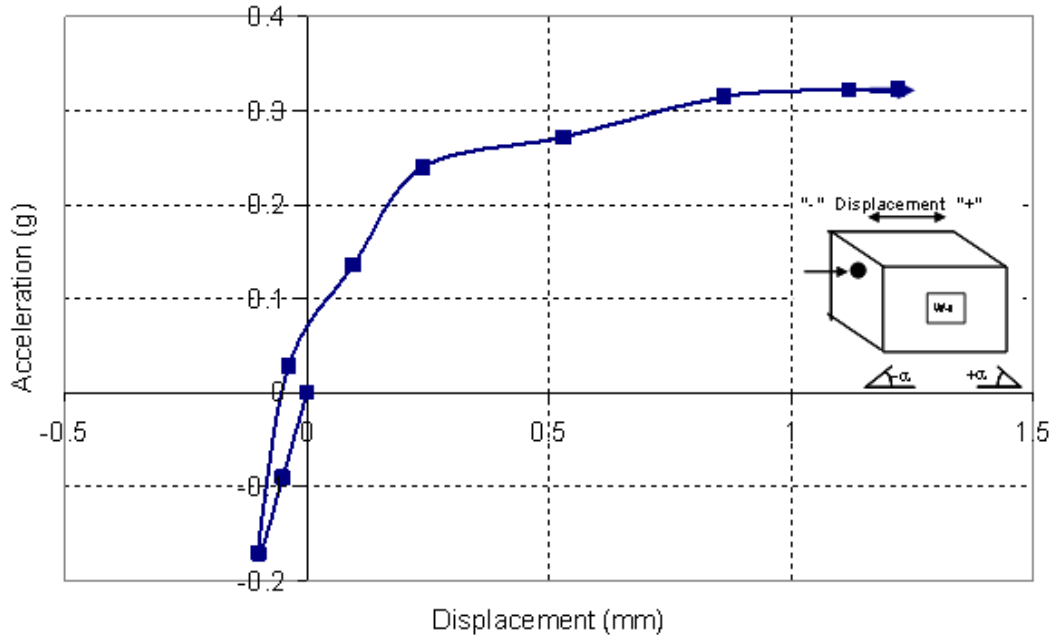

(a)

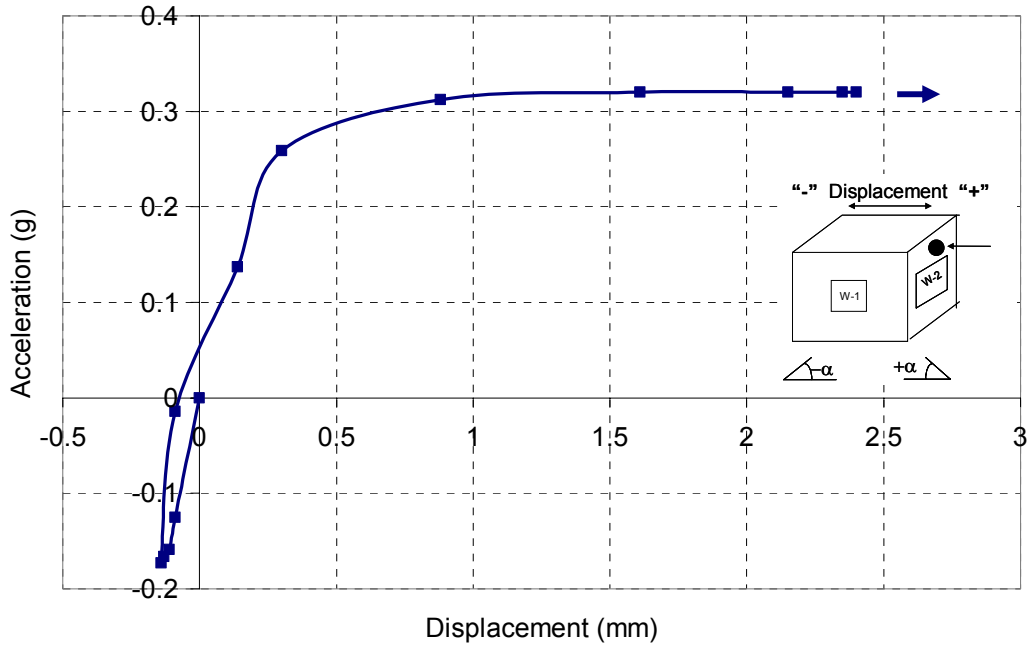

(b)

Figure 3.73 Bi-diagonal acceleration vs. out-of-plane diagonal displacements (Model #1)

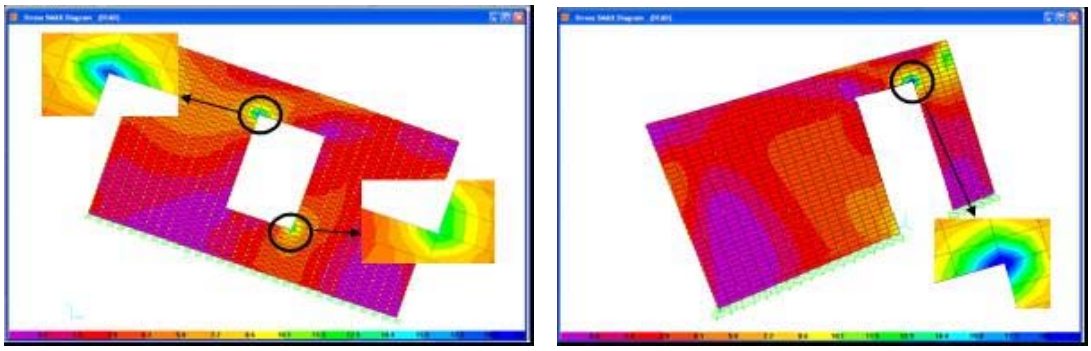

Figure 3.74 Shear Stress Distribution on in-plane walls

No clear crack formation was observed on the surface of masonry walls prior to the sudden collapse. With the increase of the value of the applied lateral force, the wall displacements increased linearly up to the collapse of the structure showing brittle behavior due to the characteristics of the used material in the construction of the model.

The measured displacements (Figure 3.73), in the elastic range, of walls in the out-of plane direction were approximately two times greater than the displacements in the in-plane direction (Figure 3.72). The deflections of the walls bending in out-of-plane direction were added on in-plane wall deformations; therefore, out-of-plane deflections are always expected to be larger than the in-plane wall deformations.

The crack formations commenced around the corners of the window and the door when the level of the shear stress reached to the limits of the walls in the in-plane direction (see Figure 3.75) and progressed diagonally. The failure of in-plane walls exposed the out-of-plane walls to an increased load and deformation demand beyond their limits thus leading to a sudden and progressive total collapse of the house. The crack formations following the collapse of the masonry house are shown in Figure 3.75 and Figure 3.76.

Figure 3.75 Diagonal Cracks on in-plane walls (Model #1)

Figure 3.76 Diagonal Cracks on out-of-plane walls (Model #1)

3.3.4. Second Model: Strengthened Masonry House

The in-plane and out-of-plane effects of post-tensioning on masonry walls are theoretically explained in Figure 3.77 and Figure 3.17, respectively. The vertically and horizontally applied post-tensioning loads change the normal stress values of points A and B toward A^1 and B^1 generating a general compression field reducing tensile stresses. As the shear stresses are increased, the location of A^1 and B^1 are shifted towards A^2 and B^2 until the Mohr-circle reaches to the tensile stress capacity of the material in the principal direction (Figure 3.77).

The effect of application of post-tensioning load on the walls in out-of-plane direction is explained in Section 3.2.3 and experimentally proven in sections between 3.2.5 and 3.2.10.

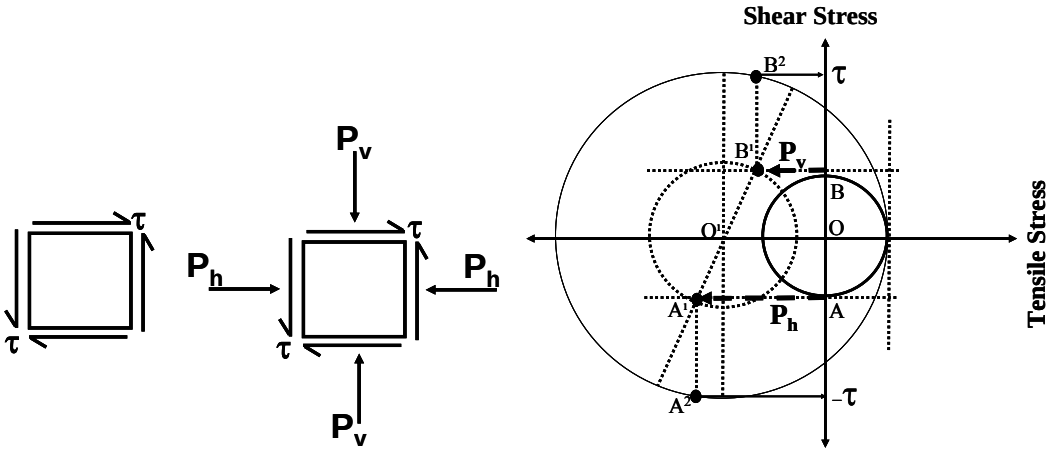

Figure 3.77 Mohr circle representation of post-tensioning

The position of the post-tensioned forces applied on the walls of the second model by Sacs in Figure 3.78 were determined by the results of previous experiments where shear stress concentration for in-plane walls and bending moment concentration for out-of-plane walls were maximum (see Figure 3.74, Figure 3.75 and Figure 3.76). 50 kN and 25 kN post-tensioning force were applied on the walls in the vertical and horizontal directions respectively. The magnitude of post-tensioning force was determined according to the strength properties of materials (i.e., STR, brick and mortar) and out-of-plane test results.

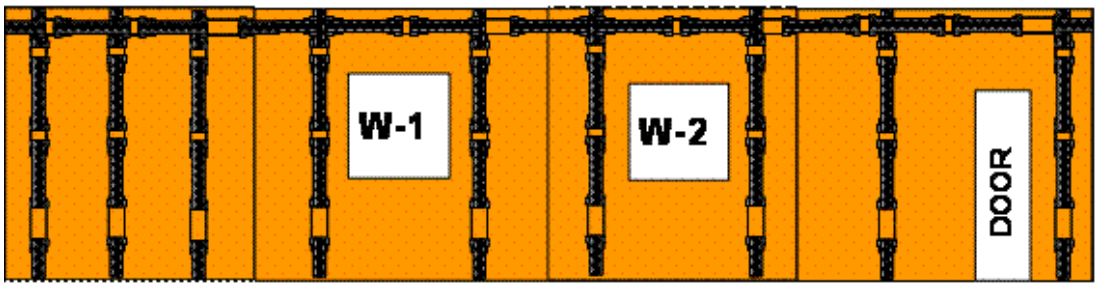

Figure 3.78 Location of Sacs on the masonry walls

The second model (strengthened using scrap tires) was subjected to inclined loading of gravitational acceleration at all points of the house to statically simulate the lateral earthquake forces. The applied lateral acceleration graph is shown in Figure 3.79, using the tilting table. The model resisted tilting up to 34.4 degrees which was equivalent to 56% of the gravitational acceleration (i.e., 0.56 g) about 75% larger

compared to the original house. The measured diagonal displacement values of the in-plane and bending displacement values of out of-plane walls are given in Figure 3.81(a)&(b) and Figure 3.80, respectively. The out-of-plane displacement values of the east wall were not taken in the test of the second model because of problems experienced with the LVDT during the experiment. The cracks pattern formation of shear and out-of-plane walls are illustrated in Figure 3.82.

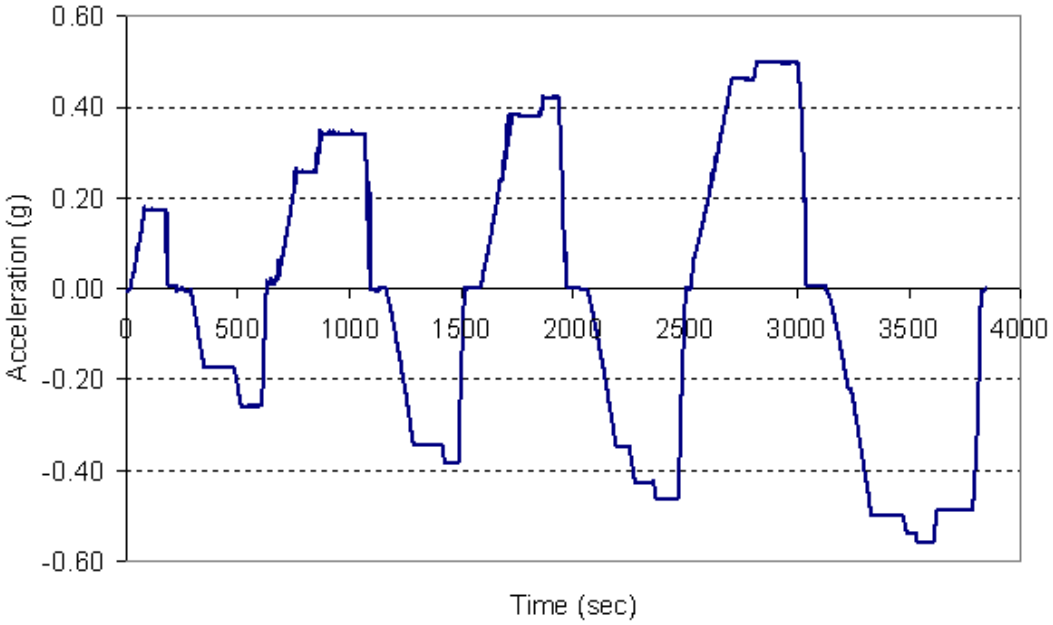

Figure 3.79 Applied acceleration value Model #2

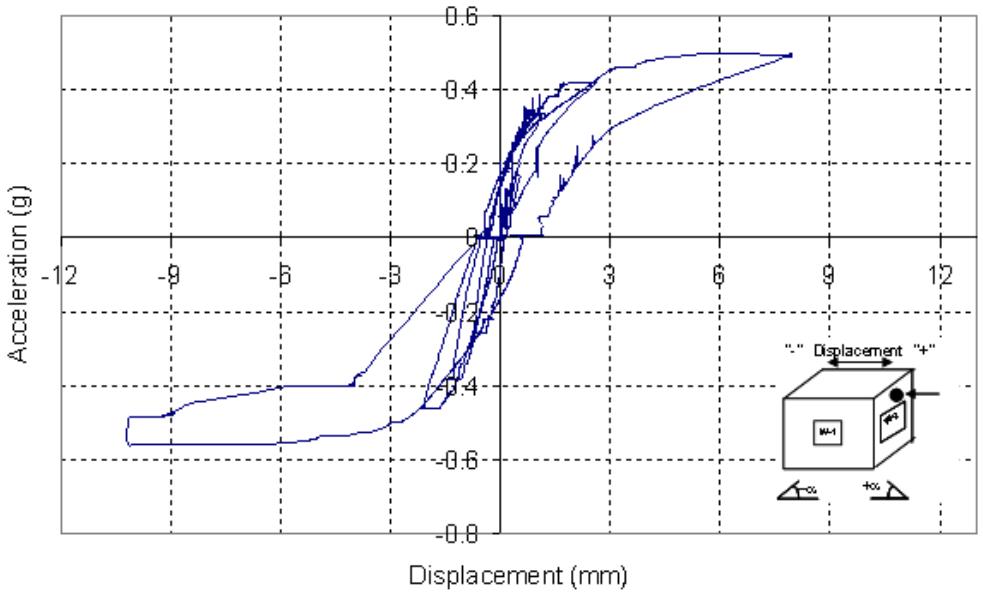

Figure 3.80 Bi-diagonal acceleration vs. out-of-plane diagonal displacements (Model #2)

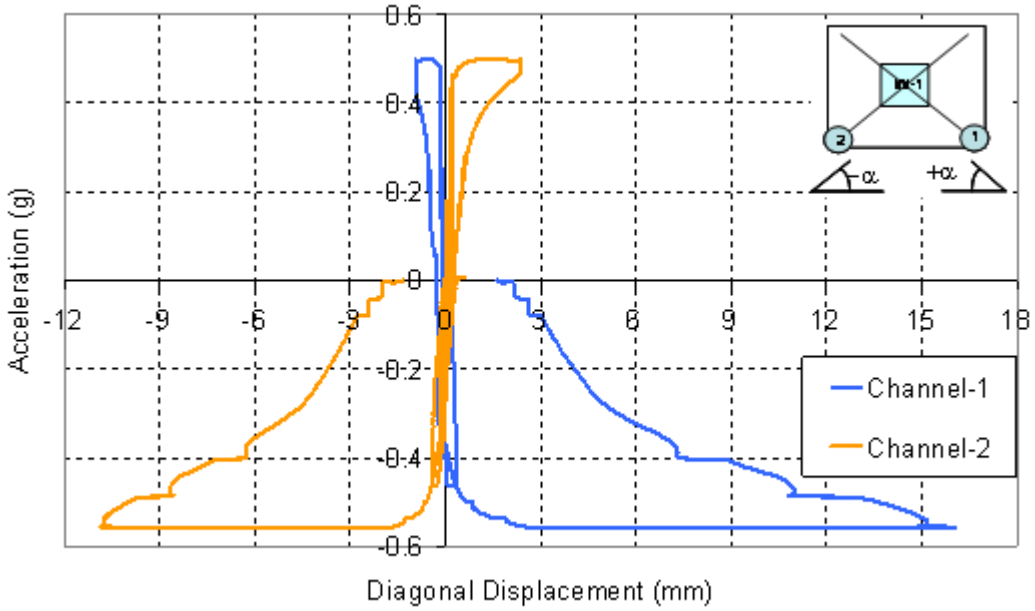

(a)

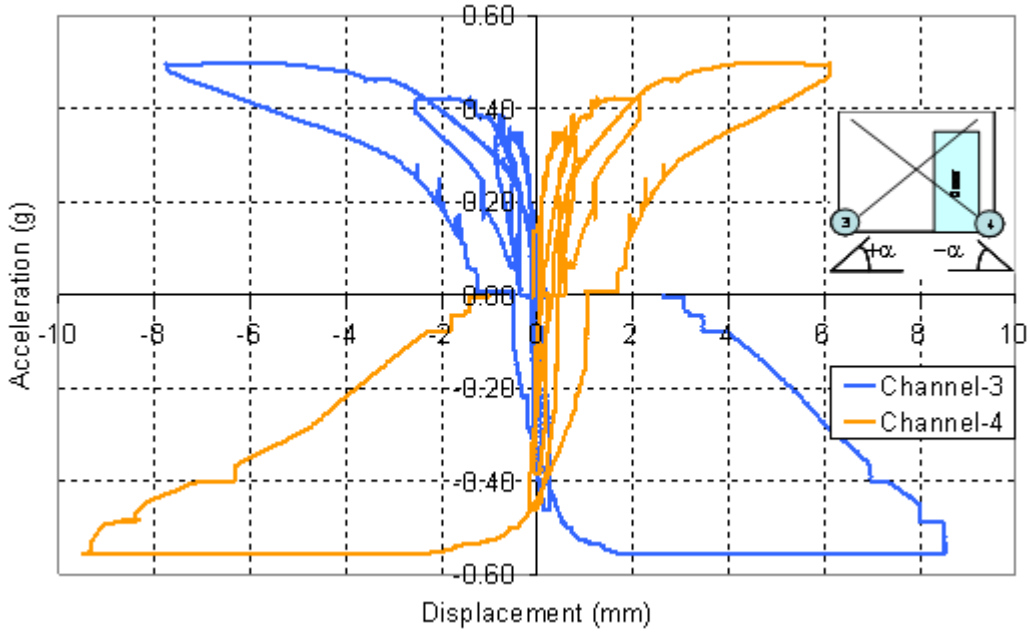

(b)

Figure 3.81 Bi-diagonal acceleration vs. in-plane diagonal displacements (Model #2)

Figure 3.82 Crack pattern formations during the experiment (Model #2)

3.3.5. Discussion of results

The first model, subjected to 0.32 g lateral acceleration, collapsed suddenly, whereas the second model did not collapse and endured acceleration of 0.56g. In other words, the strength of the masonry walls, post-tensioned by Sacs in the vertical and horizontal directions, was enhanced by 75%.

Applied post-tensioning forces altered the directions of the cracks of the second (strengthened) model. Moreover, the cracks were much smaller in numbers and size compared to the first model. They were mostly concentrated at the base and under windows while in the first model the wall cracks were very large and located at all levels, especially in diagonal direction around the corners of the window and the door. It is also important to note that, when the table was brought back to initial

condition, all cracks were closed and the house was returned to its original shape due to the elastic post-tensioning effect of scrap tires.

During the tilting experiments, the in-plane load carrying walls acted as supports to the walls which carry load in out-of plane direction. The entire roof load was successfully transferred from the out-of-plane direction walls to the in-plane direction walls. The collapse of the walls being loaded in out-of-plane direction were strengthened by vertical and horizontal post tensioning preventing any premature failure. The in-plane walls were also strengthened by post-tension in vertical and horizontal directions. The large diagonal cracks in in-plane direction were prevented and failure of the second test was governed by a rigid body motion as the walls started to separate from the footing level by means of horizontal cracks.

During the experiment, the first model showed brittle behavior. When the system exceeded the linear range, crack initiation is followed by sudden collapse of the house (see Figure 3.81). However, after applying post-tensioning force on the walls, ductility of the system was improved (see Table 3.8). In contrast to the first model, the second model showed elastic behavior. Furthermore, the energy dissipation capacity of the walls of the strengthened model was enhanced significantly.

Table 3.8: Ductility demand improvements of each wall

Wall	Diagonal Displacement Unstrengthened (mm)	Diagonal Displacement Strengthened(mm)	Ductility Enhancement
North[1]	1.65	4.59	2.78
South	1.48	4.45	3.01
East	1.5	10.2	3.01
West	1.12	-	-

[1] See Figure 3.67 for the plan view

Maximum design acceleration is defined to be 0.4g by TEC-1998 [32] in first degree earthquake regions. Single story houses are usually rigid and have periods close to the left side of the Spectral Design Acceleration Spectra, "S(T)" spectrum. However, once cracking is initiated the natural periods increases moving on the ascending portion of the S(T) curve towards 2.5 to 1.0 [32]. Consequently, the energy dissipation and damping factors increase causing an increase in Strength reduction factor (R). Overall, measured capacity increase from 0.32g to 0.56g together with improved ductility is considered to be a significant improvement in the performance of the structure. Although damaged, the house would not collapse in a brittle manner, resisting lateral acceleration beyond the code requirements. Note that R factor measured is equal to 3.19 from experimental results (Figure 3.83).

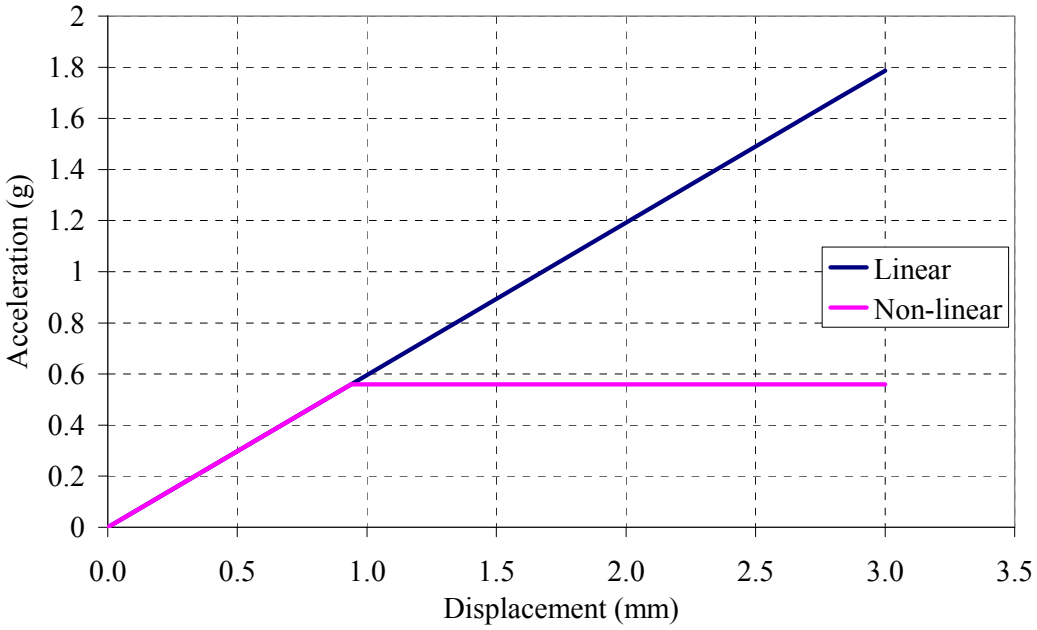

Figure 3.83 Strength Reduction factor calculation

CHAPTER 4

ANALYTICAL SIMULATION OF BRICK WALLS

Various studies to understand the linear and nonlinear out-of-plane bending behavior of masonry walls are found in the literature [13, [15]. However, analytical studies done on post-tensioning of masonry walls are rare.

In this part, an analytical study of brick strip walls exposed to out-of-plane direction force is developed using simplistic equilibrium equations. The force values corresponding to experimentally measured displacements are analytically calculated by taking advantage of the statically determinate nature of the test specimens (see Figure 4.2). The analytically calculated forces are compared against experimental counterparts.

The strip wall cross sectional area is equal to 1.637×10^5 mm^2 (185 mm x 885 mm). Void ratio of 60% makes the net area 6.55×10^6 mm^2 and moment of inertia (I) equal to 1.87×10^8 mm^4. The moment of inertia at the mortar connection between brick layers changes since the mortar layer is placed as a 50 mm wide band close to the edges of the wall (Figure 4.1) causing 'I' value of the section to further drop down to about 1.71×10^8 mm^4 at the mortar-brick interface. Similarly, the net mortar area reduces down to about 3.88×10^4 mm^2.

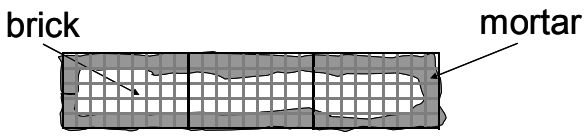

Figure 4.1 Masonry wall cross section

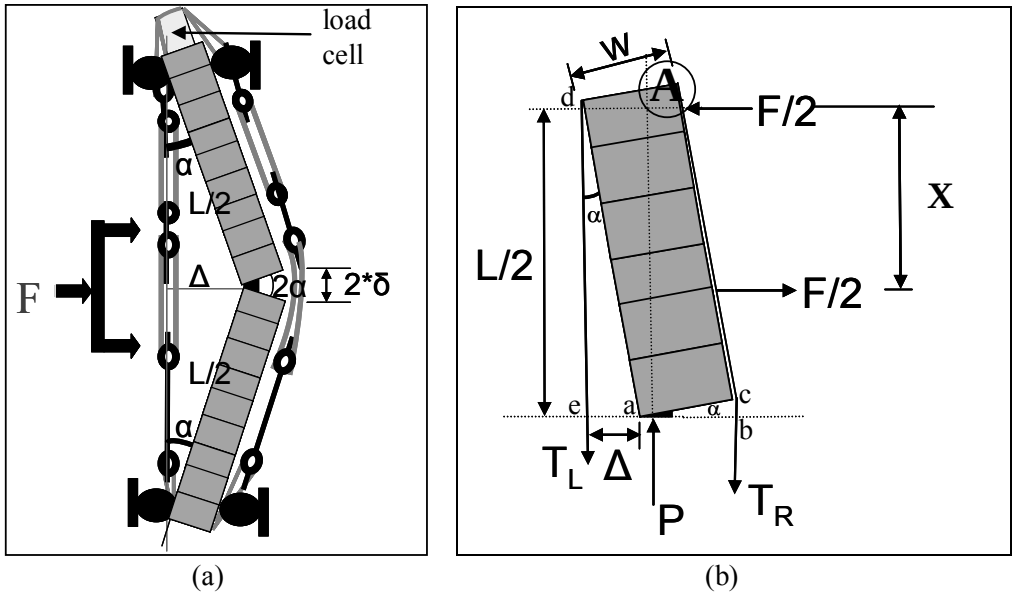

Figure 4.2 Masonry strip wall non-linear range deflection and forces illustration

The linear-range (cracking) bending moment capacity (M_{cr}) can be simply calculated using Equation 4.1 by taking average tensile strength as $1/10^{th}$ of the compressive strength of the mortar ($\sigma_{tensile}$=0.36 MPa; Section 2). The 'c' variable in Equation 4.1 is the distance from the neutral axis to the outermost layer of the wall and was taken as 92.5 mm. The moment of inertia (I) and the sectional area (A) were calculated as 1.71 x 10^8 mm^4 and 3.88 x 10^4 mm^2, respectively. The relationship between the laterally applied force (F) and the corresponding bending moment (M) in the constant moment region is given in Equation 4.2 for the statically determinate test setup in the linear range. The measured F values from the experiments and the calculated corresponding F values from the analytical study are listed in Table 4.1. Comparisons of the average experimental and analytical F values for different stages of testing (0, 50, and 100 kN post-tensioning load) are shown in Figure 4.3. For testing stages #2 and #3, the initial tensile strength of the wall was not taken into account in the calculation of analytical cracking moments (i.e., $M_{r.}$ in Equation 4.2) since during testing stage #1 the wall was already cracked (except for specimen #3). The self-weight contribution of the wall was ignored in all calculations due to the negligibly small lateral force difference of about 0.15 kN that self weight creates.

$$\frac{M_{cr} * c}{I} - \frac{P}{A} = \sigma_{tensile} \tag{4.1}$$

$$M_{cr} = \frac{F}{2} \cdot (X) \tag{4.2}$$

Table 4.1: Linear range computed versus measured lateral forces (F=kN)

Specimen	Post-Tension=0 (kN)		Post-Tension=50 (kN)		Post-Tension=100(kN)	
	Measured	Calculated	Measured	Calculated	Measured	Calculated
#1	1.21	1.6	5.25	5.60	6.34	11.20
#2	1.1	1.6	6.34	5.60	9.82	11.20
#3	-	1.6	-	5.60	13.40	12.80
#4	2.01	1.6	5.32	5.60	9.14	11.20

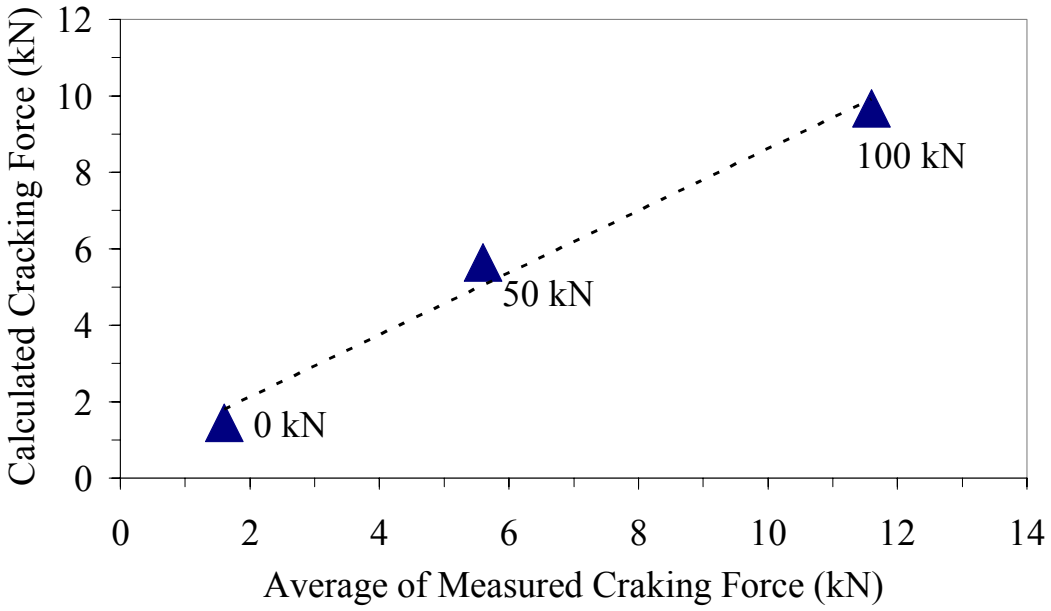

Figure 4.3 Comparison of analytical versus experimental cracking (average) lateral forces

The strip wall was post-tensioned using a chain of six scrap tire rings (STRs); 3 STRs on each side of the wall. The average stiffness of a single STR (k_{estrel}) was

calculated from the experimentally obtained values as about 1.2 kN/mm and 1.92 kN/mm under 25 kN and 50 kN tensile loads, respectively (Figure 3.6(a) and (b)). The stiffness of the STR chain (k_{etch}) located on either side of the wall is the effective stiffness of three STRs connected in series. Using Equation 4.3, k_{etch} were calculated as 0.4 kN/mm under 25 kN and 0.64 kN/mm under 50 kN, respectively.

$$\frac{1}{k_{STC}} = \frac{1}{k_{STR}} + \frac{1}{k_{STR}} + \frac{1}{k_{STR}} = \frac{3}{k_{STR}} \tag{4.3}$$

The analytical studies were also conducted for the nonlinear range. The applied lateral forces (F) were calculated for all wall tests for loading stages #2 and #3 (i.e., 50 kN and 100 kN post-tensioning forces, respectively). The tensile strength of the masonry units in stages #2 and #3 were assumed to be zero (except test #3) since the sections had already been cracked in stage #1. The linear range for the post-tensioned stages (#2 and #3) was exceeded when the maximum tensile stress caused by bending at the cross-section became larger than the axial compressive stress generated by post-tensioning (see Equation 4.1). After the wall passed into the nonlinear range, a hinge mechanism was formed at the middle joint of the wall (see Figure 4.2). The relative displacement between the two corners of the crack opening is a function of 2α and is equal to 2δ as shown in Figure 4.2(a). The crack opening stretches the STC which causes the axial post-tensioning at the front side of the wall (T_R) and consequently the total force (P) to increase (see Figure 4.2(b)). The STC on the other side of the wall shortens as a function of $1-\cos(\alpha)$ which can be ignored for small angles. Therefore T_L was assumed to be constant.

Writing a moment equilibrium equation with respect to the top support location (point 'A' in Figure 4.2(b)) enables the analytical calculation of the lateral force (F), which is given in Equation 4.4 as a function of lateral displacement (Δ) and total axial post-tensioning force (P). Constants "X" and "w" refer to support to loading point distance and width of the wall, respectively and shown in Figure 4.2.

$$F = \frac{P*(w-\Delta)+T_R*\Delta-(T_L*w)}{(X/2)} \tag{4.4}$$

Additional parameters such as rotation angle ($\alpha=\Delta*2/L$), axial force change on the tensed side of the STC ($\Delta F=2*\delta*k_{etch}$), crack opening ($\delta=2*w*\Delta/L$), axial force on front side of the wall ($T_R= T_L+\Delta F$), total post-tensioning force acting on the wall ($P=TL+TR$) can be defined as functions of parameters P and Δ. Using these dependent variables, Equation 4.4 can be simplified into Equation 4.5.

$$F = f(\Delta, P) = P \cdot \frac{(w-\Delta)}{X} + (k_{STR} \cdot \Delta) \cdot \frac{4 \cdot w \cdot (w+\Delta)}{X \cdot L} \cdot \tag{4.5}$$

For example, the steps are followed during the calculation of third stage analytical load-deflection envelope of first brick wall test are explained as follow:

- From Figure 3.25, force versus displacement envelop of the third stage test result of first brick wall is drawn in Figure 4.4. Then, the post-tensioning force values corresponding to measured force and displacement values (Figure 4.4) are taken into account from Figure 3.26 and Figure 3.27.

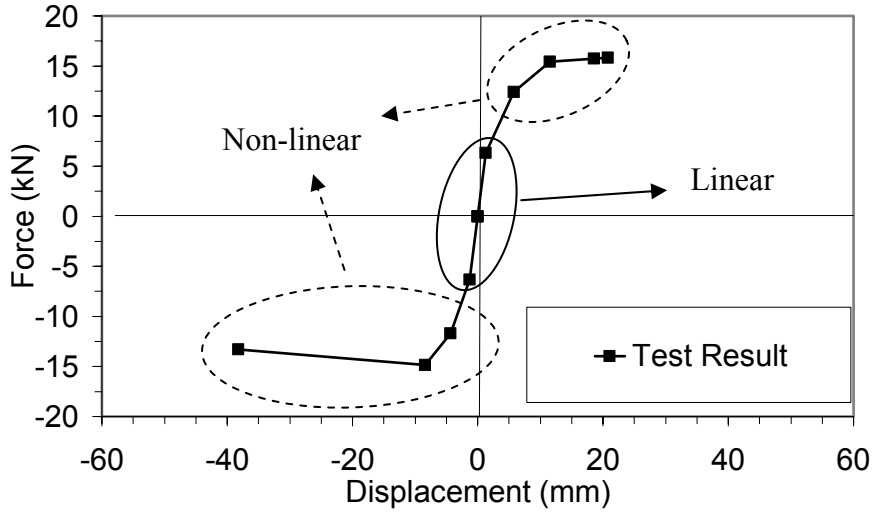

Figure 4.4 Measured force versus displacement envelop of first brick wall in third stage

- Linear and non-linear ranges of measured force versus displacement envelop are indicated in Figure 4.4.
- Firstly, in analytical calculations, the linear capacity of the wall is calculated (Table 4.1) as 11.20kN under 100kN of post-tensioning. This value is plotted against the measured linear displacement value obtained from Figure 4.4 into Figure 4.5.

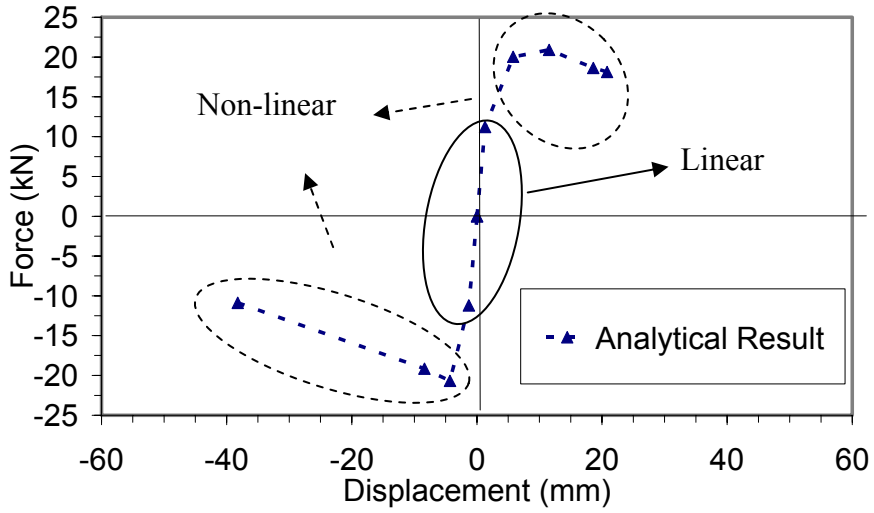

Figure 4.5 Analytical force versus displacement envelop of first brick wall in third stage

- Then, using Equation 4.5, the out-of-plane forces in non-linear range are calculated corresponding to P and Δ values in Figure 4.5.
- Finally, the linear and non-linear calculated values and measured values are plotted together in Figure 4.9

Comparisons of the analytical and experimental load-deflection graphs are presented in Figure 4.6 till Figure 4.12. The experimentally measured load-deflection envelope and the analytically generated curves correlate well and are in sufficient agreement with each other.

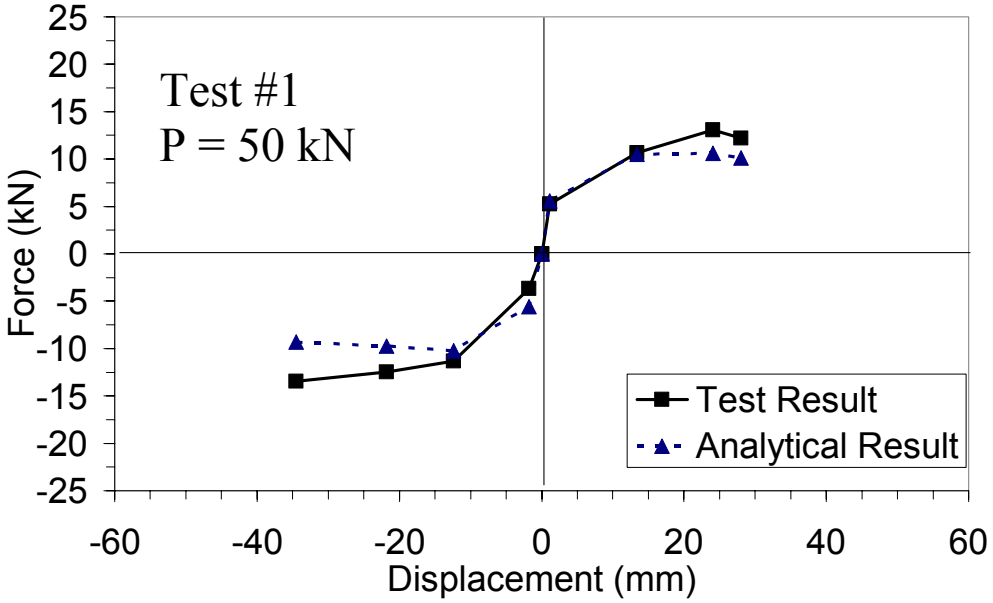

Figure 4.6 Comparison for second stage analytical and experimental load-deflection graph of first brick wall test

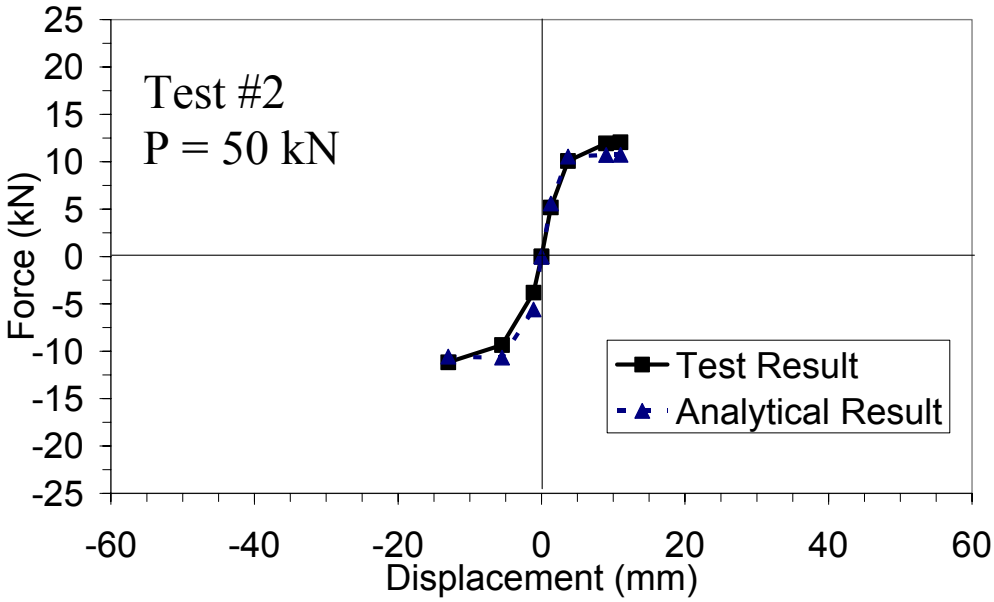

Figure 4.7 Comparison for second stage analytical and experimental load-deflection graph of second brick wall test

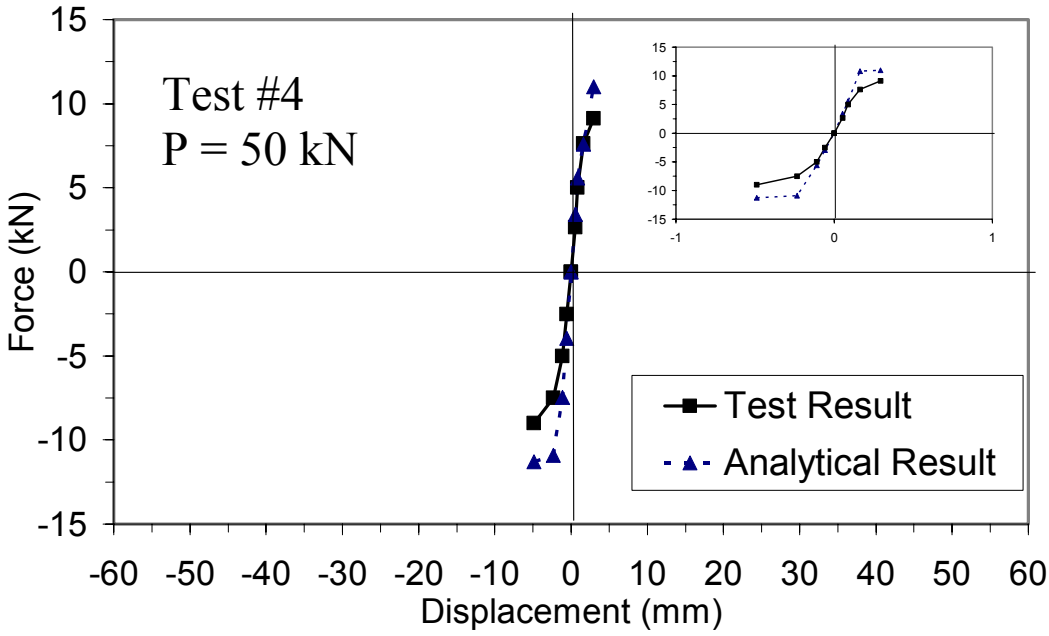

Figure 4.8 Comparison for second stage analytical and experimental load-deflection graph of fourth brick wall test

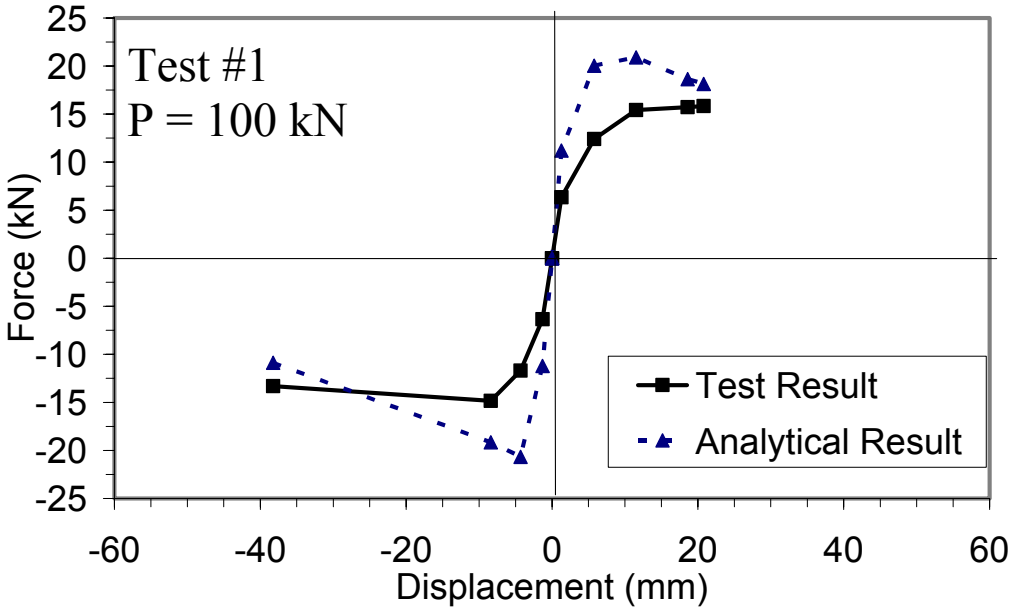

Figure 4.9 Comparison for third stage analytical and experimental load-deflection graph of first brick wall test

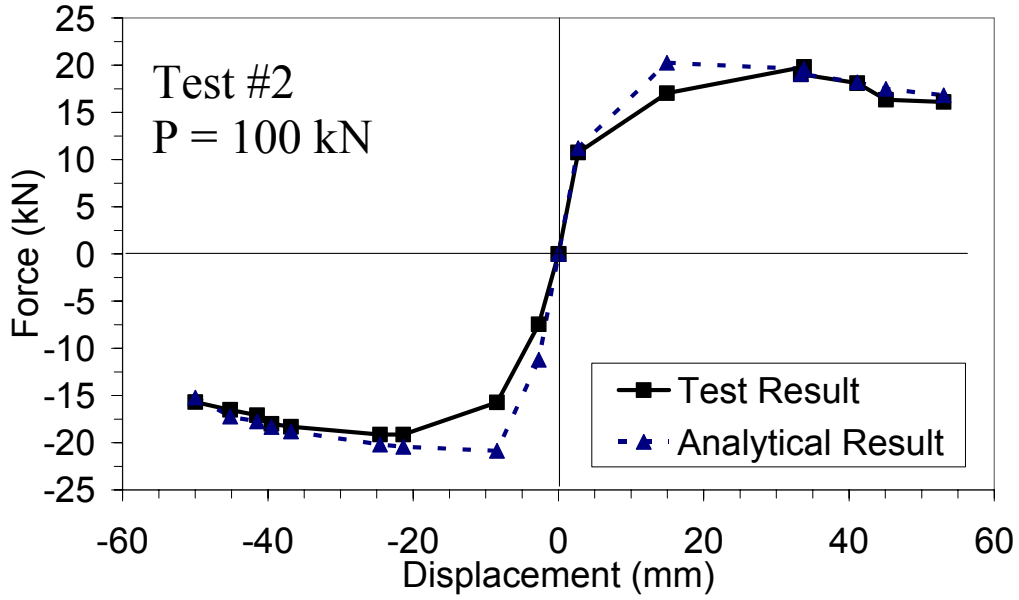

Figure 4.10 Comparison for third stage analytical and experimental load-deflection graph of second brick wall test

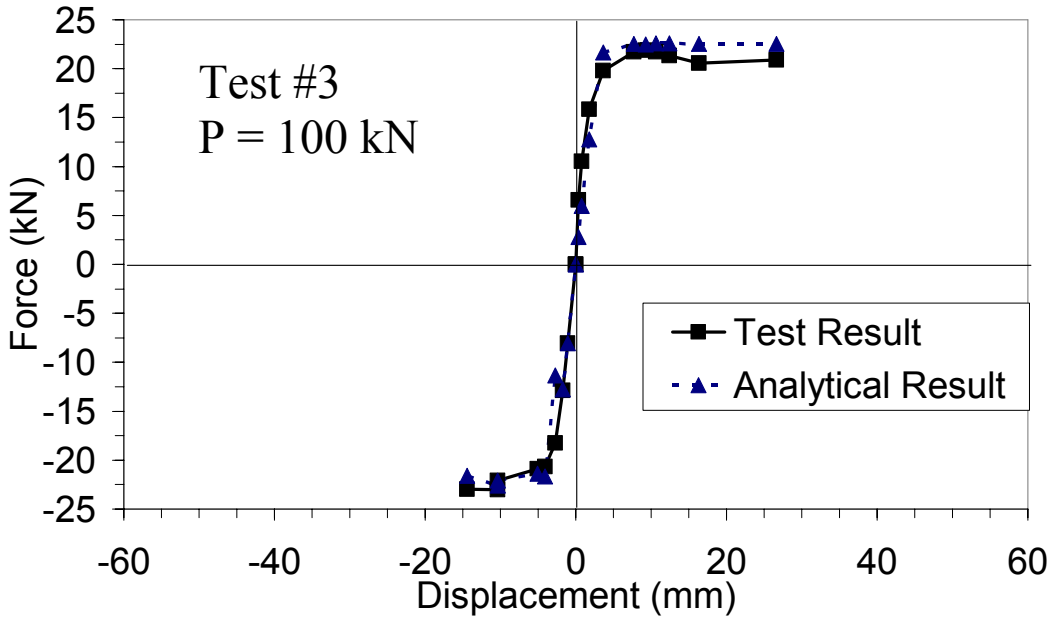

Figure 4.11 Comparison for third stage analytical and experimental load-deflection graph of third brick wall test

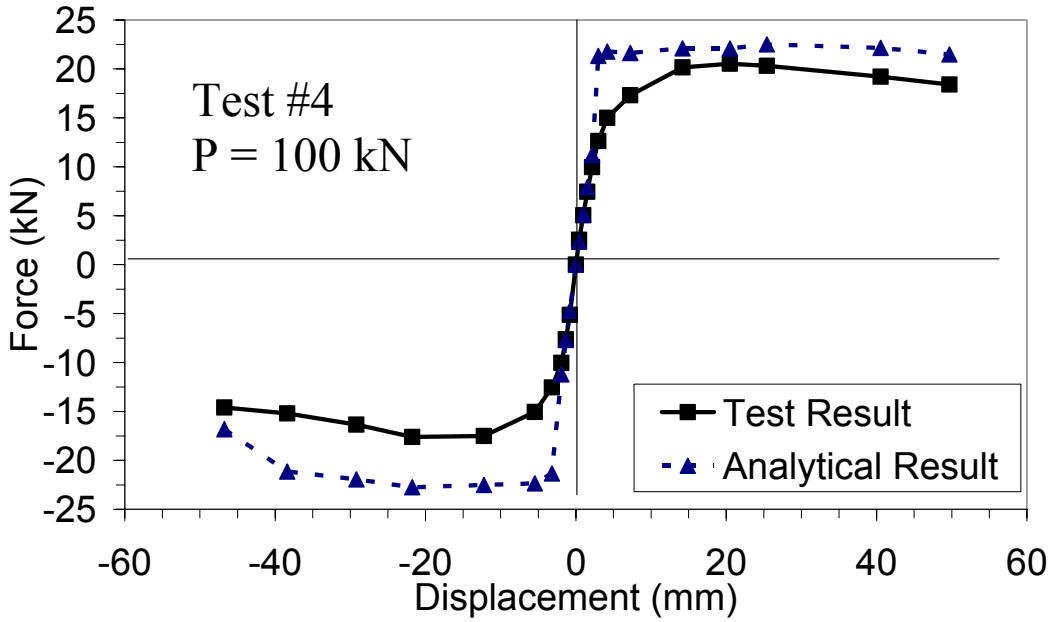

Figure 4.12 Comparison for third stage analytical and experimental load-deflection graph of first brick wall test

CHAPTER 5

CONCLUSIONS

The conclusions which were derived from the results obtained in this study are given in the following sections under separate headings referring to each part of the study.

5.1. SCRAP TIRE MATERIALS TEST RESULTS

The mean and standard deviation for the ultimate tensile load capacities of STRs were calculated as 132.6 kN and 27.72 kN; whereas, the same values for rim-rings were found to be 53.5 kN and 10.9 kN, respectively. Although the average capacity of rim-rings is smaller than that of STRs, two rim-rings are obtained from a single scrap tire (total capacity of about 107 kN with standard deviation of 21.8 kN) and the standard deviation of rim-rings are still smaller than that of STRs (about 78%). for comparison purposes.

Using the Kolmogorow-Simirov test [33] for STR and rim-rings tests results at 5% significance level, the measured data are investigated whether they are appropriate for normal distribution. The cumulative distribution of the test results and the theoretical distribution function for proposed normal models of STR and rim-ring are plotted together in Figure 5.1 and Figure 5.2. Then the maximum discrepancies between measured and theoretical distribution functions are calculated as 0.078 and 0.181 for STRs and rim-rings, respectively. After that, these values are compared with obtained values 0.24 for 43 data (of STRs) and 0.44 for 9 data (of rim-rings) [33]. The calculated discrepancy data are smaller than the given data, consequently

the normal model of STRs and rim-ring are verified at the %5 significance level.

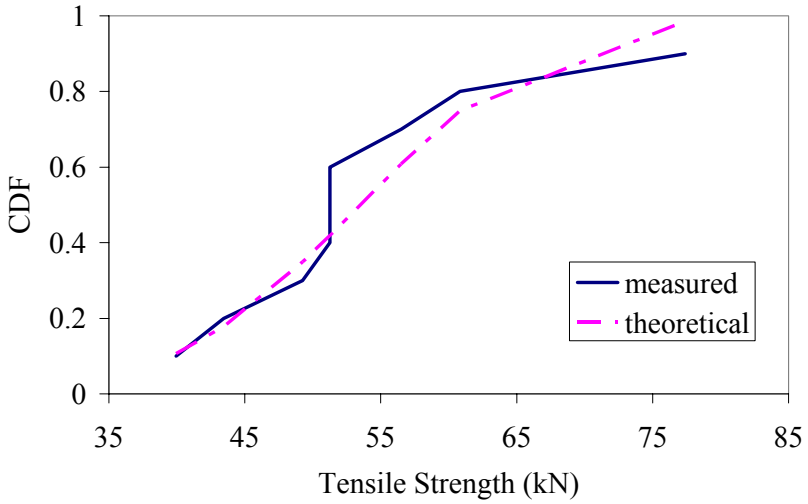

Figure 5.1 Cumulative Distribution of STR tensile strength

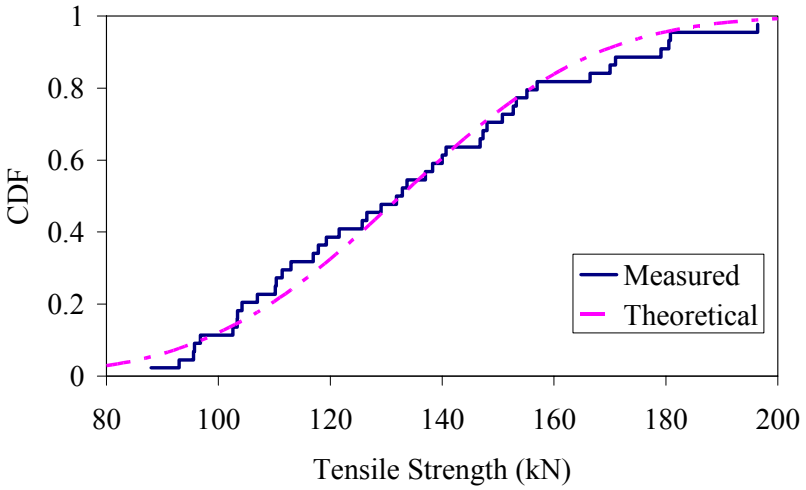

Figure 5.2 Cumulative Distribution of rim-ring tensile strength

The normal distributions for STRs and rim-rings are plotted in Figure 5.3 Three times the standard deviation is marked in the negative direction to label for a confidence level of 97.7% to remain below the average ultimate tensile capacity, which are 78.2 kN and 31.7 kN (63.4 kN for double) for the STR and rim-rings, respectively. Considering STR and rim-ring chains would surround the wall from the

inner and outer sides, the total post-tensioning load on the wall can be calculated as 156.4 kN and 126.8 kN, respectively.

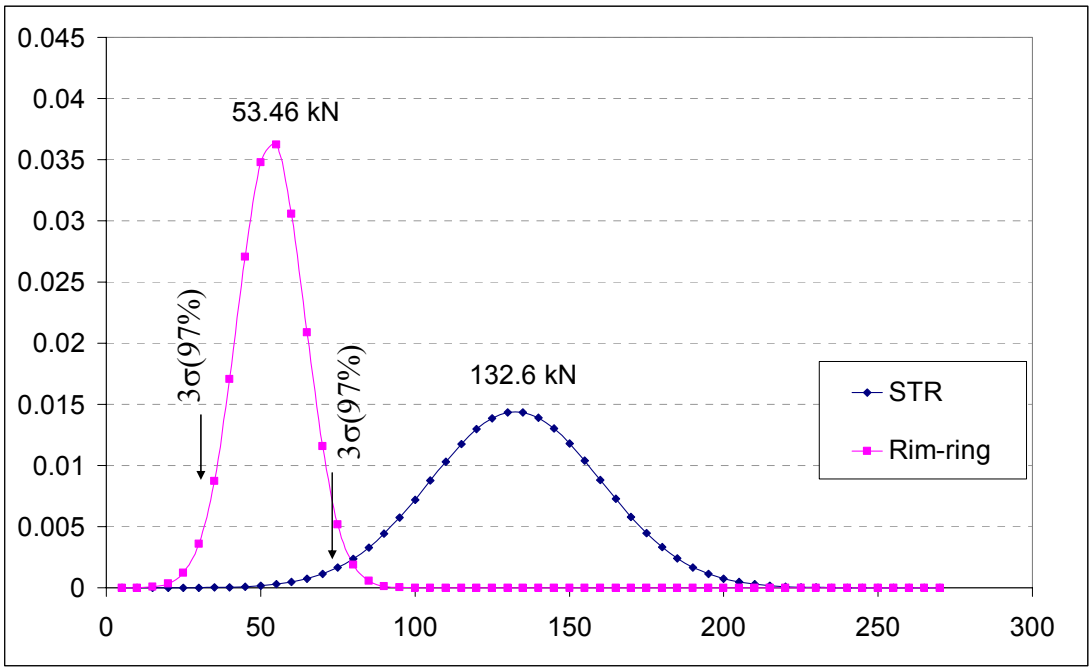

Figure 5.3 STR and rim-ring ultimate strength normal distributions

The fifth connection design for the STRs (Figure 3.7(e)) proved to be the most successful connection since the tension tests of two-tires connected by connection type 5 were able to withstand forces up to 90 kN. No apparent damage was observed to the connector such as punching, bending or bearing failures and failure was governed by scrap tire tearing.

The best performance for the connection of rim-rings was obtained using knots with a single steel pipe inserted in the middle of the knot. Although the wooden log and U-shaped bolt designs showed similar tensile load capacities, the steel pipe response was the most stable one. Overall, the connections of rim-rings are simpler and cheaper than those of the STRs.

50 kN of axial load was deemed adequate (at about 97% confidence level) for both the STR-chain and the double rim-ring chain design purposes (F.S. > 2). However, the tensile force could be reduced down to 25 kN considering the unknown long-term behavior of viscoelastic rubbery composite material. On the other hand, any post-tensioning force losses can be recovered by tightening the bolted connections. The use of double parallel rim-rings for post-tensioning may seem to be more advantageous since they have similar strengths, smaller deviations, lesser rubber content, and lower cost compared to the STRs. However, the use of STRs is preferable since their behavior is more elastic and less brittle. Stretching of STC is easier - more convenient compared to the rim-ring chain. Long-term behavior of STRs and rim-rings should also be investigated.

5.2. STRIP WALL TEST RESULTS

The experimental studies have shown that the nominal lateral load capacities of the brick walls in out-of-plane direction can be improved up to about 8.5 times by applying 100 kN (per 0.885m of wall width) axial post-tensioning force using STC and hybrid system.

On the other hand, the nominal lateral load capacity of the briquette walls in the out-of-plane direction can be improved up to about 4 times by applying 30 kN (per 1.0m of wall width) axial post-tensioning force using STC and about 6 times using hybrid system.

Both the drift and energy dissipation capacities of all tested walls were increased after applying post-tensioning.

The usage of STR, i.e., rubber-like elastic material, improved the elasticity of the strip walls even beyond the linear range. The cracks were closed and the walls have elastically returned back to their original shapes as the lateral load was removed even when the displacements were in the nonlinear range.

Post-tensioning forces of the brick walls were decreased approximately 1.5% after each cycle due to crushing of mortar layers and brick corners.

The post-tensioning using STRs, including the hybrid system, was applied to the outer surfaces of the masonry walls as opposed to the conventional post-tensioning methods for vertical load carrying members where the post-tensioning material is applied on the inside (centric) of the section. The application of STR to the outer surface of the walls permits easy access for strengthening of existing masonry houses. The increase in EI of the wall is negligible due to the large difference between stiffness terms of the STC and masonry wall.

Usage of hybrid system lowers the cost of the application while retains advantages associated with the usage of scrap tires at the support locations. Replacement of the half-circular wooden log and STR at the support with the steel plates is not recommended since the thick support plate would elevate strengthening cost while additional elasticity supplied by STR is lost. Plastic deformation would generate when only steel plate is used and self-centering (recovery) property of STR is lost.

The bending failure of masonry walls are strengthening using scrap tires for maximum moment at the middle section which resembles a simply supported beam behavior rather than a cantilever beam which have cracks forming at the base. The improvements obtained at the middle section of the wall improve bursting resistance of the wall as well as preventing bi-directional bending failure (Figure 3.76). The shear capacities of the walls were improved in in-plane direction as the formations of large cracks (Figure 3.75) are prevented by post-tensioning load (Figure 3.82).

5.3. FULL SCALE TILTING TABLE TEST RESULTS

The first (nominal) model collapsed suddenly when subjected to 0.32 g lateral acceleration; whereas, after wrapping the walls by pre-stressed Sacs in the vertical and horizontal directions, the strength of the masonry house is enhanced 75% percent and was capable of resisting 0.56 g of lateral acceleration.

Large cracks were formed around the corners of the windows and doors during the first test at the location of stress concentrations as seen in Figure 3.74. However, after applying the post-tensioning force on the walls in horizontal and vertical directions, the major diagonal cracks (Figure 3.75) have disappeared; the cracks were concentrated below the window and close to the footing levels (Figure 3.82). The size of the cracks was also reduced. Out-of-plane bending failures observed in the first test (Figure 3.76) were prevented by application of STC post-tensioning.

The energy dissipation capacity of the house was increased after applying post-tensioning on the walls. Applied post-tensioned force increased ductility of the house about three times with respect to the unstrengthened masonry house (Table 3.8). Preliminary laboratory experiments show high promise that STC based masonry wall strengthening can be used as low-cost strengthening method. However, it will take much effort to prepare design guidelines and improper application or incorrect masonry type selection (such as stone-boulder masonry) can cause legal and social problems.

To summarize, the use of post-tensioning on masonry walls is a theoretically sound method which was experimentally proved at laboratory environment. However, problems that might be faced at the implementation phase still remains to be solved. Variety in masonry type construction and scrap tire brands in Turkey imposes a thread to the success of implementation phase. Pilot studies are recommended before extensive application program launched. If proper steps are taken, Turkey can benefit from STC strengthening as a low-cost, friendly strengthening method to be used at-low-income housings.

5.4. RECOMMENDATIONS FOR FUTURE WORK

Based on the conducted studies and results, the following recommendations can be drawn:

1. The unpleasant appearance of STR chains after post-tensioning can be camouflaged by using U shaped bricks at the outer side of the walls. Gypsum plates can be easily cut using a utility knife and conveniently used to cover the STC from the inside. In addition to the improved view, fire safety, protection of rubber from harmful ultraviolet (UV) light, and possible rubber smell isolation are achieved by covering STR material.

2. Although scrap tire is a composite material containing steel mesh inside the rubber treads, the viscoelastic properties are expected to release some of the post-tensioning force. Initial studies conducted by Ms. Tuğba Eroğlu have shown that about 20% of the initial force is lost in the first few months, exponentially converging to a 30% total loss. Initial application of 130% of the optimal post-tensioning force would eliminate potential losses. It might be necessary to check post-tensioning force on Sacs once a year during summer to make sure that adequate amount of post-tensioning exists at all times. Time dependent behavior of STRs will continue to be investigated.

3. Since scrap tires are found in abundance in developed countries, exportation of used tires to other developing and/or undeveloped countries would have positive influence on the environment as well as earthquake safety of masonry house residents.

REFERENCES

[1] DIE - State Institute of Statistics Prime Ministry Republic of Turkey (2000) Building Census.

[2] OHIO Department of Natural Resources, "A history of rubber recycling" http://www.dnr.state.oh.us, fast accessed, July (2005)

[3] J.A. Epps, Uses of recycled rubber tires in highways, Synthesis of Highways Practice, vol.198, Transportation Research Board, National Research Council, Washington, DC; 1994.

[4] S. Amirkhanian, Utilization of waste materials in highway industry- a literature survey, J. Solid Waste Manag. 1997; 24(2): 94-103.

[5] S. Douglah, J.W. Everett, Scrap Tire disposal: I. Survey of the state programs, J. Solid Waste Technol. Manag. 1998; 25(1): 40-50.

[6] Li G., Stubblefield M.A., Garrick G., Eggers J., Abadie C., Huang B., Development of waste tire modified concrete, Cement and Concrete Research. December 2004; 34(12): 2283-2289.

[7] N.N. Eldin, A.B. Senouci, Rubber-tire practices as concrete aggregate,
J. Mater. Civ. Eng. 5 (4) (1993) 478– 496.

[8] Ghobarah, A. and El Mandooh Galal, "K. Out-of-plane strengthening of unreinforced masonry walls with openings", Journal of Composites for Construction, ASCE, 2004:8(4):298-305.

[9] Tan K. H. and Patoary M. K. H., "Strengthening of Masonry Walls Against Out-of-Plane Loads Using Fiber-Reinforced Polymer Reinforcement", the Journal of Composites for Construction ASCE, Vol. 8, No.1, February 1, 2004, pp. 79-87.

[10] Sameer Hamoush, Mark McGinley, Paul Mlakar and Muhammad J. Terro, "Out-of-plane behavior of surface-reinforced masonry walls", Construction and Building Materials, April 2002, pp-341-351

[11] M.R. Ehsani, Fellow, H. Saadatmanesh, and J.I Velazquez-Dimas, "Behavior of Retrofitted URM Walls Under Simulated Earthquake Loading ", Journal of Composites for Construction ASCE, Vol. 3, No.3, August 1999, pp. 134-142

[12] Ahmad A. Hamid, C. Chia-Calabria, and H.G. Harris, "Flexural Behavior of Joint Reinforced Block Masonry Walls", ACI Structural Journal, Vol.89, No.1, January-February 1992.

[13] Zeiny, A and Larralde, J. Out-of-Plane Performance of Full-Size Un-Reinforced Brick Walls Retrofitted with Expansive Epoxy. 9th Canadian Masonry Symposium, Fredericton, Canada, June 2001.

[14] Michael Craig Griffith, Nelson T. K. Lam, John Leonard Wilson and Kevin Doherty, "Experimental Investigation of Unreinforced Brick Masonry Walls in Flexure", Journal of Structural Engineering ASCE, Vol. 130, No. 3, March 2004, pp-423-432

[15] Roberto Rodriguez, Ahmad A. Hamid, and Jesus Larralde, "Flexural Behavior of Post-Tensioned Concrete Masonry Walls Subject to Out-of-Plane Loads", ACI Structural Journal, Vol.95, No.1, January-February 1998, pp-61-70

[16] Peter T. Laursen and Jason M. Ingham, "Structural Testing of Large-Scale Post tensioned Concrete Masonry Walls", the Journal of Structural Engineering ASCE, Vol. 130, No. 10, October 2004, pp-1497-1505

[17] Mohamed A. H. ABdel-Halim and Samer A. Bakarat, "Cyclic Performance of Concrete-Backed Stone Masonry Walls", the Journal of Structural Engineering ASCE, Vol. 129, No. 5, May, 2003, pp- 596-604

[18] Owen A. Rosenboom and Mervyn J. Kowalsky, “Reversed In-Plane Cyclic Behavior of Post-tensioned Clay Brick Masonry Walls”, “the Journal of Structural Engineering ASCE, Vol. 130, No. 5, May , 2004, pp-787-798

[19] Frank J. Vecchio, Omar A. Haro de la Pena, Filippo Bucci, and Daniel Palermo, “Behavior of Repaired Cyclically Loaded Shearwalls ”, ACI Structural Journal, Vol. 99, No. 3, May-June 2002, pp-327-334

[20] OHIO Department of Natural Resources, “The nature of Rubber”, http://www.dnr.state.oh.us, fast accessed, July (2005)

[21] OHIO Department of Natural Resources, “Charles Goodyear”, http://www.dnr.state.oh.us, fast accessed, July (2005)

[22] Continental, “History of the Tire” http://www.contionline.com, fast accessed, July (2005)

[23] Tire School, “Manufacturing Flowchart” http://www.maxxis.com, fast accessed, July (2005)

[24] Discount Tire Direct, “Tire Terminology”, http://www.discounttiredirect.com, fast accessed, July (2005)

[25] Discount Tire Direct, “Tire Term”, http://www.discounttiredirect.com, fast accessed, July (2005)

[26] Turkish Standards Institute (TS) (1985). “Solids Bricks and Vertically Perforated Bricks.”, TS 705, Ankara, Turkey.

[27] Key to Steel “High-Alloy Hardenable Steels” http://www.key-to-steel.com, fast accessed, July (2005).

[28] Sandvik Materials Technology, “New ultra-high strength stainless steel”, http://www.smt.sandvik.com, fast accessed, July (2005).

[29] High Tensile Steel for Tires , “ Steel Developments”, http://www.azom.com fast accessed, July (2005).

[30] Ersoy, U., “Reinforced Concrete” Middle East Technical University, Ankara, 2000, pp.231-256.

[31] Chopra, A.K, “Dynamics of Structures”, 2nd Ed, Prentice Hall, California, 2001, pp.102.

[32] Turkish Earthquake Code (TEC) (1998). “Specification for Structures to be Built in Disaster Areas, PART III - Earthquake Disaster Prevention” TEC 98, Istanbul, Turkey.

[33] Alfredo H-S. Ang and Wilson H. Tang, “Probability Concepts in Engineering Planning and Design”, Volume I, University of Illinois Press, New York, 1975, pp. 277-281.

APPENDIX A

APPLIED FORCE VALUES IN OUT-OF-PLANE TESTS

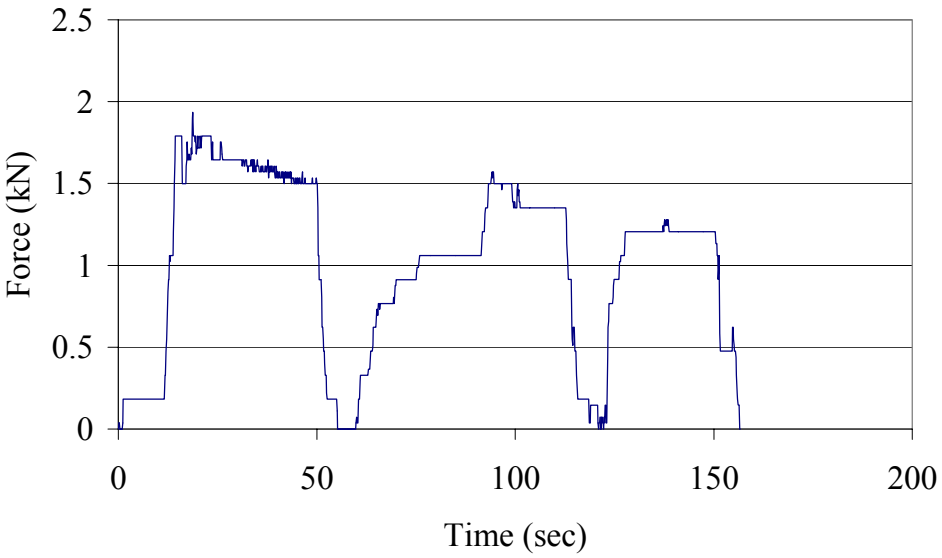

Figure A.1 Applied acceleration value for stage 1(0kN) of brick wall #1

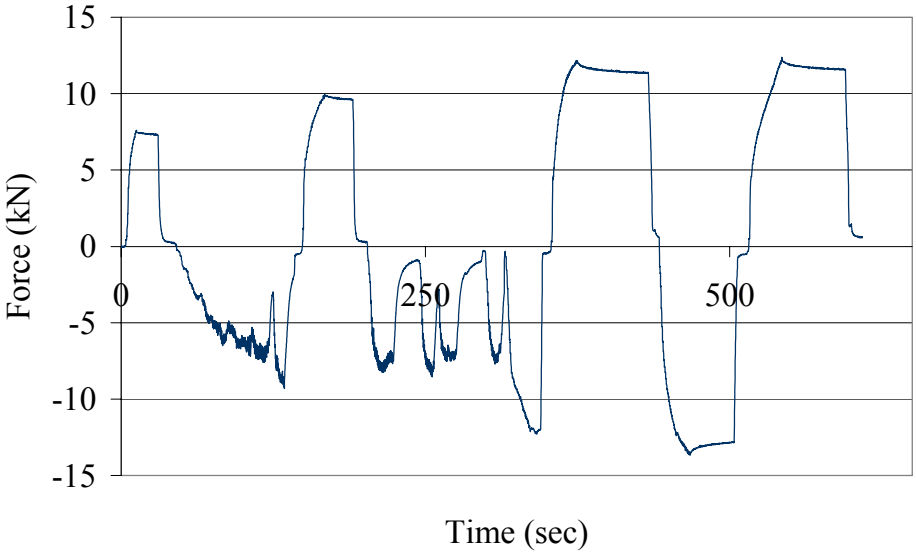

Figure A.2 Applied acceleration value for stage 2(50kN) of brick wall #1

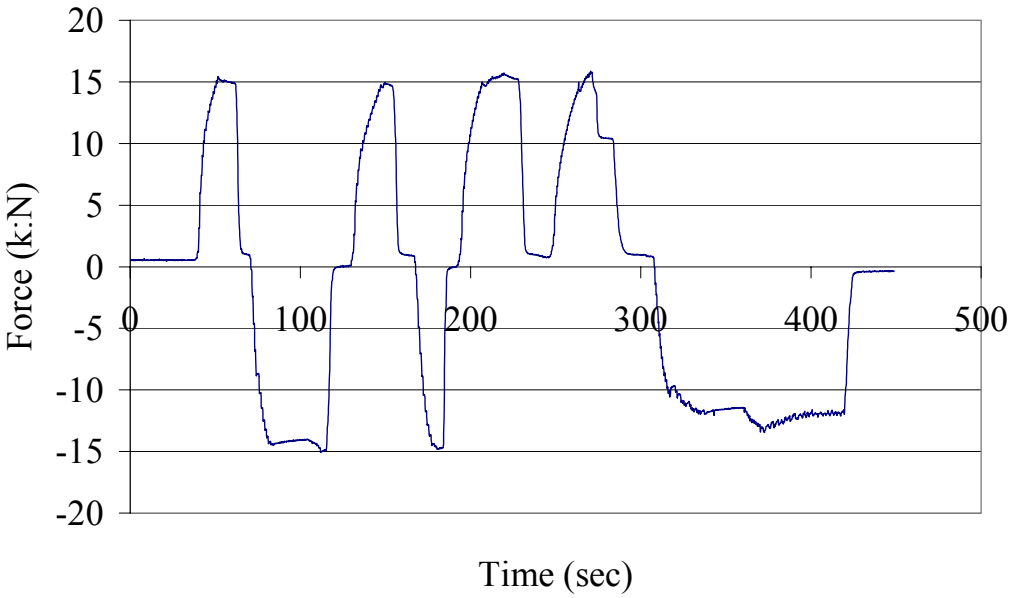

Figure A.3 Applied acceleration value for stage 3(100kN) of brick wall #1

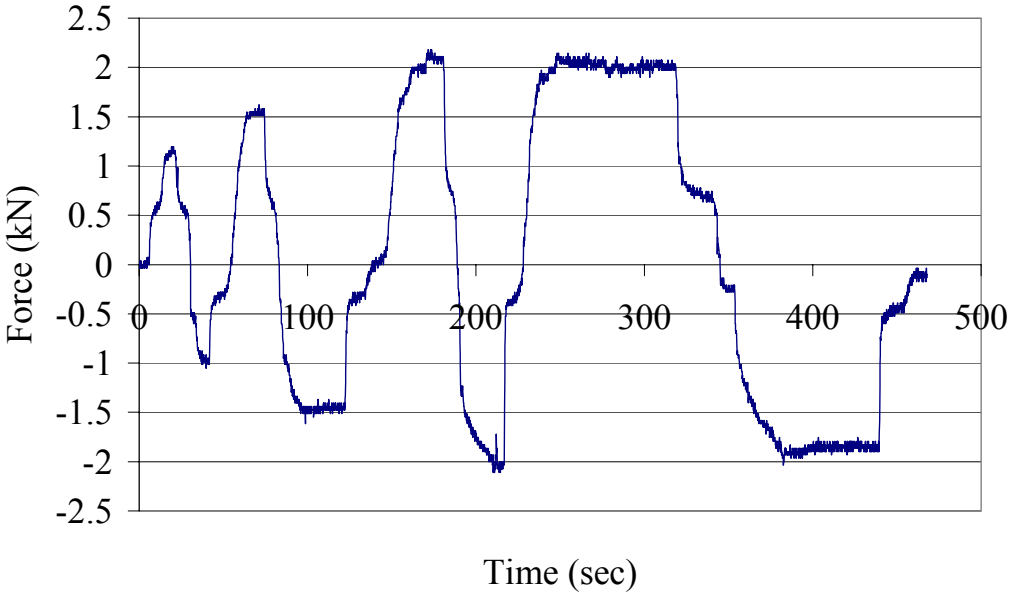

Figure A.4 Applied acceleration value for stage 1(0kN) of brick wall #2

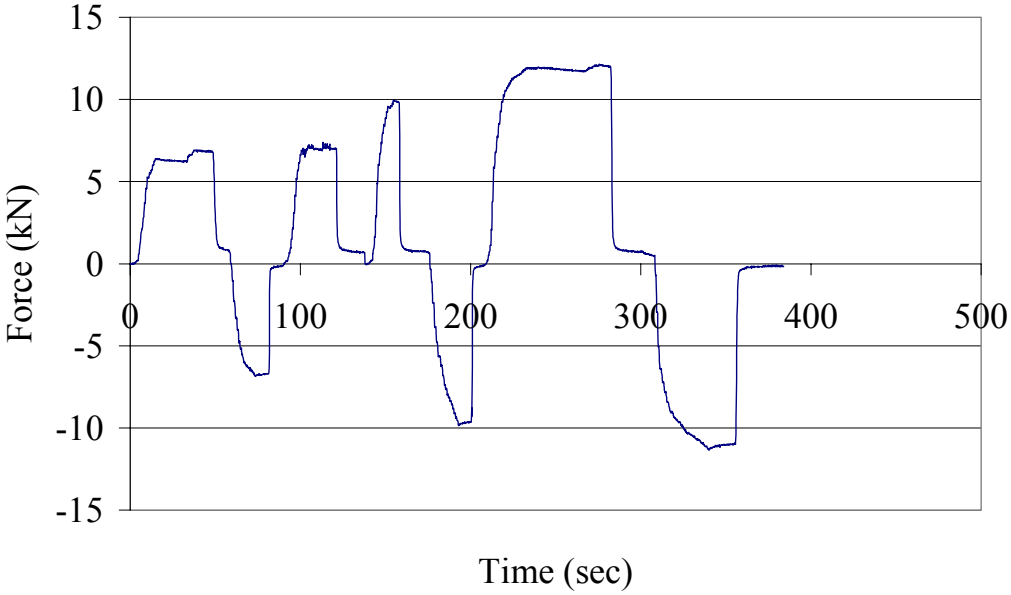

Figure A.5 Applied acceleration value for stage 2(50kN) of brick wall #2

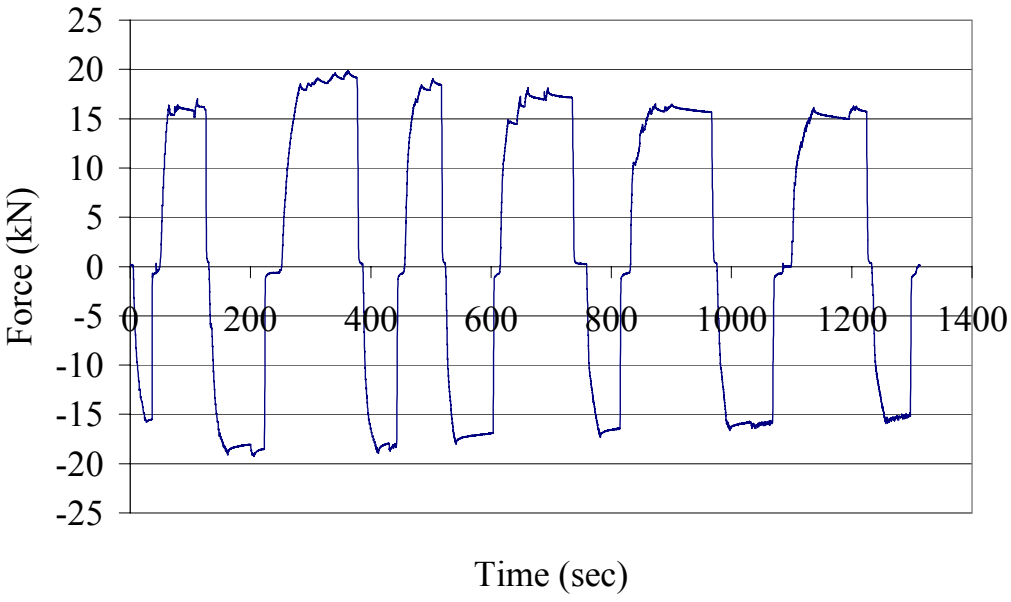

Figure A.6 Applied acceleration value for stage 3(50kN) of brick wall #2

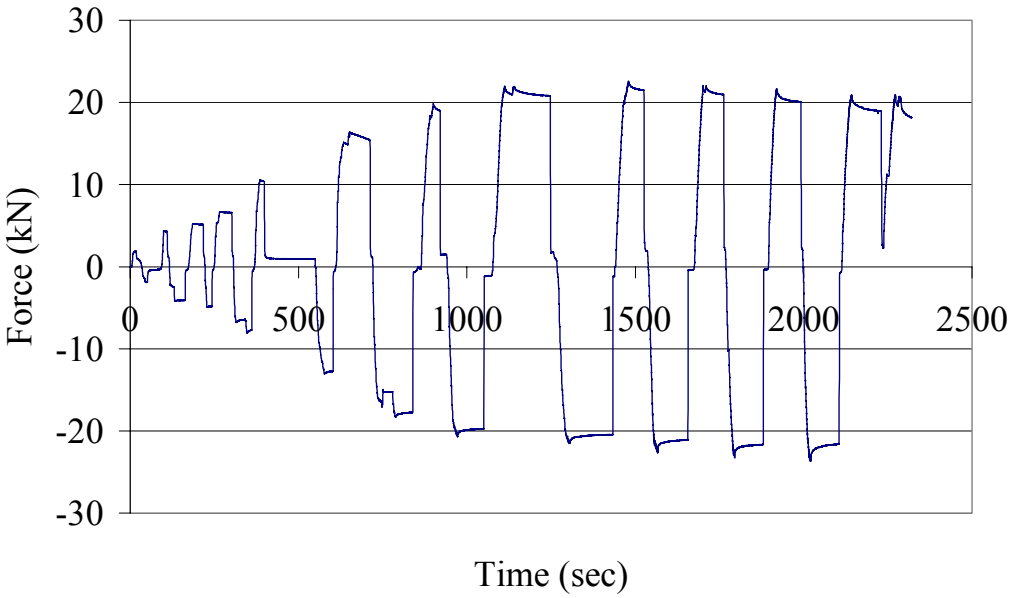

Figure A.7 Applied acceleration value for stage 3(100kN) of brick wall #3

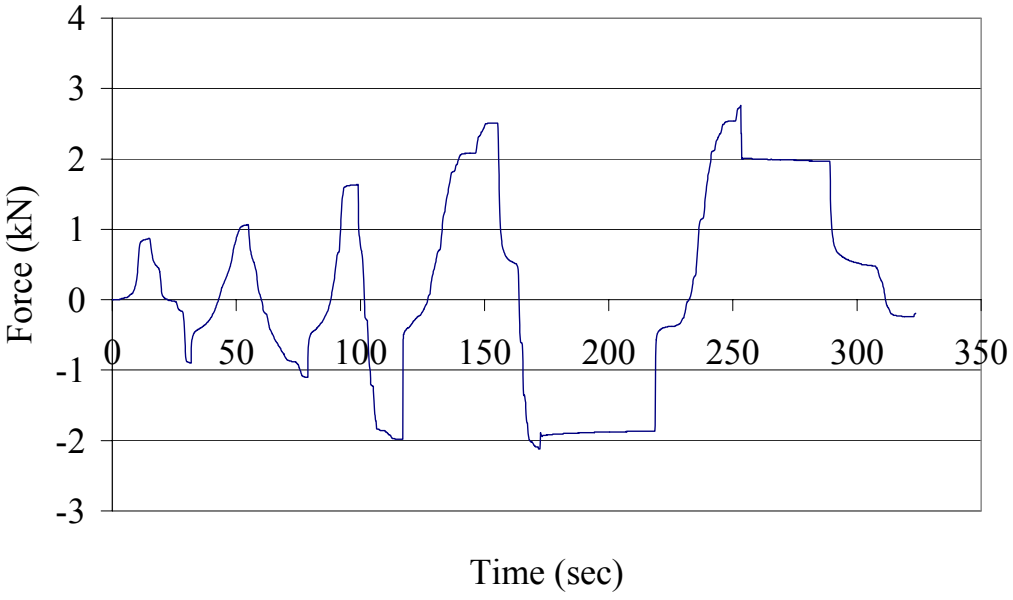

Figure A.8 Applied acceleration value for stage 1(0kN) of brick wall #4

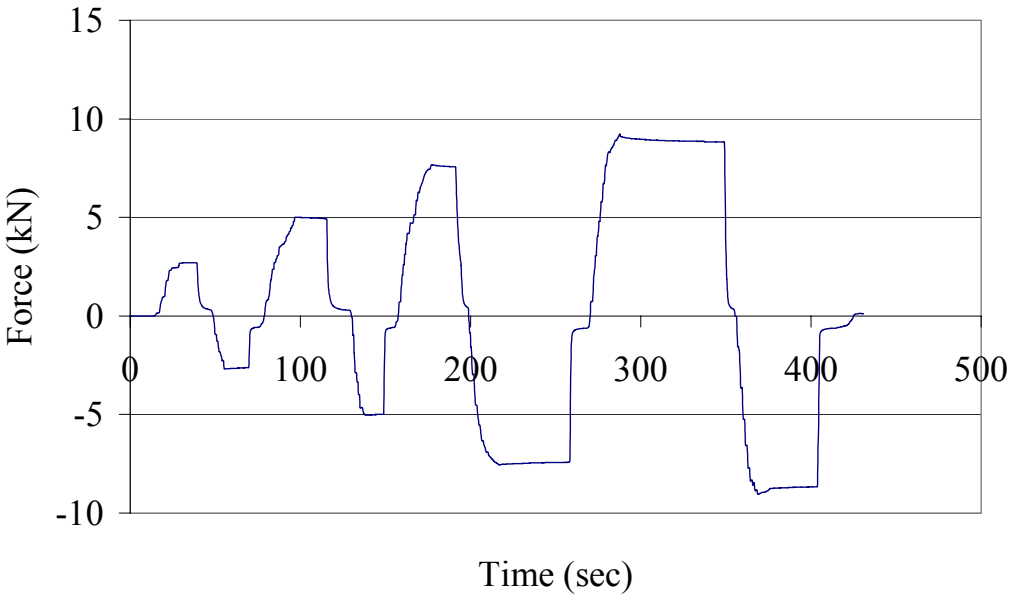

Figure A.9 Applied acceleration value for stage 4(50kN) of brick wall #4

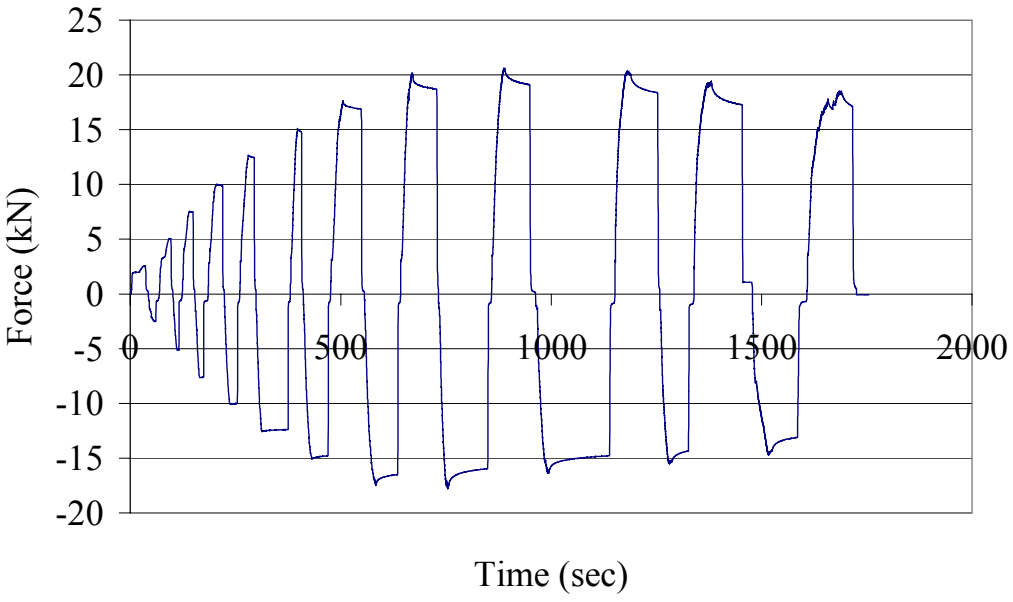

Figure A.10 Applied acceleration value for stage 4(100kN) of brick wall #4

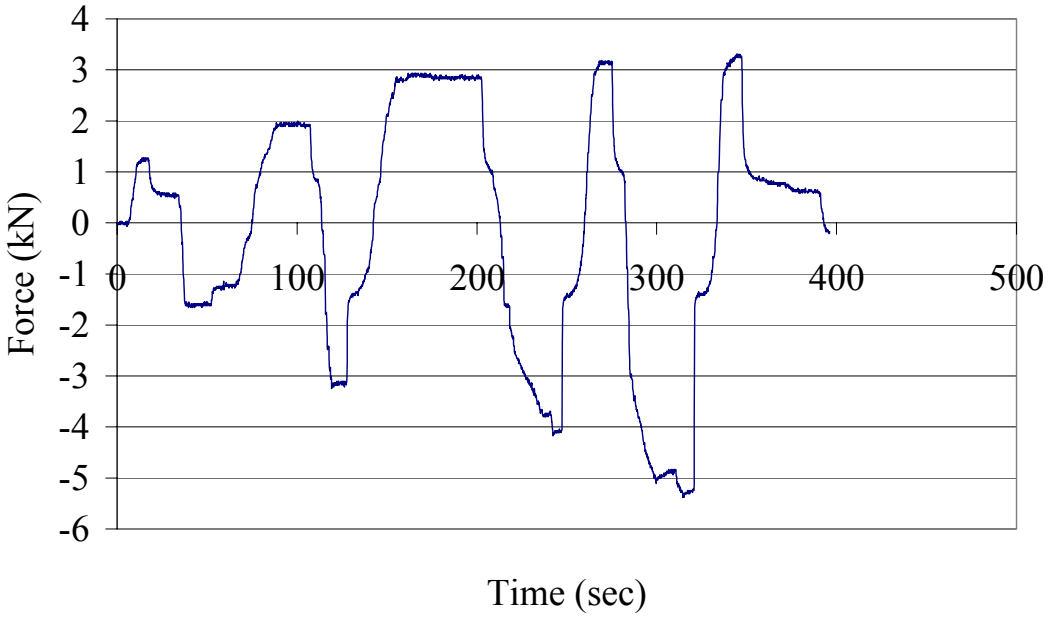

Figure A.11 Applied acceleration value for stage 1(0kN) of briquette wall #1

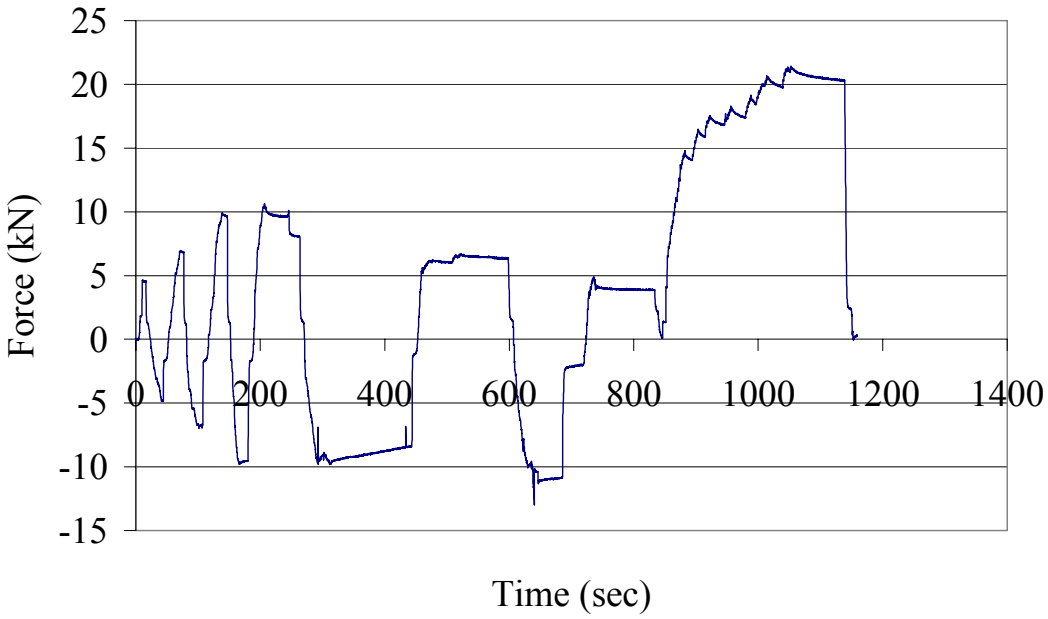

Figure A.12 Applied acceleration value for stage 2(30kN) of briquette wall #1

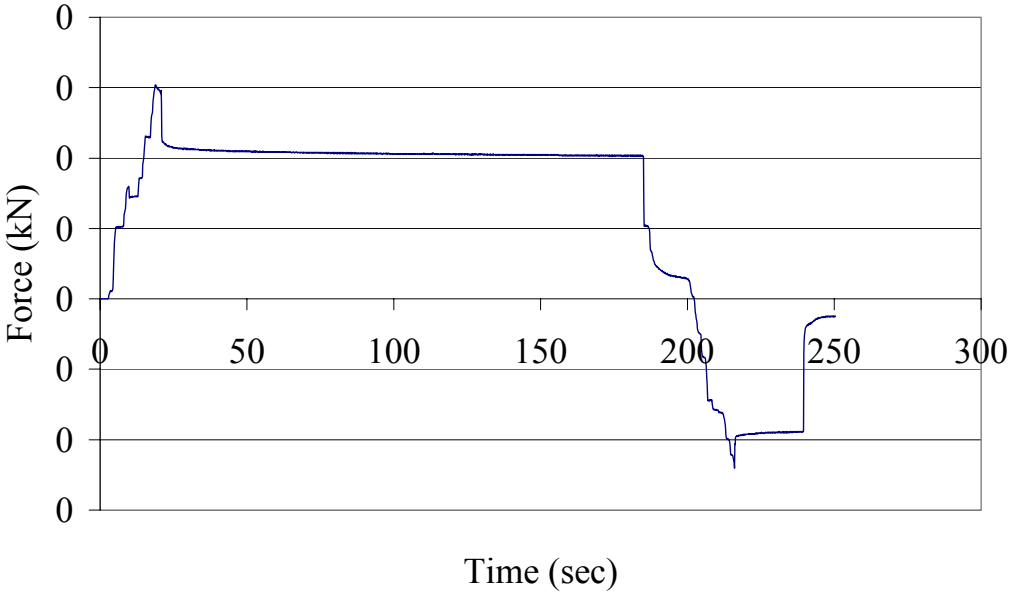

Figure A.13 Applied acceleration value for stage 1(0kN) of briquette wall #2

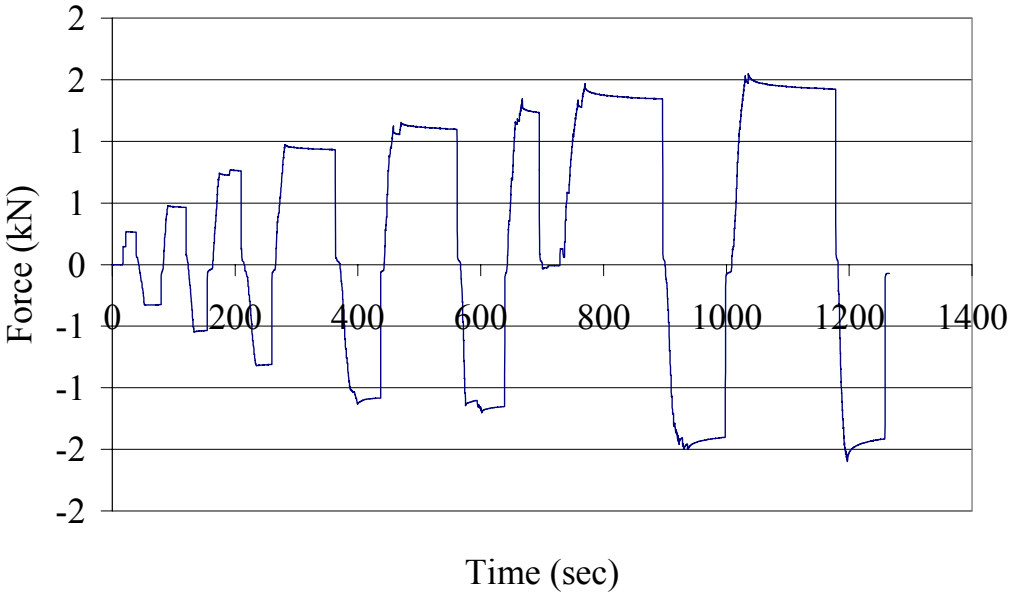

Figure A.14 Applied acceleration value for stage 2(30kN) of briquette wall #2